4-8-2014 12:00 AM

Mechanism of Dissolution of High Valence Lead Oxides in Water Under Depleting Chlorine Conditions

Daoping Guo, *The University of Western Ontario*

Supervisor: Dr. Clare Robinson, *The University of Western Ontario*
Joint Supervisor: Dr. Jose Herrera, *The University of Western Ontario*
A thesis submitted in partial fulfillment of the requirements for the Master of Engineering Science degree in Civil and Environmental Engineering

MECHANISM OF DISSOLUTION OF HIGH VALENCE LEAD OXIDES IN WATER UNDER DEPLETING CHLORINE CONDITIONS

(Thesis format: Monograph)

by

Daoping Guo

Graduate Program in
Civil and Environmental Engineering

A thesis submitted in partial fulfillment
of the requirements for the degree of
Master of Engineering Science

The School of Graduate and Postdoctoral Studies
Western University
London, Ontario, Canada

Abstract

Destabilization of lead corrosion scales present in plumbing materials used in water distribution systems results in elevated lead concentrations in drinking water. Lead release caused by changes in water chemistry (e.g., redox conditions) is often due to the destabilization of lead carbonate and oxide solid phases. Although prior studies have examined the effects of varying water chemistry on the stability of β-PbO_2 (plattnerite), β-PbO_2 stability under depleting chlorine conditions is poorly understood. In addition little is known regarding the mechanisms by which Pb_3O_4 (minium) dissolves under drinking water conditions. In this thesis, long-term batch dissolution experiments were performed for pure phase β-PbO_2 and Pb_3O_4 under depleting chlorine conditions. Results indicate that the initial availability of free chlorine effectively depresses dissolved lead concentrations released from both solid phases. From the Pb_3O_4 dissolution experiments, it was found that Pb_3O_4 was first oxidized by free chlorine to form β-PbO_2. After chlorine was depleted, Pb_3O_4 solvolytic disproportionation resulted in growth of β-PbO_2 and an increase in dissolved lead concentrations. The formation of lead carbonates controlled the final lead concentrations (~0.1 mg/L) for Pb_3O_4 dissolution. In contrast, for the β-PbO_2 dissolution experiments, the dissolved lead levels remained low (~0.004 mg/L) even after free chlorine was depleted. Detailed characterization of solid samples collected during the β-PbO_2 experiments indicate that Pb^{2+} impurities present in crystalline β-PbO_2 play a dominant role in the stability of this solid phase.

Keywords

β-PbO_2 dissolution, Pb_3O_4 dissolution, free chlorine, solid phase transformation, UV/Vis/NIR spectroscopy, FTIR, Raman spectroscopy, XRD.

Co-Authorship Statement

All the experiments were performed by the candidate under the guidance of Dr. Clare Robinson and Dr. Jose Herrera.

The candidate wrote the draft manuscripts in the following chapters:

Chapter 4: Dissolution of minium (Pb_3O_4) in water under depleting chlorine conditions

By Daoping Guo, Clare Robinson, and Jose Herrera

Chapter 5: Dissolution of plattnerite (β-PbO_2) in water under depleting chlorine conditions

By Daoping Guo, Jose Herrera, and Clare Robinson

Contributions:

D. Guo: performed all the experiments, collected, analyzed, and interpreted all the data and wrote the draft of the paper.

C. Robinson and J. Herrera: initiated the research topics, provided guidance on the experiments, assisted in data interpretation, and reviewed/revised the draft chapters.

Acknowledgement

I would like to express my greatest gratitude to my supervisors Dr. Clare Robinson and Dr. Jose Herrera for giving me this opportunity to do the research with them. Their guidance, assistance, and patience though my Master study help me not only gain knowledge, also find out the interests in doing research. I would also like to thank the suggestions and guidance from Dr. Denis O'Carroll and Dr. Jason Gerhard during the RESTORE group meeting.

I would like to thank the help from the faculty and staff in the Faculty of Engineering at Western University, especially to Mr. Tim Stephens for his great guidance and suggestions to my experiments, and Ms. Whitney Barrett giving me support for the study life. In addition, the grateful thanks will give to my fellow graduate students for their support, advice, and assistance.

My special grateful thanks will give to my parents, parents-in-law, and my husband, Yu Guo, for their unending love, encouragement, and support.

Table of Contents

List of Tables

List of Figures

Chapter 1

1 Introduction

1.1 Lead in drinking water

Lead-bearing plumbing material was used in the past for the construction of drinking water distribution networks. This practice continued up until the late twentieth century at which time the health issues caused by the consumption of drinking water with elevated lead levels became widely recognized (NTP 2012). Exposure to extremely low amounts of lead (≤2 μg/dl) may trigger serious health issues (Wu et al. 2003; NTP 2012). Elevated lead concentrations occur in drinking water due to the corrosion of lead-bearing plumbing materials, such as lead pipes, solder, fittings, and brass (Schock and Neff 1988; Schock 1990; Schock et al. 1996; Korshin et al. 2000; Edwards and Dudi 2004). Although the use of lead pipes in drinking water distribution systems (DWDS) was banned in the second half of the twentieth century, many homes built before the mid-1950s are likely to be serviced by lead pipes. Furthermore, the National Plumbing Code of Canada permitted the use of lead-based solder until 1986 (Health.Canada 2007), and so homes build up until this time may have elevated lead levels in the drinking water due to brass faucets, and fixtures.

In recent years, lead contamination of drinking water has re-emerged as a major concern, particularly with respect how changes made to water treatment systems (e.g., changing the disinfectant type) can affect lead concentrations (Edwards and Dudi 2004; Renner 2004; Schock and Giani 2004). Heightened concern has led to modifications to national and local guidelines for lead action levels and also stricter regulations for monitoring of drinking water lead levels (Schock et al. 1996). These updated guidelines present new expenses for municipal water utilities, such as expenditures related to lead monitoring, as well as the implementation and assessment of lead corrosion control strategies. The dissolution of the corrosion scale present inside lead-bearing pipes is influenced by site-specific conditions including the water chemistry (e.g., pH, oxidation and reduction potential [ORP], alkalinity, dissolved inorganic carbonates [DIC], natural organic matters [NOM]) and the composition of the corrosion scales in the pipes. Enhanced understanding of the

fundamental physicochemical processes governing lead dissolution in DWDS is required to develop generalized knowledge and tools that can be applied independent of a specific site. The effect of the water chemistry parameters on lead concentrations depends on specific composition of the corrosion scale, and the potential solid phase transformations that may occur in response to the changing water chemistry. While prior studies have characterized corrosion scales collected from DWDS and examined the influence of different water quality parameters on the dissolution of the major lead solid phases present (Schock 1980; Schock et al. 1996; Schock et al. 2001; Schock and Giani 2004; Schock et al. 2005; Kim and Herrera 2010; Kim et al. 2011; Xie and Giammar 2011), long-term solid phase transformations, the specific mechanisms of these transformations and their impact on dissolved lead levels are not well understood. This knowledge is needed to predict lead levels in customer's tap and to developed more effective corrosion control strategies.

1.2 Research objectives

The research presented in this thesis is part of a large project that aims to understand the physicochemical processes that influence dissolved lead levels in drinking water. The objective of this thesis is to characterize the fundamental processes associated with the dissolution of the solid oxide phases minium (Pb_3O_4) and plattnerite (β-PbO_2). β-PbO_2 is generally present in lead corrosion scales under typical drinking water conditions (Schock et al. 1996; Schock et al. 2001; Schock et al. 2005), while Pb_3O_4 was observed in London's corrosion scale and hypothesized as an intermediate phase in solid phase transformations (Kim and Herrera 2010). The specific objectives of this thesis are as follows:

1. Determine the equilibrium solubility of Pb_3O_4 and β-PbO_2 under depleting chlorine conditions.
2. Identify the influence of free chlorine concentrations on the dissolution of Pb_3O_4 and β-PbO_2.
3. Characterize solid phase samples collected during the dissolution of Pb_3O_4 and β-PbO_2 to identify the long-term transformations in the solid phases. This characterization provides valuable insights into the fundamental physicochemical processes governing Pb_3O_4 and β-PbO_2 dissolution.

1.3 Original contribution

The solubility of Pb_3O_4 including the influence of water quality parameters on the stability of this mixed valence lead oxide phase under drinking water conditions has not previously been investigated. In addition, while many prior studies have focused on the solubility of β-PbO_2 (e.g., (Schock et al. 2001; Lin and Valentine 2009; Xie et al. 2010; Wang et al. 2012)), the dissolution of β-PbO_2 under depleting chlorine conditions and the long-term solid phase transformations occurring during this dissolution process are not well understood. In this thesis we aim to fill these gaps by performing batch dissolution experiments that quantify the equilibrium solubility of Pb_3O_4 and β-PbO_2, and identify the effect of chlorine on the dissolution of these phases under depleting chlorine conditions. The work present in Chapter 4 is the first comprehensive study of the mechanisms of Pb_3O_4 dissolution under conditions relevant for DWDS. Furthermore for both Pb_3O_4 and β-PbO_2 dissolution experiments, solid phase samples are characterized via various techniques (UV/Vis/NIR, FTIR, Raman, and XRD) to quantify the long-term solid phase transformations.

1.4 Thesis outline

Chapter 1 presents general background for the thesis and the research objectives.

Chapter 2 reviews previous studies that have characterized lead corrosion scales present in DWDS and describes the influence of various water chemistry parameters on lead corrosion scale formation, dissolution and transformation.

Chapter 3 presents the materials and methods including details of the experimental and analytical protocols used for this work.

Chapter 4 and 5 present and discuss the experimental results of Pb_3O_4 and β-PbO_2 dissolution under depleting chlorine conditions, respectively.

Chapter 6 summarizes the experimental findings and provides recommendations for future work.

1.5 References

Edwards, M. and A. Dudi (2004). "Role of chlorine and chloramine in corrosion of lead-bearing plumbing materials." Journal of the American Water Works Association **96**(10): 69-81.

Health.Canada. (2007). Fact Sheet-Minimizing Exposure to Lead from Drinking Water Distribution Systems. Health Canada. Available: http://www.hc-sc.gc.ca/ewh-semt/pubs/water-eau/lead-plomb-eng.php. Last accessed 15th January 2014.

Kim, E. J. and J. E. Herrera (2010). "Characteristics of lead corrosion scales formed during drinking water distribution and their potential influence on the release of lead and other contaminants." Environmental Science and Technology **44**(16): 6054-6061.

Kim, E. J., J. E. Herrera, D. Huggins, J. Braam and S. Koshowski (2011). "Effect of pH on the concentrations of lead and trace contaminants in drinking water: A combined batch, pipe loop and sentinel home study." Water Research **45**(9): 2763-2774.

Korshin, G. V., J. F. Ferguson and A. N. Lancaster (2000). "Influence of natural organic matter on the corrosion of leaded brass in potable water." Corrosion Science **42**(1): 53-66.

Lin, Y. and R. L. Valentine (2009). "Reduction of Lead Oxide (PbO2) and Release of Pb(II) in Mixtures of Natural Organic Matter, Free Chlorine and Monochloramine." Environmental Science and Technology.

NTP. (2012). NTP Monograph-Health effects of low-level lead. National Toxicology Program-U.S. Department of Health and Human Services. Available: http://ntp.niehs.nih.gov/?objectid=4F04B8EA-B187-9EF2-9F9413C68E76458E. Last accessed 15th January 2014.

Renner, R. (2004). "Plumbing the depths of DC's drinking water crisis." Environmental Science and Technology **38**(12): 224A-227A.

Schock, M. R. (1980). "Response of lead solubility to dissolved carbonate in drinking water." Journal of the American Water Works Association **72**(12).

Schock, M. R. (1990). "Causes of temporal variability of lead in domestic plumbing systems." Environmental Monitoring and Assessment **15**(1): 59-82.

Schock, M. R. and R. Giani (2004). Oxidant/disinfectant chemistry and impacts on lead corrosion. Proceedings of 2004 American Water Works Association Water Quality and Technology Conference.

Schock, M. R., S. M. Harmon, J. Swertfeger and R. Lohmann (2001). "Tetravalent lead: a hitherto unrecognized control of tap water lead contamination." Proceedings AWWA Water Quality Technology Conference, Nashville: 11-15.

Schock, M. R. and C. H. Neff (1988). "Trace metal contamination from brass fittings." Journal of the American Water Works Association **80**(11): 47-56.

Schock, M. R., K. Scheckel, M. DeSantis and T. L. Gerke (2005). Mode of occurrence, treatment, and monitoring significance of tetravalent lead. Proceedings AWWA Water Quality Technology Conference. Quebec City, Quebec.

Schock, M. R., I. Wagner and R. Oliphant (1996). The corrosion and solubility of lead in drinking water. Internal corrosion of water distribution systems. Denver, CO., AWWA Research Foundation/TZW**:** 131-230.

Wang, Y., Y. Xie and D. E. Giammar (2012). Lead(IV) oxide formation and stability in drinking water distribution systems.

Wu, T., G. M. Buck and P. Mendola (2003). "Blood lead levels and sexual maturation in US girls: the Third National Health and Nutrition Examination Survey, 1988-1994." Environmental Health Perspectives **111**(5): 737.

Xie, Y., Y. Wang and D. E. Giammar (2010). "Impact of chlorine disinfectants on dissolution of the lead corrosion product PbO2." Environmental Science and Technology **44**(18): 7082-7088.

Xie, Y. J. and D. E. Giammar (2011). "Effects of flow and water chemistry on lead release rates from pipe scales." Water Research **45**(19): 6525-6534.

Chapter 2

2 Literature review

2.1 Introduction

Several drinking water distribution systems (DWDS) in North America and Europe use lead-bearing plumbing materials in their drinking water distribution infrastructure. Over time, lead corrosion scales formed on these plumbing materials. There is considerable concern regarding elevated lead levels in drinking water from the destabilization of these corrosion scales. Destabilization can be caused by the changes in water treatment methods which trigger transformations and dissolution to the corrosion scales. Since a complete replacement of lead service lines is economically prohibitive, it is, therefore, necessary to develop corrosion control strategies to reduce lead concentrations at the customer's tap. It is well acknowledged that dissolved lead concentrations in drinking water are mainly controlled by the solubility of the lead corrosion scales present in lead-bearing plumbing. Therefore, a clear understanding of the characteristics of lead corrosion scales under different water quality conditions is essential to develop effective long-term corrosion control strategies. This chapter summarizes previous studies that have examined the characteristics of site-specific corrosion scales using various analytical techniques, and also investigated the influence of water quality parameters on the lead corrosion dissolution processes.

2.2 Current lead issue in Canada

Although sources of drinking water in Canada contain almost no lead, and water treatment processes are regulated to ensure that lead is not introduced during water treatment, drinking water is recognized as a potential source of lead exposure to Canadians (Health.Canada 2007; Health.Canada 2013). Elevated lead levels in drinking water are caused by dissolution of corrosion phases formed inside lead-bearing plumbing used in drinking water distribution systems (DWDS). As lead is not metabolized, and accumulates in the body, it may trigger serious health issues particularly for infants and young children (Wu et al. 2003; COEH 2005; NTP 2012). Health Canada's Maximum Acceptable Concentration (MAC) of lead in drinking water is 10 µg/L (Health.Canada 2012). A recent

report by Health Canada (2013) showed that lead concentrations in water samples obtained in residential homes exceeded 10 µg/L in municipalities in Saskatchewan, Ontario, Quebec, and Newfoundland and Labrador. Table 2.1 shows drinking water lead tests results obtained for eight Ontario cities. From the table it can be seen that five out of eight cities were reported to have elevated lead levels in drinking water.

Table 2.1 Concentrations of lead (µg/L) in residential tap water in eight Ontario cities (Reproduced from Health Canada, 2013)

Sample location	Year	n	% > 10 µg/L	Concentration (µg/L)			Reference
				Median	Min[a]	Max[a]	
Ontario[c]	2007/8[j]	37 517	2.3	Average: 2.0	-	-	OMOE 2009
	2008[k]	37 895	3.1	Average: 1.9	-	491	
Hamilton[c]	2009	634	8	-	<1	97	Hamilton 2010
(North) Hamilton[c]	2008	-	-	-	<0.5[n]	28[n]	Richardson et al. 2011
Waterloo[c]	2009	121	0	-	<1	4	Waterloo 2009
Barrie[c]	2009	512	0.2	-	0.11	23.9	Barrie 2010
Kingston[c]	2009	198	8	-	<0.02	48.1	Kingston 2009
Ottawa[c]	2009	264	4	-	<0.5	38	Ottawa 2011
St. Catharines[c]	2009	2	0	-	<0.02	0.03	St. Catharines 2009
Sudbury[c]	2009	790	0.5	-	1	17	Sudbury 2009

The most effective way to reduce the health risks associated with dissolved lead in drinking water is the complete replacement of the lead service lines. However, full replacement of lead pipes is a lengthy and cost intensive process. Thus municipalities with lead service lines are required to develop and have a corrosion control plan to mitigate against elevated lead levels in drinking water according to the amendments to Ontario's Reg. 170/03.

2.3 Chemistry of the formation of lead corrosion scales

Lead corrosion scales form by reactions between the plumbing materials and the drinking water in DWDS. The quality of the drinking water determines the composition of the corrosion scales that develop inside a lead pipe. Generally, lead corrosion scale formation is a passivation process. Pb(II) ions form as the elemental lead (Pb^0) in the pipe matrix is oxidized by dissolved oxygen (DO) and/or the disinfectant (e.g., free chlorine) present in water. Pb(II) ions then undergo complexation by ligands such as hydroxyl ions (OH^-), carbonates (CO_3^{2-}, HCO_3^-), phosphates, nitrates, etc. Some Pb(II) phases with low solubility will precipitate resulting in the formation of a passivation layer which prevents

further contact between Pb^0 and water. Pb(IV) oxides can eventually form as well under highly oxidative conditions (Schock et al. 2001; Schock and Giani 2004; Kim and Herrera 2010). Soluble Pb^{4+} ions however are not formed during this process as they are thermodynamically unstable under typical drinking water conditions (Pourbaix 1974).

The speciation of Pb^{2+} under typical drinking water conditions has been extensively studied (Schock 1980; Schock et al. 1996a; Powell et al. 2009). Monomeric $PbOH^+$, $Pb(OH)_{2(aq)}$, and $Pb(OH)_3^-$ are the major species resulting from Pb(II) hydrolysis reactions. Polymeric species (eg. $Pb_3(OH)_4^{2+}$, $Pb_4(OH)_4^{4+}$ etc.) generally do not form in considerable amounts in typical surface or ground water (Powell et al. 2009). Figure 2.1 illustrates the speciation of soluble lead for the $Pb^{2+}/H^+/CO_3^{2-}$ system, showing that $PbCO_{3(aq)}$ dominates over lead hydroxo complexes in the 7.6<pH<8.9 range. The experimental results of Xie et al. (2010b) also demonstrated that $PbCO_{3(aq)}$, $Pb(CO_3)_2^{2-}{}_{(aq)}$, and $PbHCO_3^-{}_{(aq)}$ dominate at pH 7.5 with 10 and 50 mg C/L DIC. For multicomponent systems containing $Pb^{2+}/H^+/CO_3^{2-}/Cl^-/PO_4^{3-}/SO_4^{2-}$, the lead carbonato-complexes are still dominant species with small amounts of soluble $PbSO_{4(aq)}$ species in the 7.6<pH<8.9 range. Complexation by Cl^- and PO_4^{3-} are thought to be negligible (Powell et al. 2009).

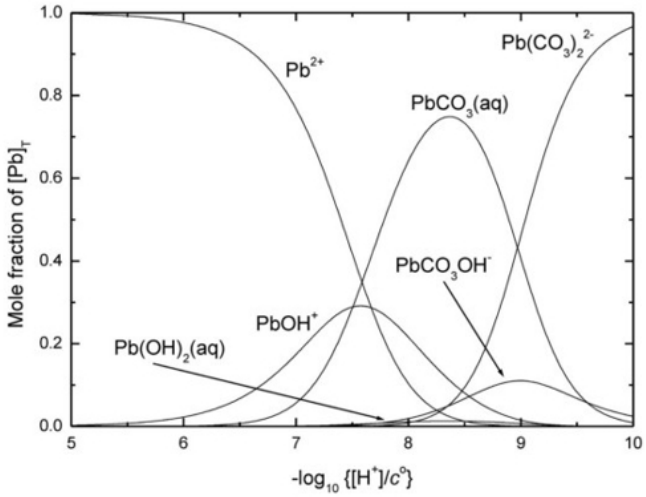

Figure 2.1 Speciation diagram for Pb^{2+}+H^++CO_3^{2-} system (Powell et al. 2009)

2.4 Characteristics of lead corrosion scales

Previous studies have focused on characterizing lead corrosion scales from DWDS to identify their chemical and physical properties (Schock et al. 1996a; Schock et al. 2001; Schock and Giani 2004; Kim and Herrera 2010; Kim et al. 2011; Xie and Giammar 2011). These studies reported that the formation of lead corrosion scales is governed by site-specific conditions, in other words their composition and dominant phases are determined by the chemistry of the drinking water flowing through the DWDS.

Generally, lead corrosion scales contain several layers. Lead (II) carbonates and lead oxides are the two major lead phases observed in corrosion scales. Hydrocerussite ($Pb_3(CO_3)_2(OH)_2$) and cerussite ($PbCO_3$) are the most common crystalline lead carbonates found in lead corrosion scales in the absence of phosphates. Therefore, many studies have examined the solubility of these solid phases under drinking water conditions (Schock 1980; Schock and Gardels 1983; Kim et al. 2011; Xie and Giammar 2011). Plattnerite (β-PbO_2) and scrutinyite (α-PbO_2) are frequently found together with lead carbonates in lead corrosion scales collected from DWDS subjected to aggressive chlorination since lead (II) phases can be oxidized by free chlorine. For instance, Schock et al. (2001) reported the presence of α-PbO_2 and β-PbO_2 in Cincinnati's DWDS. These lead (IV) oxides were found to coexist with minor amounts of hydrocerussite, quartz, and calcite. The presence of a thin surface layer of PbO_2 was also reported in the corrosion scale of Madison, WI with cerussite as the bulk underlying phase (Schock and Giani 2004). For corrosion scales analysed from the DWDS of London, ON, hydrocerussite and cerussite have been reported as the dominant crystalline phases together with lead oxides (PbO, Pb_3O_4, and PbO_2) and aluminum silicates (Kim and Herrera 2010).

The highly soluble litharge (α-PbO) phase has also been found in corrosion scales harvested from some lead service lines. However it has only been observed in the inner layers of the corrosion scale where it is not in direct contact with water (Schock et al. 1996b; Schock et al. 2005; Kim and Herrera 2010). The mixed valent oxide phase minium (Pb_3O_4) has been also observed in lead corrosion scales, and it is thought that it may act an intermediate in the transformation of Pb(II) to Pb(IV) phases (Kim and Herrera 2010).

2.5 Structural and physicochemical properties of Pb_3O_4 and PbO_2

As mentioned in section 2.4, lead oxides often presented in the surface layer of corrosion scales found in DWDS, and therefore dissolved lead concentrations in drinking water are determined by their solubility. It is, therefore, essential to have a clear understanding of the physicochemical processes governing lead oxides dissolution under typical drinking water conditions. The physicochemical properties of Pb_3O_4 and PbO_2 control their dissolution. Lead oxides are widely used as electrodes in lead-acid batteries (Rüetschi 1992; Pavlov 2011), and have been studied in the field of lead-containing thin films and glasses (Lappe 1962; Mindt 1969; Salagram et al. 2002; Aly et al. 2013). As a result their crystalline structure and electrochemical characteristics have been extensively investigated. We present below a summary of their most notable structural and physicochemical properties.

2.5.1 Crystalline structure of Pb_3O_4

Minium (Pb_3O_4) is recognized as a good semi-conductor (Terpstra et al. 1997; Dinnebier et al. 2003). This arises mainly from the fact that Pb_3O_4 is a mixed valence compound, consisting of divalent and tetravalent lead. Its chemical formula is properly written as PbO_2•2PbO. Figure 2.2 illustrates the crystalline structure of Pb_3O_4. Lead occupies two different types of sites in this structure. One site has Pb^{4+} coordinated with six oxygen atoms in an octahedral crystal field ($Pb(IV)O_6$). These octahedra are joined together along opposite edges forming two dimensional chains in a similar arrangement as those found in β-PbO_2 (Gross 1943; Dickens 1965; Vigouroux et al. 1982; Le Bellac et al. 1995; Terpstra et al. 1997). These chains are connected in an asymmetric tetragonal fashion through the formation of four Pb(II)-O bonds to form a three dimensional crystal. This coordination geometry for Pb^{2+} is similar to the one in massicot (β-PbO) except that the Pb(II)-O-Pb(II) angle in Pb_3O_4 is different from that present in β-PbO (Dickens 1965). Indeed both $Pb(IV)O_6$ octahedra and $Pb(II)O_4$ tetrahedra in Pb_3O_4 are heavily distorted compared with the structures observed in the single valence oxides (Terpstra et al. 1997).

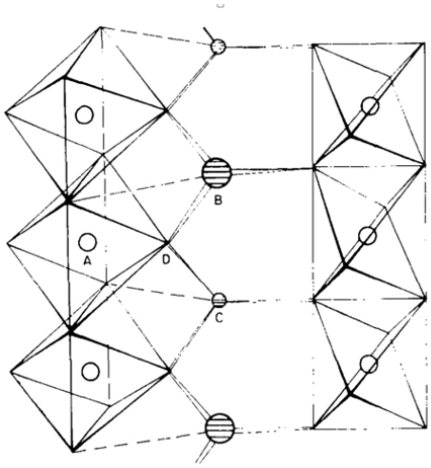

Figure 2.2 The coordination of Pb_3O_4 (Dickens 1965). Atoms A is Pb(IV), and atoms B and C are Pb(II). Atom D is oxygen.

2.5.2 Solubility of Pb_3O_4

Very few studies have reported the solubility of Pb_3O_4 in water, although Pb_3O_4 has been found in lead corrosion scales and historically used in industrial products. One of the few studies found reported the solubility of Pb_3O_4 as 1.1 x 10^{-17} mol/L at 17 °C. This value was obtained using a $Pt \mid \frac{Pb_3O_4}{PbO}$ electrode in sodium hydroxide solution without dissolved carbonates. The proposed dissolution process is given in Equation 2.1 (Glasstone 1922).

$$Pb_3O_4 \leftrightarrow 2Pb^{2+} + PbO_4^{4-} \quad (1)$$

This reported solubility value suggests that only small amounts of dissolved lead are released from Pb_3O_4 under strong alkaline conditions. A different experimental study reported that 0.553 mg/L (8.9 x 10^{-7} mol/L) of lead was released from Pb_3O_4 dissolution in distilled water at room temperature (Fraser and Fairhall 1959). Furthermore, a recent study reported that the equilibrium lead concentration of powder Pb_3O_4 (20 g/L) was 68.5 mg/L in ultra-pure water at constant pH 4-4.5 after a three-day dissolution at 22 °C (Brokbartold et al. 2013). Although these two studies suggest a relative high solubility of Pb_3O_4 in highly purified water, two additional studies reported the water solubility of Pb_3O_4 as 6.86 ng/L (McKinley et al. 2002) and 0.0207 mg/L (Pavlov 2011). Unfortunately, the authors did not mention the water quality conditions of their study. As described above there is no agreement on the solubility of Pb_3O_4 in water.

Studies focused on the mechanism of Pb_3O_4 dissolution in dilute nitric acid suggested that the removal of Pb^{2+} caused the collapse of the Pb_3O_4 crystalline structure. β-PbO_2 like octahedra chains are held by Pb^{2+} ions in Pb_3O_4. Thus the structural collapse of Pb_3O_4 results in the formation of β-PbO_2 (Bagshaw et al. 1966; Kang et al. 1988). To the best of our knowledge there is no published study on the dissolution of Pb_3O_4 under drinking water conditions. This may be because Pb_3O_4 has only recently been identified in lead corrosion scales (Kim and Herrera 2010).

2.5.3 Crystalline structure of PbO_2

Crystalline PbO_2 exists in two modifications: scrutinyite (α-PbO_2) and plattnerite (β-PbO_2). α-PbO_2 crystallizes in an orthorhombic structure, while β-PbO_2 does it in the tetragonal rutile structure. In both cases, the tetravalent lead ion is in the center of a distorted octahedron surrounded by six oxygen ions (Mindt 1969; Carr and Hampson 1972; Li et al. 2011). The main difference between these two modifications is the arrangement of the octahedra in the crystal structure. Specifically, in β-PbO_2 the neighboring octahedra share opposite edges to form a linear chain, while α-PbO_2 forms zig-zag chains as neighboring octahedra share non-opposing edges. The resulting chains are connected with each other by sharing corners for both modifications. Figure 2.3 shows the structure of these two PbO_2 modifications.

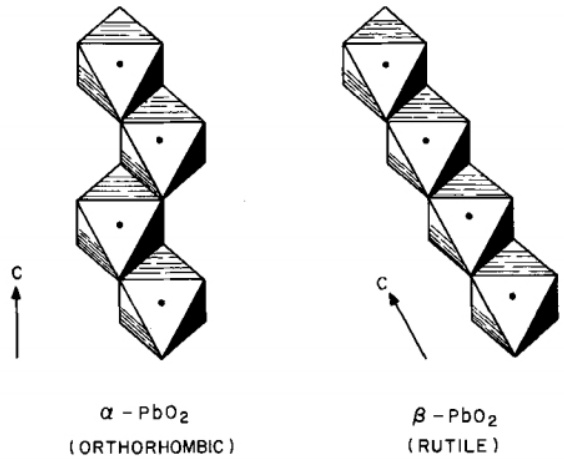

Figure 2.3 The coordination of α-PbO_2 and β-PbO_2 (Mint 1969)

Generally the two modifications have similar electrochemical properties, and both are good semi-conductors. It is well acknowledged that fully stoichiometric PbO_2 does not exist as impurities are always present in the PbO_2 structure. Previous studies have reported that these impurities are responsible for the relatively good conductivity of PbO_2, however, the nature of the impurities is still under debate. One possibility is that the deficiency of oxygen in the PbO_2 structure generates vacancies responsible for electronic conduction (Bagshaw et al. 1966; Scanlon et al. 2011). Rüetschi and Cahan (1957) proposed that some hydroxyl ions replaced oxygen in the PbO_2 crystal lattice, and provided extra free electrons for conduction. Another study by Rüetschi (1992) suggested that the oxygen sites in the crystal corresponded to the stoichiometry content of PbO_2, whereas Pb^{2+} ions substituted some Pb^{4+} sites in PbO_2, providing extra electrons for conduction. In terms of their thermodynamic stability, α-PbO_2 can transform into β-PbO_2 under normal conditions (room temperature and ambient humidity) (White et al. 1961). This has been explained in terms of the stable β-PbO_2 recrystallizing on the superficial layers of the metastable α-PbO_2 crystals (Carr and Hampson 1972). White et al. (1961) reported that β-PbO_2 could undergo an irreversible phase transition to form α-PbO_2 under high pressures.

The mechanisms of formation of α-PbO_2 and β-PbO_2 in aqueous phase have been studied in the field of electrochemistry (Bagshaw et al. 1966; Li et al. 2011). Bagshaw et al. (1966) suggested that the nucleation energy barrier determines the pathway for forming the specific PbO_2 phase from oxidation of Pb(II) in solution. The highly charged tetravalent lead ions attract the hydroxyl ions rather than water molecules to form octahedra at high pH due to ionic size considerations. The nucleation process will then occur through these octahedra packing in the α-PbO_2 pattern, which is more compact than β-PbO_2 pattern. In contrast, the conjugate base anions likely play a role in the arrangement of the Pb^{4+} coordinated octahedra in acidic solutions since the concentration of hydroxyl groups is extremely low. As these anions are larger than hydroxyls, the octahedra would face opposite directions to form linear chains to minimize steric hindrance and β-PbO_2 will form instead. The experimental results reported for oxidation of Pb(II) to Pb(IV) phases in chlorinated water are consistent with this mechanism: α-PbO_2 was the dominant phase at high pH, while β-PbO_2 was the major phase at neutral pH levels (Lytle and Schock 2005; Wang et al. 2010).

2.5.4 Solubility of PbO_2

In comparison with Pb_3O_4, several studies have addressed the solubility of PbO_2. Thermodynamically, reported Gibbs free energies of formation predict extremely low PbO_2 solubility values (in the order of nanograms to picograms per liter), and usually lower than experimental results obtained under drinking water conditions (Schock et al. 2001; Xie et al. 2010a). For instance, Schock et al. (2001) predicted the solubility of β-PbO_2 around 5 μg/L under Cincinnati's drinking water conditions at pH 8.8. He also indicated that the solubility of plattnerite increased with higher pH. This dependence of PbO_2 solubility on pH was also observed by Wang et al. (2012) on plattnerite batch dissolution experiments with constant 2 mg/L free chlorine and 50 mg C/L DIC. In this case the reported dissolved lead concentrations were well below 2 μg/L at pH 6, while the lead levels increased to about 10 μg/L at pH 7.5 and about 30 μg/L at pH 8.5 after 20 days. The study conducted by Lin and Valentine (2009) reported the equilibrium lead concentrations slightly below 8 μg/L after 21 days at pH 7 observed in PbO_2 batch dissolution experiments with 2 mg/L initial free chlorine and 1mM DIC. All these experimental results show higher dissolved lead concentrations than those predicted values using thermodynamic data. This is likely caused by the fact that PbO_2 Gibbs free energy of formation values were obtained from electrochemical measurements of dissolution processes under strongly acidic electrolyte solutions (Schock et al. 2001; Xie et al. 2010a), in contrast, batch dissolution experiments are normally performed under neutral or slightly alkaline drinking water conditions.

2.6 Solid phase transformations

2.6.1 The mechanism of precipitation and dissolution of PbO_2

Lytle and collaborators have studied the transformation of dissolved Pb(II) ions to Pb(IV) solid phases in chlorinated water (Lytle et al. 2009). In this study hydrocerussite initially precipitated out from a dissolved Pb (II) solution containing 2.82 mg Cl_2/L (free chlorine) and 10 mg C/L DIC at pH 8.02. The solid transformed to cerussite with small amounts of plattnerite and scrutinyite formed after 14 days (Lytle et al. 2009). The proposed pathway for PbO_2 formation at pH 8 was Pb^{2+}→hydrocerussite→cerussite→PbO_2. The color of the

solid phase changed from white to reddish brown during these 14 days; this is in agreement with the color changes reported by Lytle and Schock (2005) who observed that α-PbO_2 and β-PbO_2 were the dominant phases present after a Pb^{2+} solution was mixed with 3 mg/L free chlorine and 10 mg C/L DIC at initial pH of 8 for more than 80 days. Edwards and Dudi (2004) also observed a similar color change during the oxidation of Pb^{2+} ions by free chlorine at pH 5.5 and 8.5. Besides the changes in color, a decrease in dissolved lead concentrations was also observed in all these studies; this is likely caused by the formation of the low solubility PbO_2 phases.

Hydrocerussite and cerussite have also been used as starting materials to study solid phase transformations in chlorinated water (Lytle and Schock 2005; Liu et al. 2008; Liu et al. 2009; Wang et al. 2010). The formation of Pb(III) intermediates was hypothesized to explain the slight consumption of free chlorine at the beginning of experiments for hydrocerussite (pH 7.3-8.1 with 1mM total carbonates and 10mM ionic strength) and cerussite dissolution (pH 7 with 1-3mM total carbonates and 10mM ionic strength). $PbO_{2(s)}$ was not observed at the early stages of dissolution (Liu et al. 2009). During the later stages, both Pb(II) carbonates transformed to $PbO_{2(s)}$, while cerussite was also observed embedded in the original hydrocerussite matrix. This is consistent with previous observations (Liu et al. 2008). Lytle and Schock (2005) also observed a similar pathway for PbO_2 formation from hydrocerussite or cerussite in chlorinated water. There was, however, no precipitation of PbO_2 within the first 30 min reaction even in superchlorinated water (about 30 mg/L as Cl_2). Both studies suggest that the formation of PbO_2 from lead(II) carbonates is a time-dependent phenomena regulated by kinetic processes (Lytle and Schock 2005; Liu et al. 2009).

Wang et al. (2010) performed a set of batch experiments to determine the pathways and mechanism for the formation of Pb(IV) oxides from four different Pb(II) phases: aqueous lead(II) chloride solutions, massicot (PbO), cerussite, and hydrocerussite. All these four lead(II) phases transformed to PbO_2 after 28 days in the presence of free chlorine (Figure 2.4). Figure 2.5 depicts the hypothesized mechanism through two possible ways: a) $Pb^{2+}_{(aq)}$ oxidized by some free chlorine to form $Pb^{4+}_{(aq)}$ in the aqueous phase followed by $PbO_{2(s)}$

deposition (1A-2B-3A/3B); and b) solid phase oxidation (2A) where Pb(II) carbonates are transformed to $PbO_{2(s)}$.

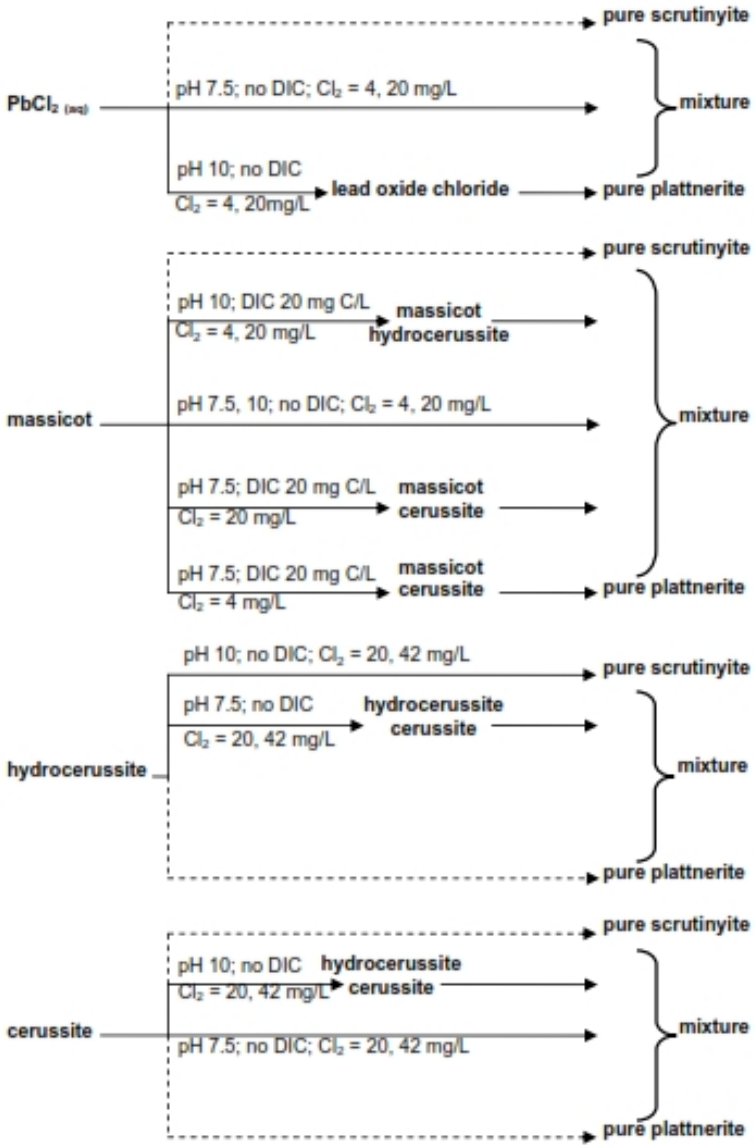

Figure 2.4 Formation of PbO_2 from Pb(II) phases. Reprinted (adapted) with permission from (Wang et al. 2010). Copyright (2014) American Chemical Society.

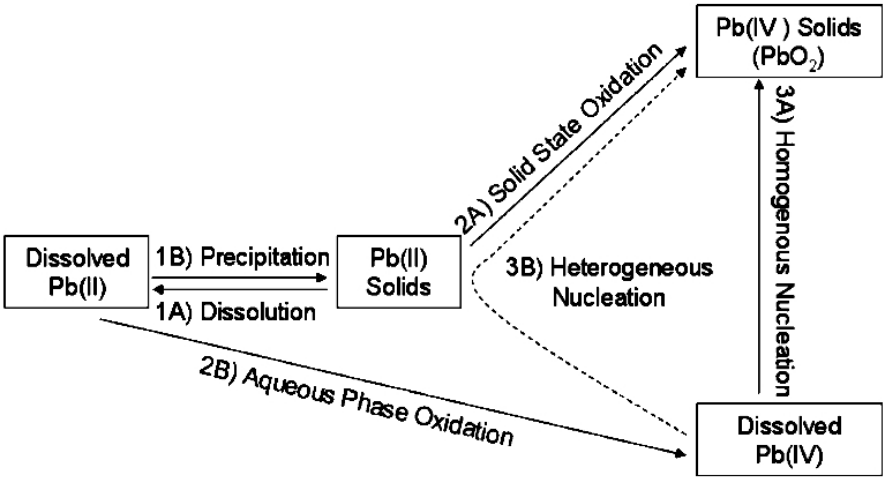

Figure 2.5 The mechanisms of PbO_2 formation from Pb(II) phases. Reprinted (adapted) with permission from (Wang et al. 2010). Copyright (2014) American Chemical Society

These studies indicate that the stability of different lead phases is highly dependent on the ORP levels. Elevated lead concentrations have been observed in some municipalities after there is a switch in disinfectant (e.g., chloramines replacing free chlorine). Studies found that the associated decrease in ORP levels led to the dissolution of PbO_2 (Edwards and Dudi 2004; Switzer et al. 2006). As a result several studies have focused on identifying the dissolution pathways for PbO_2 under drinking water conditions in the presence and absence of free chlorine. Values between 25-88 µg/L were reported for dissolved lead levels in PbO_2 dissolution experiments in the absence of free chlorine at pH 7 with DIC ranging from 1 – 5 mM (Lin and Valentine 2008a; Lin and Valentine 2008b; Lin and Valentine 2009). The dissolution was attributed to the reduction of PbO_2 by water (Eq. 2) (Lin and Valentine 2008b).

$$PbO_{2(s)} + H_2O_{(l)} \leftrightarrow Pb^{2+}{}_{(aq)} + 2OH^-{}_{(aq)} + 0.5O_{2(aq)} \quad (2)$$

Solid lead carbonates were observed in PbO_2 dissolution experiments without free chlorine, and so the proposed pathway for PbO_2 dissolution is the reverse process of PbO_2 formation: $PbO_2 \rightarrow PbCO_3$ and/or $Pb_3(CO_3)_2(OH)_2$ (Edwards and Dudi 2004; Lytle and Schock 2005). In contrast, lower dissolved lead concentrations were observed in PbO_2 dissolution experiments at pH 6 - 8.5 in the presence of free chlorine (Section 2.5.4), where water-reduced Pb^{2+} ions (Eq. 2) were transformed back into $PbO_{2(s)}$ (Eq. 3). The kinetics of Eq.

2 and 3 determine the dissolved lead concentrations under specific water quality conditions. Furthermore the modification (plattnerite vs. scrutinyite) of formed PbO_2 is determined by the pH and types of ions in solution (Section 2.5.3) (Petersson et al. 1998).

$$Pb^{2+}{}_{(aq)} + OCl^{-}{}_{(aq)} + H_2O_{(l)} \leftrightarrow Cl^{-}{}_{(aq)} + PbO_{2(s)} + 2H^{+}{}_{(aq)} \quad (3)$$

2.6.2 The mechanism of precipitation and dissolution of Pb_3O_4

As Pb_3O_4 is an important industrial product used as pigment, additive for glasses, and in lead-acid batteries, its manufacturing method and subsequent solid phase transformation have been relatively well studied. Pb_3O_4 is industrially produced by the oxidation of α-PbO by oxygen through thermal treatment (Aze et al. 2008b). A study on the thermal decomposition of hydrocerussite reported that Pb_3O_4 formed in oxygen or air at 838K via a gas-solid diffusion process (hydrocerussite→ β-PbO→ Pb_3O_4) (Dan et al. 1996). For lead-acid batteries, a non-stoichiometric mid-layer containing PbO_x ($1<x<2$) forms between the α-PbO and β-PbO_2 layers (Pavlov 2011). This mid-layer may contain Pb_3O_4 and α-PbO_2. Intense laser irradiation or heating over 375 °C can decompose β-PbO_2 into Pb_3O_4. This process has been industrially exploited for the restoration of darkened Pb_3O_4 pigments in painting (Burgio et al. 2001; Aze et al. 2008a).

As mentioned in Section 2.5.2 Pb_3O_4 dissolution has only been studied under acid conditions. Kang et al. (1988) observed Pb_3O_4 underwent a disproportionation process in dilute nitric and acetic acid forming β-PbO_2. A similar redox process was observed during Pb_3O_4 dissolution in 0.1M sulfuric acid, resulting in the formation of β-PbO_2 and $PbSO_4$ (Aze et al. 2007). Reports on the mechanisms of Pb_3O_4 dissolution under drinking water conditions were not found in the literature.

2.6.3 Effect of water quality on lead oxides solid phase transformations

Previous studies have proposed that the influence of DIC on the formation of PbO_2 from hydrocerussite or cerussite is not significant in chlorinated water because carbonate ions are released from the dissolution of solid lead carbonates (Wang et al. 2010). In contrast,

DIC and pH play an important role in the formation of PbO_2 from massicot (β-PbO) and Pb (II) ions in chlorinated water based on the study of Wang et al (2010). In the absence of DIC, only a mixture of scrutinyite and plattnerite were observed together with residual massicot at pH 7.5 and 10 throughout 28-day experiments. These experiments indicate PbO_2 formation does not require lead carbonates as intermediate phase. The presence of DIC seems to accelerate the transformation of the Pb(II) phases → hydrocerussite → scrutinyite (dominant phase) at pH 10 (Wang et al. 2010). In contrast, at lower pH (7.5) a different pathway of Pb(II) phases → cerussite → plattnerite was observed. The studies discussed in Section 2.5.3 and 2.6.1 (for PbO_2 formation from hydrocerussite or cerussite) also indicate that pH plays a critical role in determining the oxidation pathway and crystalline structure of PbO_2 (Bagshaw et al. 1966; Lytle and Schock 2005; Liu et al. 2008; Li et al. 2011). Pure α-PbO_2 formed from the oxidation of hydrocerussite by free chlorine after 28 days at pH 10 (Wang et al. 2010). The formation of α-PbO_2 from hydrocerussite has also been reported by Lytle and Schock (2005) under similar experimental conditions (initial pH of 9.62-9.86, DIC 10 mg C/L, 3 mg/L chlorine). In contrast, cerussite was observed as an intermediate phase during the oxidation of hydrocerussite at lower pH (7.5), and a mixture of scrutinyite and plattnerite was observed as final solid phases (Wang et al. 2010). Hydrocerussite converting into cerussite and PbO_2 has also been reported by Lytle et al. (2005) in the pH range of 6.5 to 8.

The studies discussed in Section 2.6.1 indicate that free chlorine can effectively oxidize Pb(II) phases to form PbO_2 under drinking water conditions (Lytle and Schock 2005; Liu et al. 2008; Lytle et al. 2009; Wang et al. 2010). When relatively high ORP values are maintained by free chlorine, dissolved lead concentrations remain low as PbO_2 is thermodynamically stable under high ORP conditions. The more free chlorine, the faster PbO_2 formation was observed in the formation of PbO_2 from β-PbO in the presence of DIC (Wang et al. 2010).

In comparison with comprehensive studies investigating the influence of DIC, pH and free chlorine on the pathways for PbO_2 formation, few studies focus on the effects of these water quality parameters on the pathways for PbO_2 dissolution. It was observed by Xie et al. (2010) that DIC accelerates the dissolution rate of PbO_2 through complexation with

dissolved lead at pH 7.5, 8.5, and 10. Thermodynamically, the equilibrium dissolved lead concentrations increase with increasing pH levels under drinking water conditions. The effect of free chlorine on the dissolution of scrutinyite was studied by Liu (2009). With an increase in the concentration of free chlorine, the zeta-potential of α-PbO_2 became more negative, which suggests an increased adsorption of free chlorine on the scrutinyite surface. α-PbO_2 particles were observed to form aggregates of size smaller than 50 nm with a blunter edge after a 10-day exposure to a solution with 50 mg/L as Cl_2 at pH 7.3. Meanwhile dissolved lead levels ranging from 0.1 - 1 mg/L were observed even though α-PbO_2 is thermodynamically insoluble under these conditions. These observations strongly suggest solid phase transformations occurred, however the authors did not propose a mechanism for these apparent inconsistencies.

If Pb(IV) oxides are the dominant phase in the surface layer of the lead corrosion scale, the stability of PbO_2 may determine the dissolved lead concentrations in drinking water. Morphological changes are consistently reported in the literature for PbO_2 in chlorinated water even though it should be thermodynamically stable under these conditions. There is a lack of knowledge however on the influence of free chlorine on the solid phase transformation, particularly dissolution of PbO_2, as well as the associated changes in dissolved lead levels. Moreover, although mixed valence lead oxides such as Pb_3O_4 could be important intermediate phases for transformation of Pb(II) to Pb(IV) phases, prior studies have not addressed the effects of water quality on the solid phase transformations of Pb_3O_4 or reported solubility values under typical drinking water conditions.

2.7 Analytical methods for characterization of solid phase transformations in corrosion scales

2.7.1 X-ray powder diffraction

X-ray powder diffraction (XRD) has been widely used for identification of the crystalline solid phases present in lead corrosion scales obtained from DWDS. XRD can differentiate between crystalline solid phases by revealing distinctive diffraction patterns, but only if the solids are in defined crystalline structures. It has being recently acknowledged however that the surface layers in lead corrosion scales, which are in close contact with the flowing

drinking water, are mainly amorphous (Kim and Herrera 2010; Kim et al. 2011; Peng and Korshin 2011). XRD patterns are poorly resolved, and phase identification becomes difficult when the phases are amorphous. Even for well-defined crystalline phases, it may be difficult to interpret the composition of the scale based on its XRD results as diffraction peaks from different phases overlap with each other. For instance, Shock, et al. (2004; 2005) reported superposition of some characteristic XRD peaks for different solid phases. Carr and Hampson (1972) also reported a similar challenge. In addition, lattice distortions and peak broadening can also complicate XRD assignation. Theoretically XRD can differentiate between the α-PbO_2 and β-PbO_2 (Bagshaw et al. 1966), but the discrimination between the two phases can sometimes be problematic in practice. This is due to lattice distortion and small crystalline sizes of the new formed PbO_2 phase during solid phase transformation in real DWDS (Carr and Hampson 1972).

2.7.2 Infrared and Raman spectrometry

Infrared and Raman spectrometry have been widely used to characterize lead compounds in art painting (Bruni et al. 1999; Burgio and Clark 2001; Burgio et al. 2001; Aze et al. 2008a), minerals (Huang and Kerr 1960; Farrell 1977; Brooker et al. 1983; Burgio and Clark 2001), lead corrosion products in the field of lead-acid batteries (Bullock et al. 1983; Trettenhahn et al. 1993), and in atmospheric chemistry (Black et al. 1995). Only a few studies used these two forms of vibrational spectroscopy for the characterization of lead corrosion scales obtained from DWDS (Noel and Giammar 2008; Kim and Herrera 2010). Infrared and Raman spectra result from transitions between vibrational or rotational states in the chemical structure. As a consequence the peak position in the spectra can be linked to a particular vibrational transition in a specific chemical bond. Although all chemical bonds have vibrational or rotational transitions, not all of their transitions are IR active or Raman active. In some cases Raman active transitions are not infrared active, and vice versa, making the two techniques complementary. However, Raman spectra sometimes are difficult to obtain due to low scattering efficiencies, particularly for the case of highly self-absorbing samples such PbO_2.

2.7.3 Optical absorption spectroscopy

Optical absorption results from electronic transitions of outer shell electrons. For solids, electrons from the valence band transit to the conduction band when the energy of optical photons in the UV, Visible or Near Infrared (UV/Vis/NIR) region matches the band gap energy in the solid. The energy of the light absorbed provides information on the electronic structure of the solids, and so can be used to identify structure or even monitor electronic transfer processes. The optical band gap (E_g) is the energy difference (eV) between occupied states in their valence band and unoccupied states in the conduction band. It can be calculated from the UV/Vis/NIR spectra of semiconductors. Shifts on the absorption band energy can also provide insights regarding changes in the crystalline and band structure of solids (Hossein et al. 1994).

For lead-bearing semiconductors, UV/Vis/NIR spectroscopy has been widely used, particularly in the field of glasses and conductive thin films. Pure lead compounds ($PbCO_3$, $Pb_3(CO_3)_2(OH)_2$, PbO, Pb_3O_4, and PbO_2) display the UV/Visible spectra, only PbO_2 absorbs the near infrared light and shows an apparently defined NIR band in the optical spectra. It is acknowledged that this NIR band is the result of Pb^{2+} impurities in non-stoichiometric PbO_2 (section 2.5.3), resulting in the excess of electrons in the conduction band (Payne et al. 2009; Scanlon et al. 2011). Prior studies have suggested the possibility of obtaining average oxidation valence of lead in solids using the linear relationship between E_g and the Pb oxidation state in lead oxides (Keester and White 1969; Zhou et al. 2012). Only a limited number of literature data is available however for the band gap of lead oxides. Moreover, the values reported are somewhat inconsistent. E_g values for Pb_3O_4 are reported between 2.12-2.25 eV (Keester and White 1969; Zhou et al. 2012). For PbO_2, it was reported that the band gap is between 0.99-2.0 eV by Keester et al. (1969), Carr and Hampson (1972) and Lappe (1962). Scanlon et al. (2011) and Walsh et al. (2013), in contrast, reported that there is a small indirect band gap of about 0.20-0.23 eV. Surprisingly, to our knowledge there are no studies available that report the use of optical absorption to investigate lead oxide dissolution processes.

2.8 Summary

Detailed understanding of the dissolution mechanisms of lead oxides is necessary for developing effective lead corrosion control strategies in drinking water systems. Although β-PbO_2 dissolution processes have been extensively studied, most prior studies have presented short-term experiments that may not capture the slow kinetics associated with the transformations of solid phases. Furthermore, the dissolution processes of intermediate lead oxide phases such as Pb_3O_4 have not been studied under drinking water conditions. As discussed in section 2.7, prior studies have extensively used XRD to characterize solid phase transformations. In contrast, vibrational and optical spectroscopy are able to identify and evaluate changes in amorphous phases. It is, however, surprising the lack of application of these techniques for characterization of lead corrosion scales. Therefore we attempt to fill these gaps by performing long-term dissolution experiments on β-PbO_2 and Pb_3O_4, and use optical characterization techniques to identify solid phase transformations. Our approach combined with previously established methodologies reported in the literature enable us gain valuable insights into the fundamental physicochemical processes governing the dissolution of lead oxides under typical drinking water conditions.

2.9 References

Aly, S. A., M. A. Kaid and N. Z. El-Sayed (2013). "Some Optical Aspects of Thermally Evaporated Lead Oxide Thin Films." Acta Physica Polonica, A. **124**(4).

Aze, S., P. Delaporte, J. M. Vallet, V. Detalle, O. Grauby and A. Baronnet (2008a). Towards the restoration of darkened red lead containing mural paintings: A preliminary study of the β-PbO2 to Pb3O4 reversion by laser irradiation. Lasers in the Conservation of Artworks: Proceedings of the International Conference Lacona VII, Madrid, Spain, 17-21 September 2007, CRC Press.

Aze, S., J.-M. Vallet, V. Detalle, O. Grauby and A. Baronnet (2008b). "Chromatic alterations of red lead pigments in artworks: a review." Phase Transitions **81**(2-3): 145-154.

Aze, S., J.-M. Vallet, M. Pomey, A. Baronnet and O. Grauby (2007). "Red lead darkening in wall paintings: natural ageing of experimental wall paintings versus artificial ageing tests." European Journal of Mineralogy **19**(6): 883-890.

Bagshaw, N. E., R. L. Clarke and B. Halliwell (1966). "The preparation of lead dioxide for X-ray diffraction studies." Journal of Applied Chemistry **16**(6): 180-184.

Black, L., G. C. Allen and P. C. Frost (1995). "Quantification of Raman spectra for the primary atmospheric corrosion products of lead." Applied spectroscopy **49**(9): 1299-1304.

Brokbartold, M., E. J. M. Temminghoff, L. P. Weng and B. Marschner (2013). "Unique Characteristics of Pb in Soil Contaminated by Red Lead Anti-Corrosion Paint." Soil and Sediment Contamination: An International Journal(just-accepted).

Brooker, M. H., S. Sunder, P. Taylor and V. J. Lopata (1983). "Infrared and Raman spectra and X-ray diffraction studies of solid lead (II) carbonates." Canadian Journal of Chemistry **61**(3): 494-502.

Bruni, S., F. Cariati, F. Casadio and L. Toniolo (1999). "Identification of pigments on a XV century illuminated parchment by Raman and FTIR microspectroscopies." Spectrochimica Acta Part A: Molecular and Biomolecular Spectroscopy **55**(7): 1371-1377.

Bullock, K. R., G. M. Trischan and R. G. Burrow (1983). "Photoelectrochemical and microprobe laser Raman studies of lead corrosion in sulfuric acid." Journal of The Electrochemical Society **130**(6): 1283-1289.

Burgio, L. and R. J. Clark (2001). "Library of FT-Raman spectra of pigments, minerals, pigment media and varnishes, and supplement to existing library of Raman spectra of pigments with visible excitation." Spectrochimica Acta Part A: Molecular and Biomolecular Spectroscopy **57**(7): 1491-1521.

Burgio, L., R. J. Clark and S. Firth (2001). "Raman spectroscopy as a means for the identification of plattnerite (PbO2), of lead pigments and of their degradation products." Analyst **126**(2): 222-227.

Carr, J. P. and N. A. Hampson (1972). "Lead dioxide electrode." Chemical Reviews **72**(6): 679-703.

COEH (2005). "Lead exposure in children: prevention, detection, and management." Pediatrics **116**(4): 1036.

Dan, A. C., J. H. C. Robin, L. J. M. and O. Marianne (1996). "Studies on the thermal decomposition of basic lead (II) carbonate by Fourier-transform Raman spectroscopy, X-ray diffraction and thermal analysis." Journal of the Chemical Society, Dalton Transactions(18): 3639-3645.

Dickens, B. (1965). "The bonding in Pb3O4 and structural principles in stoichiometric lead oxides." Journal of Inorganic and Nuclear Chemistry **27**(7): 1509-1515.

Dinnebier, R. E., S. Carlson, M. Hanfland and M. Jansen (2003). "Bulk moduli and high-pressure crystal structures of minium, Pb_3O_4, determined by X-ray powder diffraction." American Mineralogist **88**(7): 996-1002.

Edwards, M. and A. Dudi (2004). "Role of chlorine and chloramine in corrosion of lead-bearing plumbing materials." Journal of the American Water Works Association **96**(10): 69-81.

Farrell, D. M. (1977). "Infrared investigation of basic double-carbonate hydrate minerals." The Canadian Mineralogist **15**(3): 408-413.

Fraser, D. A. and L. T. Fairhall (1959). "Laboratory study of the solubility of red lead paint in water." Public Health Reports **74**(6): 501.

Glasstone, S. (1922). "CLXXII.—Physical chemistry of the oxides of lead. Part IV. Red lead and lead sesquioxide." Journal of the Chemical Society, Transactions **121**: 1456-1469.

Gross, S. T. (1943). "The crystal structure of Pb_3O_4." Journal of the American Chemical Society **65**(6): 1107-1110.

Health.Canada. (2007). Fact Sheet-Minimizing Exposure to Lead from Drinking Water Distribution Systems. Health Canada. Available: http://www.hc-sc.gc.ca/ewh-semt/pubs/water-eau/lead-plomb-eng.php. Last accessed 15th January 2014.

Health.Canada. (2012). Guidelines for Canadian Drinking Water Quality - Summary Table. Available: http://www.hc-sc.gc.ca/ewh-semt/pubs/water-eau/2012-sum_guide-res_recom/index-eng.php#t2. Last accessed 15th January 2014.

Health.Canada (2013). Final Human Health State of the Science Report on Lead. H. Canada. Ottawa, Ontario, the Minister of Health.

Hossein, A. A., C. A. Hogarth and J. Beynon (1994). "Optical absorption in CeO_2-V_2O_5 evaporated thin films." Journal of Materials Science Letters **13**(15): 1144-1145.

Huang, C. K. and P. F. Kerr (1960). "Infrared study of the carbonate minerals."

Kang, Z. C., L. Machesky, H. A. Eick and L. Eyring (1988). "The solvolytic disproportionation of mixed-valence compounds: III. Pb_3O_4." Journal of Solid State Chemistry **75**(1): 52-59.

Keester, K. L. and W. B. White (1969). "Electronic spectra of the oxides of lead and of some ternary lead oxide compounds." Materials Research Bulletin **4**(10): 757-764.

Kim, E. J. and J. E. Herrera (2010). "Characteristics of lead corrosion scales formed during drinking water distribution and their potential influence on the release of lead and other contaminants." Environmental Science and Technology **44**(16): 6054-6061.

Kim, E. J., J. E. Herrera, D. Huggins, J. Braam and S. Koshowski (2011). "Effect of pH on the concentrations of lead and trace contaminants in drinking water: A combined batch, pipe loop and sentinel home study." Water Research **45**(9): 2763-2774.

Lappe, F. (1962). "Some physical properties of sputtered PbO_2 films." Journal of Physics and Chemistry of Solids **23**(11): 1563-1566.

Le Bellac, D., J. M. Kiat and P. Garnier (1995). "Electronic Lone Pair Localization and Electrostatic Energy Calculations: Application to α-PbO, SnO, Pb1-x (TiO)xO, Pb_3O_4, Pb3 $(V,P)_2O_8$, and a BiSrCaCuO-Type Superconductor." Journal of Solid State Chemistry **114**(2): 459-468.

Li, X. H., D. Pletcher and F. C. Walsh (2011). "Electrodeposited lead dioxide coatings." Chemical Society Reviews **40**(7): 3879-3894.

Lin, Y.-P. and R. L. Valentine (2008a). "Release of Pb (II) from monochloramine-mediated reduction of lead oxide (PbO2)." Environmental Science and Technology **42**(24): 9137-9143.

Lin, Y. and R. L. Valentine (2008b). "The release of lead from the reduction of lead oxide (PbO2) by natural organic matter." Environmental Science and Technology **42**(3): 760-765.

Lin, Y. and R. L. Valentine (2009). "Reduction of Lead Oxide (PbO2) and Release of Pb(II) in Mixtures of Natural Organic Matter, Free Chlorine and Monochloramine." Environmental Science and Technology.

Liu, H., G. V. Korshin and J. F. Ferguson (2008). "Investigation of the kinetics and mechanisms of the oxidation of cerussite and hydrocerussite by chlorine." Environmental Science and Technology **42**(9): 3241-3247.

Liu, H., G. V. Korshin and J. F. Ferguson (2009). "Interactions of Pb (II)/Pb (IV) solid phases with chlorine and their effects on lead release." Environmental Science and Technology **43**(9): 3278-3284.

Lytle, D. A. and M. R. Schock (2005). "Formation of Pb (IV) oxides in chlorinated water." Journal of the American Water Works Association **97**(11): 102-114.

Lytle, D. A., C. White, M. N. Nadagouda and A. Worrall (2009). "Crystal and morphological phase transformation of Pb (II) to Pb (IV) in chlorinated water." Journal of Hazardous Materials **165**(1): 1234-1238.

McKinley, J. P., M. K. Dlaska and R. Batson (2002). "Red lead: understanding red lead in lead− acid batteries." Journal of Power Sources **107**(2): 180-186.

Mindt, W. (1969). "Electrical properties of electrodeposited PbO2 films." Journal of the Electrochemical Society **116**(8): 1076-1080.

Noel, J. D. and D. E. Giammar (2008). Influence of water chemistry on dissolution rates of lead(II) carbonate solids found in water distribution systems. Water Quality Technology Conference Proceedings, American Water Works Association.

NTP. (2012). NTP Monograph-Health effects of low-level lead. National Toxicology Program-U.S. Department of Health and Human Services. Available: http://ntp.niehs.nih.gov/?objectid=4F04B8EA-B187-9EF2-9F9413C68E76458E. Last accessed 15th January 2014.

Pavlov, D. (2011). Lead-acid batteries: science and technology: science and technology, Elsevier.

Payne, D. J., G. Paolicelli, F. Offi, G. Panaccione, P. Lacovig, G. Beamson, A. Fondacaro, G. Monaco, G. Vanko and R. G. Egdell (2009). "A study of core and valence levels in β-PbO_2 by hard X-ray photoemission." Journal of Electron Spectroscopy and Related Phenomena **169**(1): 26-34.

Peng, C. and G. V. Korshin (2011). "Speciation of trace inorganic contaminants in corrosion scales and deposits formed in drinking water distribution systems." Water Research **45**(17): 5553-5563.

Petersson, I., E. Ahlberg and B. Berghult (1998). "Parameters influencing the ratio between electrochemically formed α-and β-PbO_2." Journal of Power Sources **76**(1): 98-105.

Pourbaix, M. (1974). "Atlas of electrochemical equilibria in aqueous solutions."

Powell, K. J., P. L. Brown, R. H. Byrne, T. Gajda, G. Hefter, A. K. Leuz, S. Sjöberg and H. Wanner (2009). "Chemical speciation of environmentally significant metals with inorganic ligands. Part 3: The Pb^{2+}+OH^{-}, Cl^{-}, CO_3^{2-}, SO_4^{2-}, and PO_4^{3-}systems (IUPAC Technical Report)." Pure and Applied Chemistry **81**(12): 2425-2476.

Rüetschi, P. (1992). "Influence of crystal structure and interparticle contact on the capacity of PbO2 electrodes." Journal of the Electrochemical Society **139**(5): 1347-1351.

Salagram, M., V. Krishna Prasad and K. Subrahmanyam (2002). "Optical band gap studies on xPb_3O_4–$(1-x)$ P_2O_5 lead [(II, IV)] phosphate glasses." Optical Materials **18**(4): 367-372.

Scanlon, D. O., A. B. Kehoe, G. W. Watson, M. O. Jones, W. I. F. David, D. J. Payne, R. G. Egdell, P. P. Edwards and A. Walsh (2011). "Nature of the Band Gap and Origin of the Conductivity of PbO_2 Revealed by Theory and Experiment." Physical Review Letters **107**(24): 246402.

Schock, M. R. (1980). "Response of lead solubility to dissolved carbonate in drinking water." Journal of the American Water Works Association **72**(12).

Schock, M. R. and M. C. Gardels (1983). "Plumbsolvency reduction by high pH and low carbonate solubility relationship." Journal of the American Water Works Association **75**(2): 87-91.

Schock, M. R. and R. Giani (2004). Oxidant/disinfectant chemistry and impacts on lead corrosion. Proceedings of 2004 American Water Works Association Water Quality and Technology Conference.

Schock, M. R., S. M. Harmon, J. Swertfeger and R. Lohmann (2001). "Tetravalent lead: a hitherto unrecognized control of tap water lead contamination." Proceedings AWWA Water Quality Technology Conference, Nashville: 11-15.

Schock, M. R., K. Scheckel, M. DeSantis and T. L. Gerke (2005). Mode of occurrence, treatment, and monitoring significance of tetravalent lead. Proceedings AWWA Water Quality Technology Conference. Quebec City, Quebec.

Schock, M. R., I. Wagner and R. Oliphant (1996a). The corrosion and solubility of lead in drinking water. Internal corrosion of water distribution systems. Denver, CO., AWWA Research Foundation/TZW**:** 131-230.

Schock, M. R., I. Wagner and R. J. Oliphant (1996b). The corrosion and solubility of lead in drinking water. Internal corrosion of water distribution systems. **2:** 131-230.

Switzer, J. A., V. V. Rajasekharan, S. Boonsalee, E. A. Kulp and E. W. Bohannan (2006). "Evidence that monochloramine disinfectant could lead to elevated Pb levels in drinking water." Environmental Science and Technology **40**(10): 3384-3387.

Terpstra, H. J., R. A. De Groot and C. Haas (1997). "The electronic structure of the mixed valence compound Pb_3O_4." Journal of Physics and Chemistry of Solids **58**(4): 561-566.

Trettenhahn, G. L. J., G. E. Nauer and A. Neckel (1993). "Vibrational spectroscopy on the PbO-$PbSO_4$ system and some related compounds: Part 1. Fundamentals, infrared and Raman spectroscopy." Vibrational spectroscopy **5**(1): 85-100.

Vigouroux, J. P., E. Husson, G. Calvarin and N. Q. Dao (1982). "Etude par spectroscopié vibrationnelle des oxydes Pb3O4, SnPb2O4 et SnPb(Pb2O4)2." Spectrochimica Acta Part A: Molecular Spectroscopy **38**(4): 393-398.

Wang, Y., Y. Xie, W. Li, Z. Wang and D. E. Giammar (2010). "Formation of lead (IV) oxides from lead (II) compounds." Environmental Science and Technology **44**(23): 8950-8956.

White, W. B., F. Dachille and R. Roy (1961). "High-Pressure-High-Temperature Polymorphism of the Oxides of Lead." Journal of the American Ceramic Society **44**(4): 170-174.

Wu, T., G. M. Buck and P. Mendola (2003). "Blood lead levels and sexual maturation in US girls: the Third National Health and Nutrition Examination Survey, 1988-1994." Environmental Health Perspectives **111**(5): 737.

Xie, Y., Y. Wang and D. E. Giammar (2010a). "Impact of chlorine disinfectants on dissolution of the lead corrosion product PbO2." Environmental Science and Technology **44**(18): 7082-7088.

Xie, Y., Y. Wang, V. Singhal and D. E. Giammar (2010b). "Effects of pH and carbonate concentration on dissolution rates of the lead corrosion product PbO2." Environmental Science and Technology **44**(3): 1093-1099.

Xie, Y. J. and D. E. Giammar (2011). "Effects of flow and water chemistry on lead release rates from pipe scales." Water Research **45**(19): 6525-6534.

Zhou, Y., J. Long, Q. Gu, H. Lin, H. Lin and X. Wang (2012). "Photoinduced Reactions between Pb_3O_4 and Organic Dyes in Aqueous Solution under Visible Light." Inorganic chemistry **51**(23): 12594-12596.

Chapter 3

3 Methodology

This chapter presents the materials and methods used for experimental work and data analysis. This includes details of the experimental setups, sampling methods and analytical tools. The methodology for spectra analysis and chemical parameter calculations are described as well.

3.1 Lead oxide dissolution experiments

3.1.1 Materials

Plattnerite (β-PbO_2) (Sigma-Aldrich, A.C.S reagent grade) and Minium (Pb_3O_4) (Alfa Aesar, 97%, metals basis) were used without further purification for the dissolution experiments. The average particle size of Pb_3O_4 is 10.4 μm and that of β-PbO_2 is 27.1 μm as determined via laser diffraction particle sizing technique (Mastersizer 2000). NaOCl (Fisher Scientific, 5.65-6% w/w, laboratory grade) was used as the source of free chlorine. $NaNO_3$ (Sigma-Aldrich, ≥ 99.0%) and $NaHCO_3$ (Sigma-Aldrich, ≥ 99.5%) were used to prepare a stock solution with 0.01 M ionic strength and 20 mg/L dissolved inorganic carbon (DIC), respectively. NaOH (Pellets, Sigma-Aldrich, A.C.S reagent grade) and 67-70% v/v condensed HNO_3 (EMD Milipore, Omnitrace) were used to prepare 0.1 M NaOH and 0.1 M HNO_3 solutions, respectively. All solutions were prepared using mega-pure water and A.C.S reagent grade chemicals except for the NaOCl solution.

3.1.2 Methods

3.1.2.1 Experimental methodology for the dissolution experiments

Three different sets of batch experiments were carried out. The first set, labeled "Test 1" was designed to evaluate the equilibrium solubilities of β-PbO_2 (Plattnerite: P) and Pb_3O_4 (Minium: M). Three distinct experiments were performed at different nominal initial free chlorine concentrations (A~2.5 mg/L, B~5 mg/L and C~6 mg/L) for each solid lead oxide phase. For instance, 1MA refers to Test 1 of Pb_3O_4 dissolution experiment with a nominal initial free chlorine concentration of 2.5 mg/L. The second set, labeled Test 2 was designed

to evaluate the lead release profile of β-PbO_2 and Pb_3O_4 with two different nominal initial chlorine concentrations (A~2.5 mg/L and B~5 mg/L). Two experiments (2MA and 2MB) were conducted for Pb_3O_4, while 2PA and 2PB were conducted for β-PbO_2. Test 1 and Test 2 were performed in 25 ml high density polyethylene vials (Wheaton) at a concentration of 0.88 g/L of pure solid phase. Triplicate samples were prepared for both Tests. Tables 3.1 summarizes the details for Tests 1 and 2. Test 3 was conducted to examine the solid phase transformations taking place over the course of the dissolution experiments. This test was performed using 300 ml high density polyethylene bottles (Nalgene) loaded with 0.88 g/L to collect sufficient quantity of solid sample for solid phase characterization. In Test 3, 3MA and 3MB were performed for Pb_3O_4, as well as 3PA and 3PB for β-PbO_2 (A~2.5 mg/L and B~5 mg/L). Experiments were run in duplicates or triplicates. The details of the experimental conditions for Test 3 are provided in Tables 3.2. Tests 2 and 3 were conducted simultaneously.

Table 3.1 Summary of experiments conditions for Test 1 and Test 2

Experiment	Initial solid phase	Free chlorine (mg/L as Cl2)	Elapsed time (days)	pH	DIC (mg C/L)
1MA	Pb_3O_4	2.35	200	7.93	20
1MB	Pb_3O_4	5.13	200	8.12	20
1MC	Pb_3O_4	6.16	200	7.94	20
2MA	Pb_3O_4	2.51	200	8.00	20
2MB	Pb_3O_4	4.85	200	7.96	20
1PA	β-PbO_2	2.35	330	7.93	20
1PB	β-PbO_2	5.13	336	8.12	20
1PC	β-PbO_2	6.16	330	7.94	20
2PA	β-PbO_2	2.51	200	8.00	20
2PB	β-PbO_2	4.85	200	7.96	20

Table 3.2 Summary of experiments conditions for Test 3

Experiment	Initial solid phase	Free chlorine (mg/L as Cl2)	Sampling times (days)	pH	DIC (mg C/L)
3MA	Pb_3O_4	2.51	0, 10, 30, 60, 90, 200	8.00	20
3MB	Pb_3O_4	4.85	0, 1, 10, 30, 60, 90, 120, 200	7.96	20
CM	Pb_3O_4	0	0, 10, 30, 60	8.01	20
3PA	β-PbO_2	2.51	0, 10, 30, 60, 90, 200	8.00	20
3PB	β-PbO_2	4.85	0, 1, 10, 30, 60, 90, 120, 200	7.96	20
CP	β-PbO_2	0	0, 10, 30, 60	8.01	20

All experiments were carried out in a closed system configuration with vials completely filled with the stock solution (0.01 M ionic strength, 20 mg C/L DIC, and target initial free chlorine concentrations at an initial pH value close to 8 (unbuffered)) to avoid carbonate exchange with air. Control tests were performed as well under the same conditions as Test 3 but in the absence of free chlorine. All experiments performed for this thesis were conducted at room temperature (21±2 °C). It should be noted however that temperature varies seasonally in DWDS, and that temperature is a significant factor affecting the stability and dissolution of lead corrosion scales. However, the effect of temperature on the stability of lead oxides is beyond the scope of this thesis.

3.1.2.2 Set up of Test 1 and Test 2

The required amount of $NaNO_3$ and $NaHCO_3$ was dissolved in a 20 L polyethylene container (Nalgene) containing 17 L of mega-pure water to prepare a stock solution of 0.01 M $NaNO_3$ and 20 mg C/L $NaHCO_3$. A 0.06% v/v solution of NaOCl was prepared from 6% NaOCl solution, and was dosed into the stock solution containing the $NaNO_3$ and $NaHCO_3$ described above to get the targeted initial free chlorine concentration for each experiment. pH then was measured and adjusted to 8 initially by adding 0.1 M NaOH or 0.1M HNO_3 to the chlorinated stock solution. Free chlorine was measured again with the value recorded as initial free chlorine concentration. Each 25ml vial was first loaded with approximately 20 mg of solid. Then the chlorinated stock solution was poured into each vial to achieve a 0.88 g/L solid concentration. The total solution volume in the vial was 25ml (no headspace). All vials were put in a sealed dark box to avoid light-induced degradation of free chlorine. The box was placed on a mixing shaker and the vials were continuously mixed (Thermo Scientific, MAXQ 2000) at 170 rpm. A total of 180 vials were prepared for Test 1, and 120 vials for Test 2.

3.1.2.3 Set up of Test 3 and control tests

The chlorinated stock solution was prepared following the same procedure described for Tests 1 and 2. Each 300 ml bottle reactor was loaded first with 0.26g of solid. The chlorinated stock solution was poured into each bottle (0.88 g/L final solid concentration). The total volume in the bottle was 300ml (no headspace). All bottles were placed in a

sealed dark box and were continuously mixed on a shaker at 170 rpm. 15 bottles were prepared for Pb_3O_4 and 15 for PbO_2.

For control tests, an 8 L stock solution was prepared following the same procedure described for Tests 1 and 2 but without free chlorine. Experimental set-up procedure is the same as Test 3. 10 bottles were prepared for Pb_3O_4 and 10 for PbO_2.

3.1.3 Sampling procedure

For Test 1 and Test 2, three sacrificial samples were collected regularly for each time series data point. Samples were filtered using a 0.22 μm polyethersulfone (PES) filter (VWR). For each sample, the first few drops of the filtrate were discarded. A volume of 10 ml filtrate was used for free chlorine measurements. A second 10 ml aliquot was transferred to a high density polyethylene vial for ORP and pH measurements. After pH and ORP values were obtained, 1 ml of 20% nitric acid was added to the vial. The samples were stored for at least 24 hr before sampled were analyzed for dissolved lead.

For Test 3, 25 ml aqueous sample was collected as the same manner described for Tests 1 and 2. To measure alkalinity an additional 150 ml aliquot was withdrawn into a 150 ml polyethylene bottle without headspace. The remaining sample containing most of the solid phase was transferred into 50 ml centrifuge tube (Nalgene) and was centrifuged at 8000 rpm for 15 minutes (Sorvall, RC-5B). After removing the supernatant the solid samples were dried and stored in a vacuumed desiccator. This same sampling procedure was used for the control tests, with the exception of the measurement of free chlorine.

3.1.4 Analytical methods

Dissolved lead concentrations were determined via inductively coupled plasma optical emission spectrometry (ICP-OES) (Varian, Inc., Vista-Pro Axial). Five standards (0, 0.01, 0.04, 0.4, 4 mg/L of Pb) were prepared using a certified ICP standard solution (Fluka, multielement standard solution 4, Pb 40 mg/L) and mega-pure water. The pH value was measured with a non-glass ISFET probe and pH meter (Hach, H160). ORP was measured via pH meter with a glass ORP probe. The concentration of free chlorine was measured using the standard DPD colorimetric method (Method 10069, Hach) in an UV/Vis

spectrophotometer (Hach, DR5000). Alkalinity values were obtained by titration using 0.1 N HCl (Mocron, 0.1N standard).

3.2 Methodology of spectroscopic characterization

Solid samples were characterized by Infrared and UV/Vis/NIR spectroscopy using a Fourier Transform Infrared Spectrometer (VERTEX 70) equipped with a diffuse reflectance spectroscopy cell (Harrick-Praying Mantis) and a UV-3600 SHIMADZU equipped with a Praying Mantis as well. Raman spectra on the solid samples were obtained in a Jovin Yvon-Horiba LabRam 800 (air-cooled CCD detector) with a He–Ne laser (632.8 nm) tuned at 610 uW to avoid sample decomposition. X-ray powder diffraction was also used to analyze the solid samples. The XRD patterns for aging solid samples collected from Pb_3O_4 and β-PbO_2 dissolution experiments and the control tests were obtained using Co K-α (λ=1.78890 Å) radiation over the range of 10-70° 2θ with a 0.02° step size. The XRD results were illustrated as used Cu K- α (λ=1.54059 Å) radiation.

Infrared spectra were measured in the mid-range (450-4000 cm^{-1}) in diffuse reflectance mode at a 4 cm^{-1} resolution and 64 scans per sample. The diffuse reflection spectra were transformed to pseudo-absorption using the Kubelka-Muck function by OPUS® software. UV/Vis/NIR spectra of aging samples were also obtained in diffuse reflectance mode over the range from 200 nm to 1400 nm with 1 nm step size using the highest resolution setting in the instrument. For each data point a minimum of two spectra were obtained. The absorption spectra of aging samples from experiments 3MA and 3MB were normalized and then averaged for each time data point. For experiments 3PA and 3PB, the absorption spectra were not normalized and only averaged for each data point. Obtained Raman spectra were corrected to the silicon phonon at 520 cm^{-1} and the Rayleigh peak. Integration times for the Raman spectra were around 12 seconds for each spectrum; 10 Raman spectra were averaged for each sample at 3 scans per spectra over the range of 50 to 1200 cm^{-1}.

3.3 Methodology of calculation of total carbonates

The total dissolved carbonates in the 150 mL aqueous phase sample was calculated for experiments 3MA, 3MB, 3PA, and 3PB based on the obtained pH values and alkalinity

results. The relationship between alkalinity (Alk.), pH, and total carbonates (C_T) is shown below:

$$Alk. = [\mathrm{HCO_3^-}] + 2[\mathrm{CO_3^{2-}}] + [\mathrm{OH^-}] - [\mathrm{H^+}]$$
$$= \left[\left(1\frac{eq}{mol}\right) * \alpha_1 + \left(2\frac{eq}{mol}\right) * \alpha_2\right] * C_T + \left(1\frac{eq}{mol}\right) * [\mathrm{OH^-}] - \left(1\frac{eq}{mol}\right) * [\mathrm{H^+}] \quad (1)$$

Where α_1 and α_2 represent the fraction of bicarbonate and carbonate ions in solution, respectively. They are calculated according to the equations below.

$$\alpha_1 = K_{a1} * [\mathrm{H^+}]/([\mathrm{H^+}]^2 + K_{a1}[\mathrm{H^+}] + K_{a1} * K_{a2}) \quad (2)$$

$$\alpha_2 = K_{a1} * K_{a2}/([\mathrm{H^+}]^2 + K_{a1}[\mathrm{H^+}] + K_{a1} * K_{a2}) \quad (3)$$

Where $K_{a1}=10^{-6.33}$ and $K_{a2}=10^{-10.33}$ are the acid dissociation constants of H_2CO_3 at 25°C.

For each data point, the average pH value was determined based on the measured duplicate or triplicate results. The α_1 and α_2 values were calculated using Eq. 2 and 3, then the results and obtained experimental total alkalinity were substituted into Eq. 1 to finally obtain the total concentration of carbonate species in solution for each data point.

3.4 Methodology of Calculation of first-order apparent kinetics for pH change

To understand the change of pH levels during the dissolution of Pb_3O_4, a standard first-order kinetic model was used. The first-order consumption of hydronium ion is thus described as:

$$-\frac{d[H^+]}{dt} = k[H^+] \quad (4)$$

The integrated first-order rate is

$$-ln[H^+] = k * t - ln[H_0^+]$$

$$-log[H^+] = loge * k * t - log[H_0^+]$$

$$pH = 0.4342\ k * t + pH_0 \quad (5)$$

Where pH is a measured value at each specific time data point, pH_0 is the initial pH value, k is the first order kinetic constant (day^{-1}), t is the time.

For each set of experiments, the initial pH_0 value, sampling time, and measured pH values were linearized to calculate the kinetic constant using Eq. 5.

Chapter 4

4 Dissolution of minium (Pb_3O_4) in water under depleting chlorine conditions

4.1 Introduction

Elevated lead levels are observed in the drinking water of many municipalities due to lead-bearing plumbing materials in DWDS. High lead levels pose a threat to human health. Health Canada's Maximum Acceptable Concentration (MAC) for lead in drinking water is 10 µg/L (Health.Canada 2012). This guideline value is slightly stricter than in the U.S. where the action level for lead in drinking water is 15 µg/L according to the lead and copper rule (U.S.EPA 1991). High soluble lead levels in drinking water are caused by the dissolution of corrosion scales that have built-up on lead-bearing plumbing. In the past, free chlorine was often used as the disinfectant for drinking water treatment with residual chlorine creating oxidizing conditions in a distribution system. At least 0.05 mg/L free chorine residual needs to be present in drinking water distribution systems as regulated by Ontario's Reg. 170/03. The composition of the lead corrosion scales in distribution systems exposed to these conditions typically consists of lead(II) carbonates and lead(II and IV) oxides (Schock et al. 1996; Schock et al. 2001; Kim and Herrera 2010). The corrosion scale composition may be more complex in systems where additives such as phosphate and silicate have been added in the water treatment process (Grimes et al. 1995; Hozalski et al. 2005; Schock et al. 2005). Mixed valent oxide Pb_3O_4 was found in corrosion scale samples obtained from the City of London (Kim and Herrera 2010). Pb_3O_4 is hypothesized to be an intermediate solid phase formed during the oxidation from Pb(II) to Pb(IV) phases.

It is widely acknowledged that the stability of lead corrosion scales in DWDS is significantly influenced by the water chemistry, particularly the redox conditions. A decrease in oxidation-reduction potential (ORP), for example, sudden depletion of residual chlorine in DWDS or a switch in disinfectant type in drinking water treatment, can trigger reactions that destabilize the corrosion scale and cause long-term solid phase transformations (Lytle and Schock 2005; Lin and Valentine 2009; Liu et al. 2009; Wang et al. 2012). Specifically, transformations between Pb(II) and Pb(IV) solid phases have

been shown to strongly affect the stability of corrosion scales present in lead-bearing plumbing. While significant research has focused on investigating the stability of Pb(IV) (β-PbO_2) and Pb(II) (lead carbonates) solid phases, few studies reported their solubilities under decreasing ORP conditions. In addition, little is known regarding the stability of mixed valence lead solids such as Pb_3O_4. As these mixed valence lead solids may act as intermediate products during the transformation between Pb(II) and Pb(IV) solid phases, identifying the mechanisms by which these solids dissolve is essential for understanding the factors that regulate lead concentrations in drinking water (Mosseri et al. 1990; Kim and Herrera 2010; Liu et al. 2012).

To investigate the effect of decreasing ORP, in this chapter we investigate the dissolution of Pb_3O_4 under depleting chlorine conditions via batch experiments conducted with pure phase Pb_3O_4. The effect of the initial free chlorine concentrations was examined as this variable impacts the initial redox conditions and thus the Pb(II)/Pb(IV) redox couple. In addition to analyzing the aqueous chemistry, the composition of the aging of the solid phase was determined using spectroscopic characterization techniques. The solid phase transformations observed provide valuable insight into the dissolution mechanism of Pb_3O_4.

4.2 Results and discussion

4.2.1 Influence of free chlorine on lead release profile and equilibrium lead concentrations

As described in the methodology chapter (Chapter 3), Test 1 was conducted to evaluate equilibrium dissolved lead concentrations resulting from pure phase Pb_3O_4 present with different initial free chlorine concentrations. Table 4.1 shows the equilibrium concentrations observed for experiments 1MA (initial nominal free chlorine concentration of 2.5 mg Cl_2/L), 1MB (5.0 mg Cl_2/L), and 1MC (6.0 mg Cl_2/L). The free chlorine depletion, pH, and ORP profiles for these experiments are shown in Appendix A (Figures S.A.1 and S.A.2). Despite the different initial chlorine concentrations, the final equilibrium lead concentrations for these experiments were similar (~0.1 mg/L after 200 days, Table 4.1).

To evaluate the effect of free chlorine on the dissolution profile of Pb_3O_4, experiments 2MA (2.5 mg Cl_2/L) and 2MB (5.0 mg Cl_2/L) (Test 2) were performed under similar conditions as Test 1 (Table 4.1), but with more frequent sampling during the first three days of the experiments. The free chlorine depletion and the lead concentration profiles for experiments 2MA and 2MB are shown in Figure 4.1. Three distinct stages are evident in the Pb_3O_4 lead dissolution profiles. The time at which the transition between each stage occurred varied between the experiments as the time taken for chlorine to be consumed was different.

Table 4.1 Summary of Pb_3O_4 dissolution experimental conditions and results for Test 1 and Test 2

Experiment	Initial solid phase	Free chlorine (mg/L as Cl_2)	Elapsed time (days)	pH	DIC (mg C/L)	$[Pb]_{diss.}$ mg/L			Final pH
						10 days	100 days	200 days	
1MA		2.35	200	7.93	20	0.151	0.099	0.102	8.37
1MB		5.13	200	8.12	20	0.016	0.090	0.099	8.45
1MC	Pb_3O_4	6.16	200	7.94	20	0.045	0.087	0.084	9.16
2MA		2.51	200	8.00	20	N/A	N/A	0.096	9.02
2MB		4.85	200	7.96	20	N/A	N/A	0.095	9.11

Note: Test 1 and Test 2 experiments were conducted in 25 ml vials.

From Figure 4.1b it can be seen that the lead concentrations increased immediately at the beginning of the experiments. The initial lead concentrations were similar for all experiments (~0.17 mg/L) suggesting that they were independent of the initial free chlorine availability. The lead concentrations then decreased over 1-2 days after which time they remained stable for a few days around 0.01-0.02 mg/L. We define this period as Stage I. In this stage, the lead concentrations in experiment 2MB decreased at a faster rate compared with experiment 2MA. Dissolved lead reached a stable low concentration (~0.02 mg/L) after 4 days for experiment 2MA, in contrast to after only 2 days for experiment 2MB. The free chlorine concentrations also decreased but chlorine was not completely consumed in Stage I. It is well known that free chlorine will oxidize Pb (II) species to form PbO_2, which is a very stable lead compound with a low solubility (Edwards and Dudi 2004;

Lytle and Schock 2005). The experimental results suggest that this oxidation process dominated during Stage I with the initial availability of free chlorine concentration, and as a result high ORP, driving the Pb(II) → Pb(IV) redox transformation (Figure 4.2a).

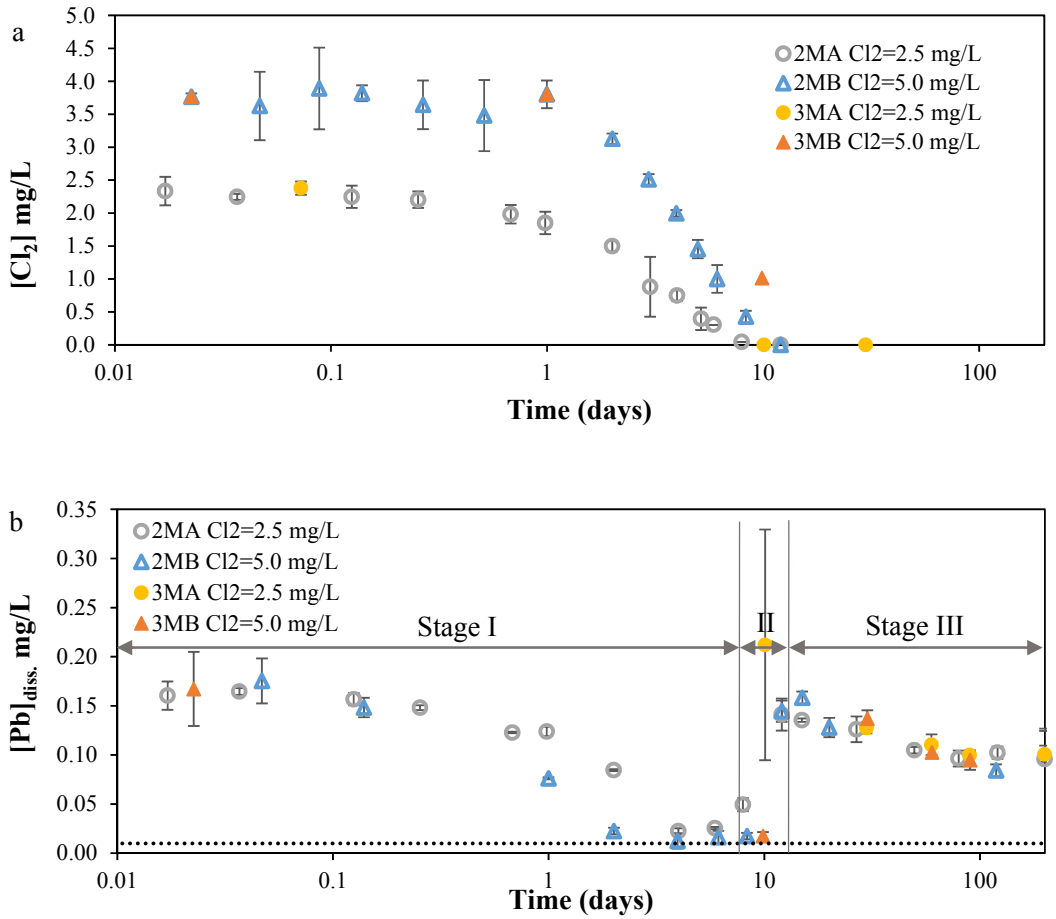

Figure 4.1 a) Chlorine and b) dissolved lead concentrations observed during Pb_3O_4 dissolution experiments at two different initial free chlorine concentrations (Tests 2 and 3). The horizontal black dotted line indicates the MAC level for lead (10 µg/L). Three stages are identified in b) for experiment 2MA.

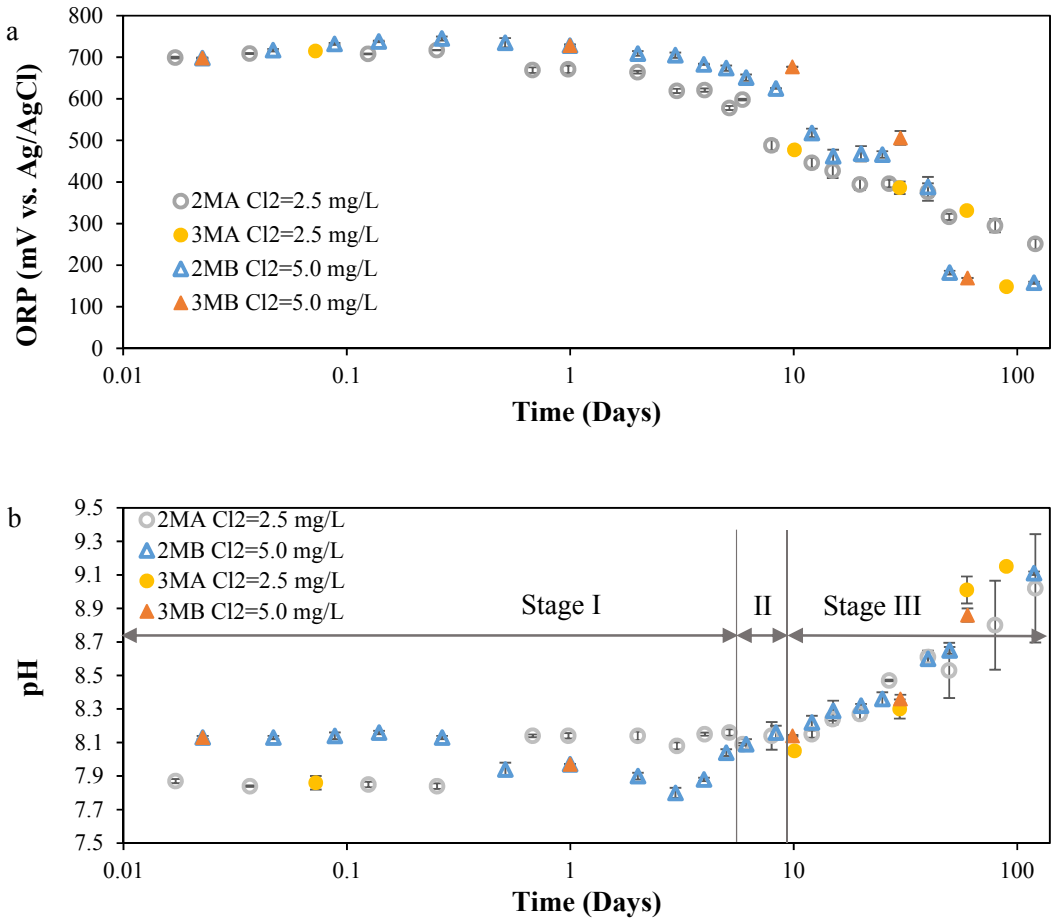

Figure 4.2 a) ORP and b) pH values obtained during Pb_3O_4 dissolution experiments at two different initial free chlorine concentrations (Tests 2 and 3). Three stages are identified in a) for experiment 2MA.

It was not until the free chlorine was completely depleted (10 days for experiment 2MA and 12 days for experiment 2MB) that the dissolved lead levels rebounded, and a sharp spike in the lead concentration was observed (Figure 4.1b). This period is defined as Stage II. Specifically, the free chlorine levels decreased below 0.3 mg/L at 6 days for experiment 2MA; this corresponds with the beginning of Stage II. At this time, the dissolved lead concentrations started to increase until a peak concentration was reached at about 12 days. This peak concentration occurred slightly later than the complete consumption of free chlorine. For experiment 2MB, the dissolved lead levels remained low until around 8 days at which time the free chlorine concentration was approximately 0.4 mg/L. As the free

chlorine depleted further, the dissolved lead levels increased and peaked at 15 days. As expected, the ORP values decreased more than 100 mV during Stage II as the free chlorine was completely consumed (Figure 4.2a).

Finally, after reaching a maximum concentration, the lead levels gradually decreased towards a final equilibrium concentration around 0.1 mg/L for both experiments 2MA and 2MB (Figure 4.1b). This final period is defined as Stage III. The ORP continued to decrease during this stage (Figure 4.2a). In contrast to Stages I and II where the pH was relatively stable, the pH values increased from about 8 to 9 during Stage III (Figure 4.2b). These changes in pH are explained below with reference to the solid phase transformations observed during Stage III (Section 4.2.3).

The final dissolved lead values in Test 2 are in agreement with the final concentrations observed in Test 1. Thus, the equilibrium lead concentrations for Pb_3O_4 is about 0.1 mg/L under depleting chlorine conditions. A slightly higher dissolved lead concentration (~0.14 mg/L) was observed for a control test conducted with Pb_3O_4 and no initial free chlorine present. Results of this control test are shown in Figure S.A.3 in Appendix A. This slight difference in equilibrium lead concentrations is discussed in Section 4.2.3. The experimental results from Test 2 indicate that the initial free chlorine concentrations affected the rate of Pb_3O_4 dissolution but did not affect the equilibrium lead concentrations. This suggests that the availability of free chlorine and associated ORP plays an important role in mechanism by which Pb_3O_4 dissolves.

4.2.2 Characterization of solid phase during Pb_3O_4 dissolution

Test 3 was carried out under similar conditions as Test 2, but for this set of experiments the solid samples were collected and analyzed in addition to the aqueous samples (Table 4.2). This enables us to identify the solid phase transformations including the effect of the initial free chlorine concentrations. The aqueous phase results for the Test 3 experiments compare well with the Test 2 experiments (Figures 4.1 and 4.2).

Table 4.2 Summary of Pb_3O_4 dissolution experimental conditions for Test 3

Experiment	Initial solid phase	Free chlorine (mg/L as Cl_2)	Sampling times (days)	pH	DIC (mg C/L)	Final pH
3MA		2.51	0, 10, 30, 60, 90, 200	8.00	20	9.5
3MB	Pb3O4	4.85	0, 1, 10, 30, 60, 90, 120, 200	7.96	20	9.67
CM		0	0, 10, 30, 60	8.01	20	8.07

Note: Test 3 experiments were conducted in 300 ml bottles.

4.2.2.1 Characterization of solid samples from Test 3

Figure 4.3 shows the FTIR spectra of the solid samples collected from experiment 3MA. It should be noted that all solid samples were collected during Stage III, except the sample collected at 0.07 days (Stage I). FTIR spectra of pure solid phase are shown in Figure S.A.4 in Appendix A. The IR spectrum of the solid sample collected and analyzed at the beginning of the experiment (0.07 days) shows identical spectral features as those observed for pure Pb_3O_4. The peak at 583 cm^{-1} is characteristic for Pb_3O_4, and attributed to the stretching of the Pb(IV)-O bond (Vigouroux et al. 1982). A small band centered at 1390 cm^{-1} is also observed. This is attributed to free adsorbed carbonates attached to the surface of Pb_3O_4 (Schrrrz and White 1977). This free carbonate band is not present in the IR spectra of the subsequent solid samples as these weakly adsorbed carbonates likely dissolved into aqueous solution. For the sample obtained at 30 days, a shoulder at 682 cm^{-1} is observed (Figure 4.3 inset). This peak is attributed to the in-plane bending of lattice carbonate ions in cerussite (Schrrrz and White 1977). The characteristic peak of cerussite is even more pronounced for the sample collected at 60 days. In addition, a shoulder at slightly higher wavenumbers (696 cm^{-1}) is present for the 60 days sample instead of a single narrow peak centered at 682 cm^{-1}. This observation suggests that a mixture of cerussite and hydrocerussite, whose characteristic peaks are at 682 and 696 cm^{-1} respectively, formed. The increase in the relative intensity of the peak at 696 cm^{-1} indicates that more hydrocerussite than cerussite was present at 90 days.

The UV/Vis spectra obtained on the same solid samples also indicate the formation of lead carbonates (Figure 4.4). It can be seen that the relative intensity of the band centered between 200 to 300nm increases rapidly over the first 10 days of the experiment. We

attribute this to the formation of cerussite and/or hydrocerussite since their main bands appear between 200 and 270nm in the UV/Vis spectra (Figure S.A.5a in the Appendix A). The formation of PbO (main band located at 297 nm, Figure S.A.5b in the Appendix A) may also have caused the observed changes in the UV/Vis spectra; this possibility is discussed further below in light of the XRD and Raman results.

Similar changes were observed in the FTIR and UV/Vis spectra of the solid samples collected from experiment 3MB (Figures 4.5 and 4.6). For this experiment three samples (0.023, 1 and 10 days) were collected during Stage I and two samples were collected during Stage III (30 and 60 days). In the FTIR spectra, the band at 1390 cm^{-1} ascribed to the free adsorbed carbonates is again observed for the samples obtained at 0.023 days and 1 day. Clear peaks at 682 and 696 cm^{-1} are observed for samples collected at 30 and 60 days. This indicates the formation of lead carbonates. In the UV/Vis spectra, the relative increase in the range of 200 to 270 nm is also observed at 10 and 30 days; this supports carbonate formation or the possible formation of PbO.

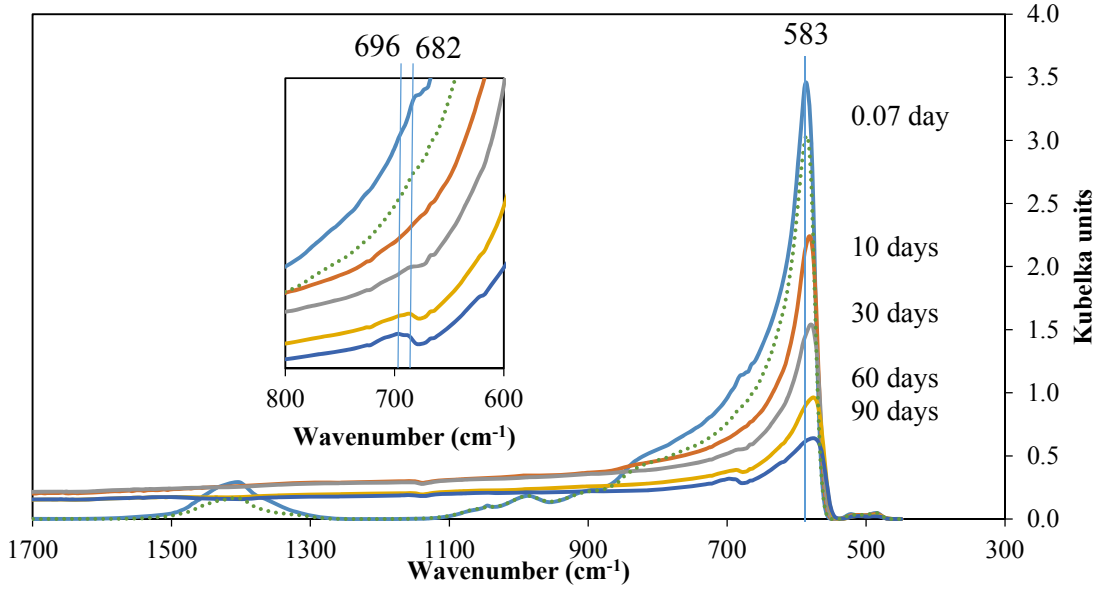

Figure 4.3 FTIR spectra obtained on solid samples collected during experiment 3MA (initial free chlorine concentration of 2.5 mg/L). The data obtained on pure phase Pb_3O_4 is also included for reference (dashed line). Inset: detail of the 550-800 cm^{-1} region.

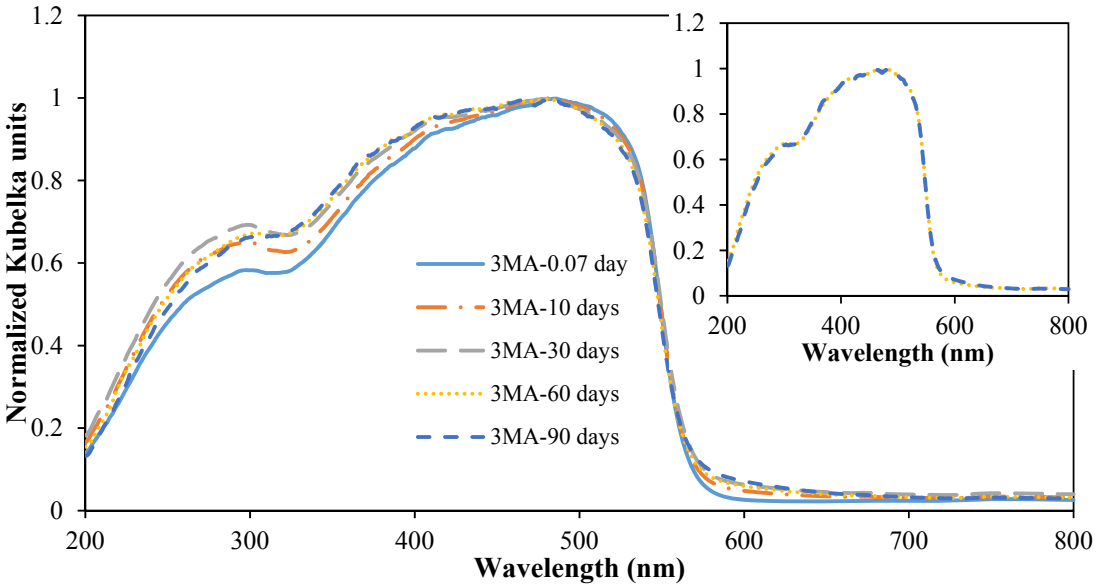

Figure 4.4 UV-Vis spectra obtained on solid samples collected during experiment 3MA (initial free chlorine concentration of 2.5 mg/L). Inset: comparison of results obtained after 60 and 90 days.

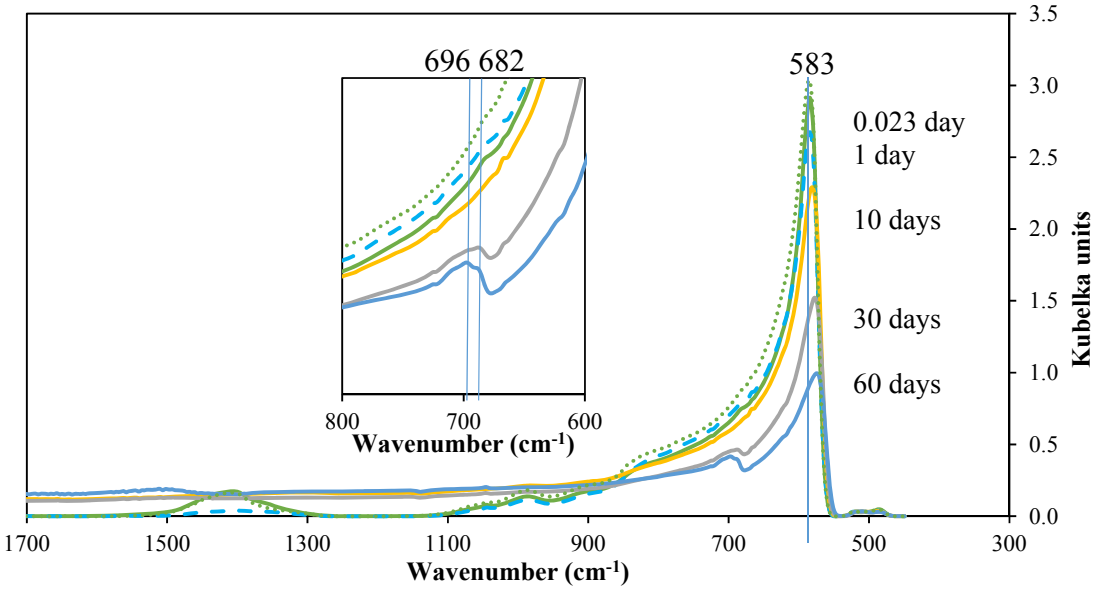

Figure 4.5 FTIR spectra obtained on solid samples collected during experiment 3MB (initial free chlorine concentration of 5.0 mg/L). The data obtained on pure phase Pb_3O_4 is included as a dashed line. Inset: detail of the 550-800 cm^{-1} region

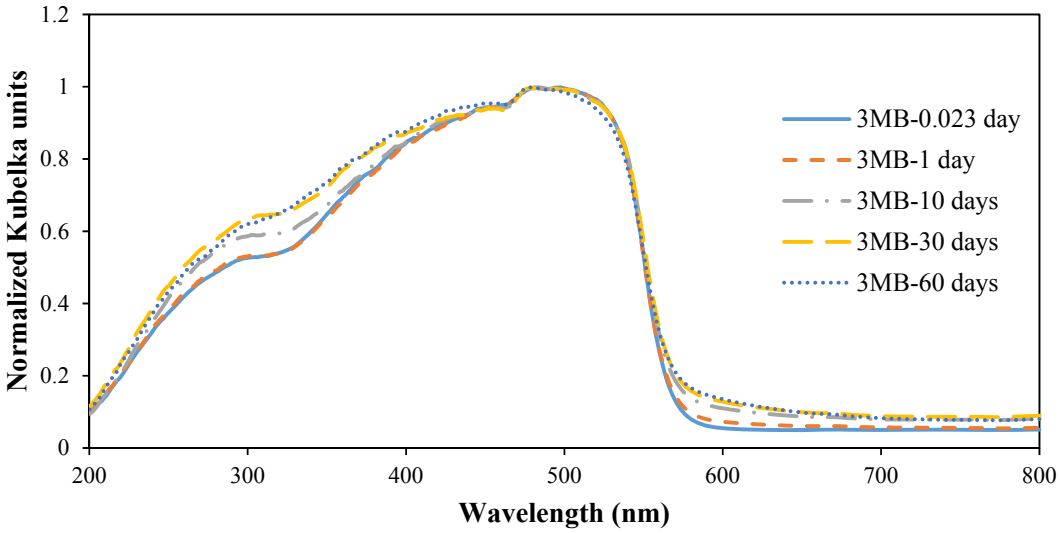

Figure 4.6 UV-Vis spectra obtained on solid samples collected during experiment 3MB (initial free chlorine concentration of 5.0 mg/L).

To further identify the solid phase transformations occurring during Pb_3O_4 dissolution, Raman spectrometry was used to characterize the samples collected from experiment 3MB. The results are shown in Figure 4.7 together with the spectra of pure Pb_3O_4 and PbO. The Raman spectra of other lead oxides and lead carbonate crystalline phases are provided in Figure S.A.6 in the Appendix A. Characteristic peaks for pure Pb_3O_4 appear at 542, 386, 307, 220, and 119 cm^{-1}, and are attributed to the vibrational modes of Pb-O bonds (Vigouroux et al. 1982; Trettenhahn et al. 1993; Dan et al. 1996). The Raman spectra of samples collected at 0.023 and 10 days show similar patterns as the spectra of Pb_3O_4. For the sample collected at 30 days, new peaks appear at 86, 139, and 283 cm^{-1}, suggesting the presence of PbO moieties. The appearance of these new peaks, and thus formation of PbO in the aging solid samples, is consistent with the UV/Vis features observed below 300nm and discussed above (Figure 4.6). However, the relative intensities of these new peaks are lower for the sample collected at 60 days, and for the 90 days sample the spectra has lost the features attributed to PbO moieties and appears similar again to the Pb_3O_4 spectra. This suggests that the concentration of the newly formed PbO species in the solid decreased over time. This disappearance of the PbO species is consistent with the UV/Vis results as the spectrum intensity in the 200 to 300 nm range for the 60 days sample is lower than for the sample collected at 30 days.

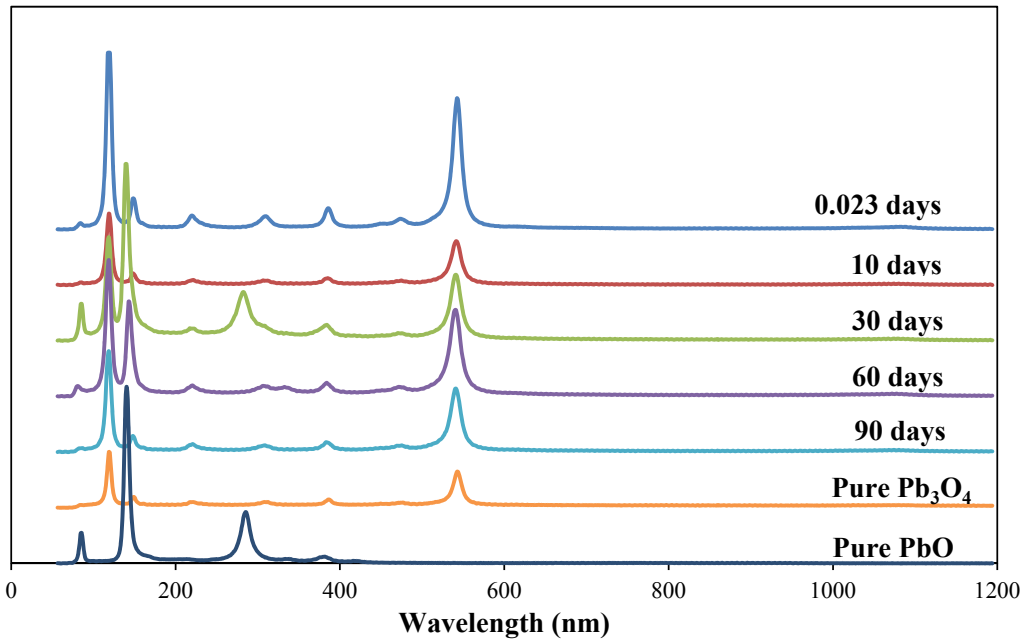

Figure 4.7 Raman spectra obtained on solid samples collected during experiment 3MB (initial free chlorine concentration of 5.0 mg/L). The spectrum obtained on pure phase Pb_3O_4 is also shown.

XRD diffractograms were obtained for the samples collected from experiments 3MB and 3MA. The results for experiment 3MB are shown in Figure 4.8 together with the diffractogram of pure Pb_3O_4, lead carbonates, PbO, and plattnerite (β-PbO_2). The diffractogram pattern of the sample collected at 10 days does not show any new peaks compared with pure Pb_3O_4. For the sample obtained at 60 days, features at 34° and 49° - characteristic of hydrocerussite – are observed. In addition, small peaks at 25° and 36° are more apparent at 60 days than at 30 days. This suggests that crystallized β-PbO_2 also formed during Stage III. The β-PbO_2 features become more apparent for the samples collected as the experiment progressed. The UV/Vis spectra (Figure 4.4 and 4.6) are consistent with the formation of β-PbO_2 through the experiments. The intensity of the tail (580 to 750 nm) increased in UV/Vis spectra over time as PbO_2 species have a broader range of absorption in the visible range (Figure S.A.5b in the Appendix A) than lower valence lead oxides. This is also consistent with our visual observations that the color of the aging solids turned darker as the dissolution experiments progressed. On the other hand, the intensity of the diffraction peak at 29° - characteristic of PbO – did not increase during the experiments. This is consistent with the fact that thermodynamically crystalline PbO is

very soluble in water. While these results indicate that crystalline PbO was not present in the solid phase, the formation of an amorphous PbO is still plausible since XRD is unable to identify amorphous phases. The formation of hydrocerussite and β-PbO_2 are also observed in the XRD diffractograms for 3MA (Figure S.A.7 in Appendix A).

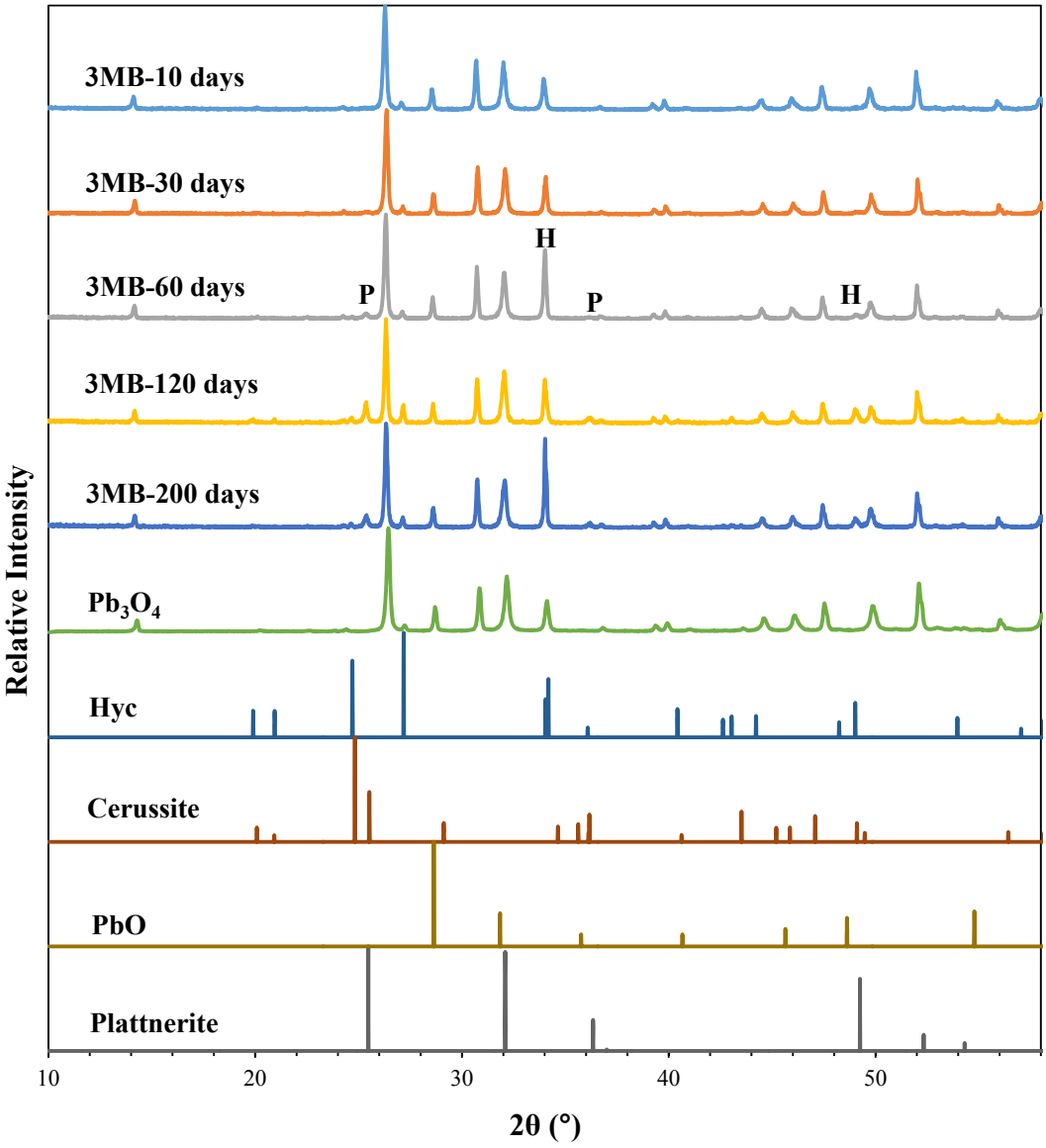

Figure 4.8 XRD patterns obtained on solid samples collected for experiment 3MB. The data for crystalline phases of lead oxides and carbonates is included for reference.

4.2.2.2 The effect of initial chlorine concentration on solid phase transformation

To evaluate the effect of free chlorine on the solid phase transformations, characterization results obtained for experiments 3MA and 3MB are compared. The FTIR spectra for the sample collected at 30 days from experiment 3MB shows that the free carbonate vibrational band disappeared and a clear peak at 682 cm^{-1} is observed (Figure 4.5). This is in contrast to the small shoulder observed at the same position for the sample obtained at 30 days for experiment 3MA (Figure 4.3). This suggests that a larger fraction of cerussite was formed for experiment 3MB which had a higher initial chlorine concentration. For the 60 days sample from experiment 3MB, the peak at 682 cm^{-1} shifted to 696 cm^{-1} and had a higher intensity, indicating the presence of hydrocerussite. The IR spectra obtained for the 60 days sample for experiment 3MA, in contrast, reveals that the main lead carbonate phase was still cerussite. These results indicate that the formation of lead carbonates was favored at the higher initial chlorine concentrations.

To verify the effect of free chlorine on the formation of lead carbonates, the alkalinity of the aqueous solution was measured (Figure 4.9a). The total aqueous carbonate concentrations for experiments 3MA and 3MB were calculated using the measured alkalinity in combination with pH measurements (Figures 4.2a and 4.9b). Details of the calculations are provided in Chapter 3. For experiment 3MB the aqueous carbonate concentrations decreased by about 5.2% over the first 60 days. If it is assumed that all carbonate removed from solution was converted into hydrocerussite, 3.8% of the initial solid Pb_3O_4 would be converted into hydrocerussite. While this calculation is not a precise representation of the solid phase transformation, it provides an upper limit for the amount of hydrocerussite present at 60 days. For experiment 3MA, the aqueous carbonate concentration remained slightly higher than in experiment 3MB. This indicates that consistent with the solid phase characterization results less carbonate ions precipitated out in experiment 3MA.

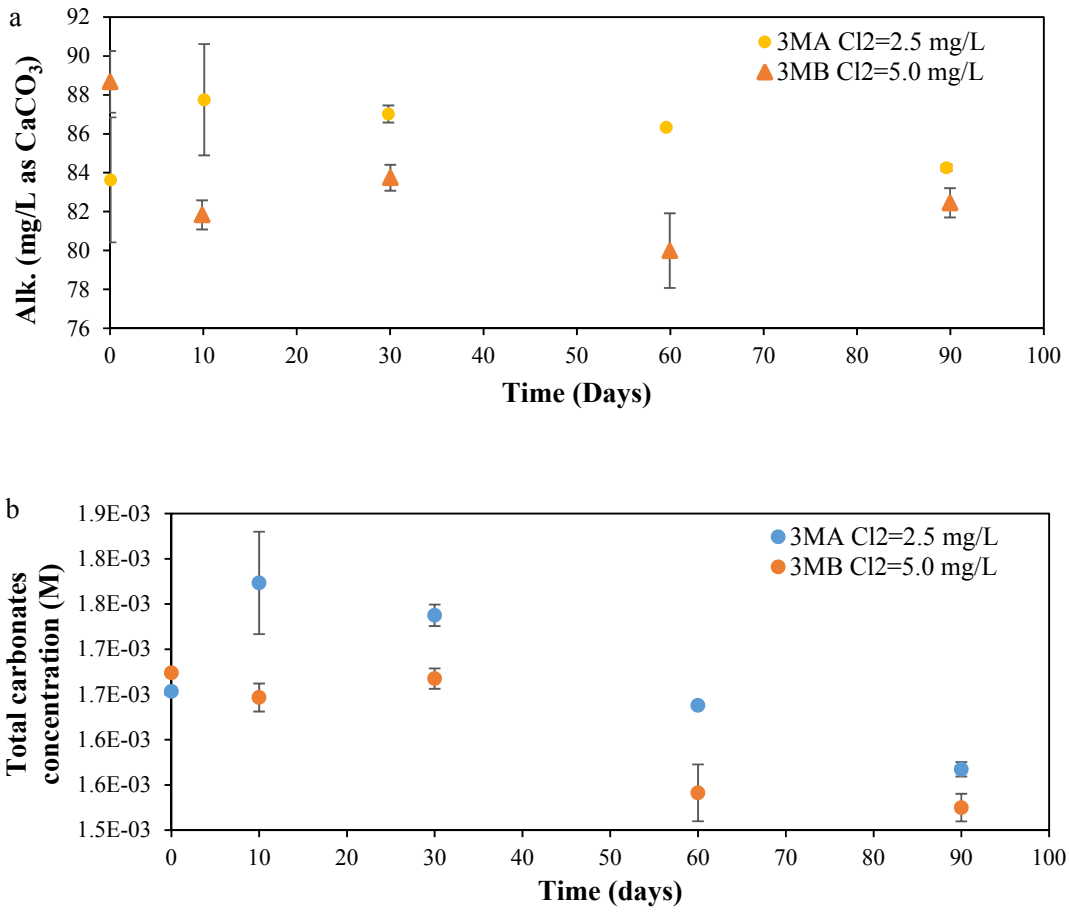

Figure 4.9 a) Alkalinity and b) calculated total aqueous carbonate concentrations obtained during experiments 3MA and 3MB.

The UV/Vis spectra obtained on the solids from experiment 3MB suggest that the initial free chlorine concentration also affected the formation of PbO_2 (Figure 4.6). The tailings of the UV/Vis spectra (580-750nm) are more pronounced for samples obtained from experiment 3MB compared with experiment 3MA (Figure 4.4). This suggests more PbO_2 formed at a higher initial chlorine concentration. To verify this result a control test was run under the same conditions but in the absence of chlorine. The UV/Vis spectra obtained on the collected solids from this control test does not show the tailing that was observed for experiments 3MA and 3MB (Figure S.A.8). This indicates that the changes in the visible region, attributed to PbO_2 formation, resulted from the availability of chlorine.

Further evidence of the formation of PbO_2 is observed in the FTIR spectra (Figure 4.5). As mentioned in Section 4.2.2.1 the main IR peak (~580 cm^{-1}) is attributed to the stretching of

the Pb(IV)-O bond present in the Pb(IV)-O-Pb(II) moiety in the Pb_3O_4 structure (Vigouroux et al. 1982). The intensity of this peak not only decreased with time but its position clearly shifted from 584 cm^{-1} at 0.023 days, to 572 cm^{-1} at 60 days, to 570 cm^{-1} at 90 days. The shift of this peak to lower wavenumbers suggests that the relative strength of this chemical bond decreased during Pb_3O_4 dissolution. Therefore, it may be hypothesized that the Pb(IV)-O bond present in the metastable PbO_2 fragment (octahedral arrangement hosting the Pb^{4+} ions in Pb_3O_4) is distorted from its original form during Pb_3O_4 dissolution. As pH is expected to affect the Pb_3O_4 dissolution process and subsequent solid phase transformation (see Section 4.2.3), the time profile of the IR peak (~580 cm^{-1}) shift together with the changes in pH observed for experiments 3MA and 3MB were plotted in Figure 4.10. For both experiments, the changes in pH levels follow a linear trend, while the IR peak shift reveals a more complex profile. This suggests that the peak shift may be not directly related to the change of pH values. Although we cannot confirm that the newly distorted structure is identical to that of β-PbO_2, we can hypothesize that the distortion of the structure is triggered by free chlorine and is part of the mechanism leading to the final formation of β-PbO_2. The FTIR spectra of the solids collected in the control test (no initial chlorine concentration, Figure S.A.9) did not show a peak shift; this further indicates that the observed changes in the structure of Pb_3O_4 are due to the presence of chlorine and could be possibly linked to the formation of β-PbO_2.

4.2.3 Mechanism of Pb_3O_4 dissolution

Stage I

Based on the experimental results, we hypothesize that Pb_3O_4 was partially oxidized by free chlorine to form PbO_2 during Stage I of the experiments. This resulted in a decrease in dissolved lead levels as PbO_2 has a very low solubility (Schock et al. 1996) compared with Pb_3O_4 (Fraser and Fairhall 1959). The UV/Vis spectra indicated that PbO_2 formation occurred in Stage I as chlorine was consumed (Figures 4.4 and 4.6). PbO_2 may have been formed by the overall oxidation reaction:

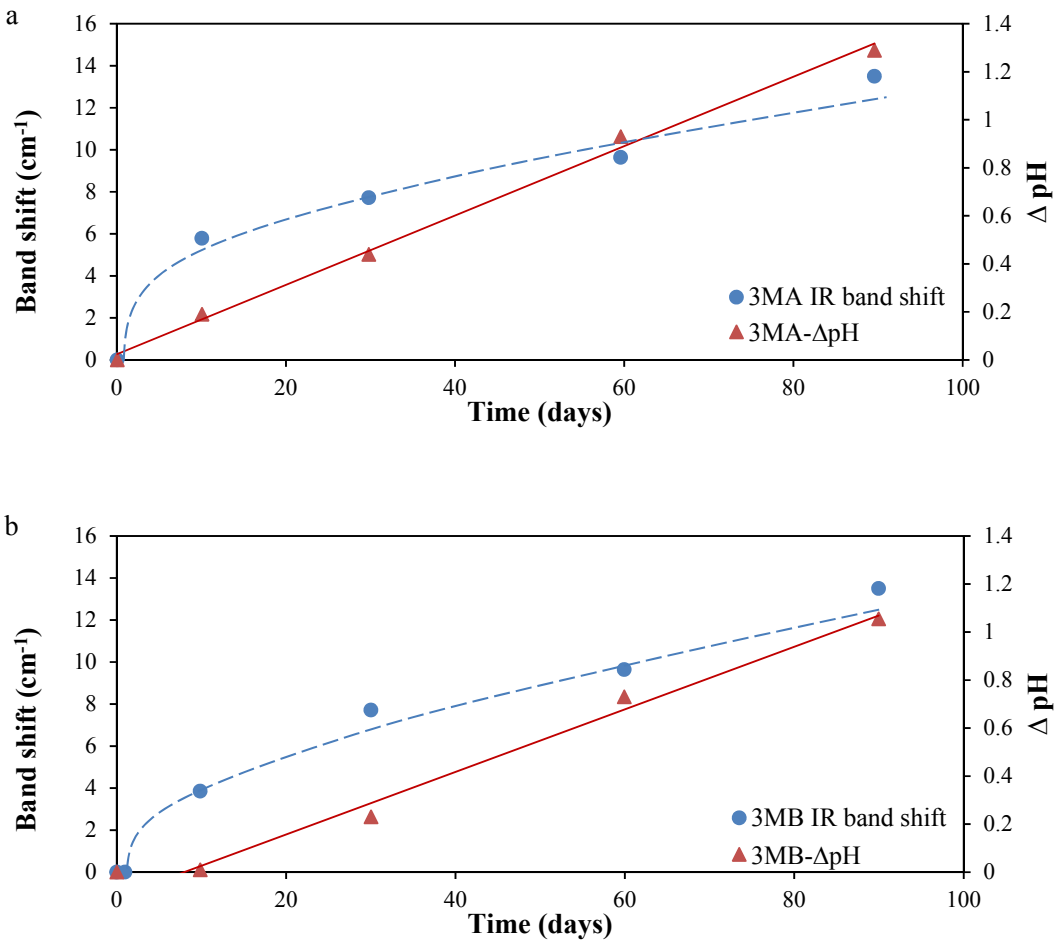

Figure 4.10 Shift of the Pb_3O_4 IR band at ~580 cm^{-1} over time and the rate of pH change for experiments a) 3MA and b) 3MB.

$$Pb_3O_{4(s)} + 2OCl^-_{(aq)} \leftrightarrow 3PbO_{2(s)} + 2Cl^-_{(aq)} \quad (1)$$

This reaction may occur in a two-step process:

$$Pb_3O_{4(s)} + 4H^+_{(aq)} \leftrightarrow 2Pb^{2+}_{(aq)} + PbO_{2(s)} + 2H_2O \quad (2)$$

$$Pb^{2+}_{(aq)} + OCl^-_{(aq)} + H_2O_{(l)} \leftrightarrow Cl^-_{(aq)} + PbO_{2(s)} + 2H^+_{(aq)} \quad (3)$$

Equation 2 describes solvolytic disproportionation for Pb_3O_4, which has been studied previously in diluted (0.075 N) nitric acid (Kang et al. 1988). In the study by Kang et al., a mechanism for Pb_3O_4 dissolution was proposed whereby Pb_3O_4 first releases Pb^{2+} species

from tetrahedrally coordinated Pb(II)O_4 sites through ligand substitution triggered by hydronium ions:

$$Pb_3O_{4(s)} + 4H^+_{(aq)} \leftrightarrow 2Pb^{2+}_{(aq)} + PbO_{2(unstable)} + H_2O \qquad (4-a)$$

Following this, two processes occur simultaneously. First, the octahedral unstable PbO_2 fragments ($PbO_{2(unstable)}$) left behind after the removal of Pb^{2+} species from Pb_3O_4 are reduced to Pb^{2+}:

$$PbO_{2(unstable)} + 2e^- + 4H^+_{(aq)} \leftrightarrow Pb^{2+}_{(aq)} + 2H_2O_{(l)} \qquad (4-b)$$

The electrons needed to complete Eq. 4-b come from a second simultaneous process (Eq. 4-c) in which newly stable β-PbO_2 phases nucleate from the Pb^{2+} ions generated in Eq. 4-a:

$$Pb^{2+}_{(aq)} + 2H_2O_{(l)} \leftrightarrow PbO_{2(stable)} + 2e^- + 4H^+_{(aq)} \qquad (4-c)$$

As both Pb_3O_4 and β-PbO_2 are semiconductors, electrons can transfer between these two solid phases. The driving force for the process described in Eq. 2 (sum of Eq. 4-a, 4-b, and 4-c) is provided by the difference in free energy between the octahedral fragment of PbO_2 in Pb_3O_4 and that of the recrystallized stable β-PbO_2. The overall mechanism is illustrated in Figure 4.11.

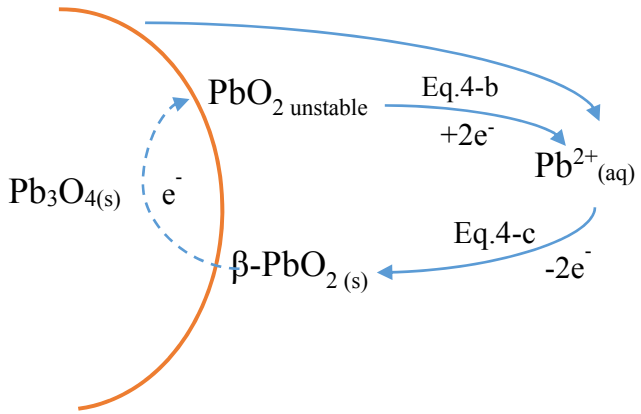

Figure 4.11 Schematic of the mechanism for the dissolution of Pb3O4 as described in Kang. et al. (1988).

For our experimental conditions, the process described in Eq. 2 may occur at a relatively slower rate than that observed by Kang et al. (1988) due to the slightly basic (pH>8) conditions in our experiments. In the presence of free chlorine during Stage I, the newly formed PbO_2 deposits on the surface of the Pb_3O_4 solid, and so passivation occurs, resulting in the observed low lead concentrations.

Stage II

With the free chlorine largely depleted and the ORP values sharply decreasing, the lead release profile for Pb_3O_4 entered Stage II. With less available oxidant, the dominant Pb_3O_4 dissolution mechanism is that described in Eq. 2 above. Once formed PbO_2 can remain either as a spectator species or be reduced by water according to (Lin and Valentine 2008; Lin and Valentine 2009; Xie et al. 2010):

$$PbO_{2(s)} + H_2O_{(l)} \leftrightarrow Pb^{2+}{}_{(aq)} + 2OH^-{}_{(aq)} + 0.5O_{2(aq)} \quad (5)$$

Due to the low solubility of PbO_2, the dissolved lead levels in solution were controlled mainly by Pb_3O_4 dissolution during Stage II. The equilibrium lead levels (~0.14 mg/L) in the control test are consistent with the peak concentration (~0.15 mg/L) observed at the end of Stage II for experiments 2MA and 2MB (Figures 4.1b and S.A.3). Analysis indicates that the total aqueous carbonate concentration remained stable through Stages I and II (Figure 4.9b) suggesting that solid lead(II) carbonate phases were not formed. This is consistent with the IR results which indicate there was no detectable solid lead carbonates formed during the first 10 days of the experiments. This may also be attributed to the fact that crystal-growth for lead carbonates is a kinetically-controlled process (Marani et al. 1995; Sánchez-Navas et al. 2013). The 20 mg C/L DIC, however, could potentially act as ligands in the complexation of aqueous Pb (II) species, leading to the observed increase in dissolved lead levels during Stage II.

Stage III

Although there was no free chlorine available in Stage III, crystalline β-PbO_2 was observed in the solid sample collected after 60 days via XRD. We hypothesize the solvolytic

disproportionation of Pb_3O_4 was the dominant process for PbO_2 formation in Stage III (Eq. 4-a, 4-b, and 4-c). The IR spectra (Figure 4.3 and 4.5) show that lead carbonates were formed also during this stage and were transformed over time from cerrusite ($PbCO_3$, Eq. 6) to a mixture of cerussite and hydrocerussite ($Pb_3(CO_3)_2(OH)_2$, Eq. 7):

$$Pb^{2+}_{(aq)} + CO^{2-}_{3(aq)} \leftrightarrow PbCO_{3(aq)} \leftrightarrow PbCO_{3(s)} \quad (6)$$

$$3PbCO_{3(s)} + 2OH^{-}{}_{(aq)} \leftrightarrow Pb_3(CO_3)_2(OH)_{2(s)} + CO^{2-}_{3}{}_{(aq)} \quad (7)$$

In Stage III, the aqueous carbonate was consumed over a long time period, particularly after 30 days, with the consumption profile following an apparent zeroth order rate. We propose that the formation of lead carbonates during Stage III is a slow process that may be limited by the available Pb^{2+} species in solution rather than the carbonate concentrations. The dissolved lead concentrations in Stage II was influenced by the initial chlorine concentrations as indicated in Figure 4.1b. Specifically, more PbO_2 formed during the experiment with higher initial free chlorine in Stage I (Eq. 1). This newly formed PbO_2 usually with smaller particle size and aggregates together (Lytle et al. 2009; Wang et al. 2010). Once free chlorine was completely consumed, the reduction of this newly formed PbO_2 by water may have led to higher Pb^{2+} concentrations in Stages II and III (Eq. 5). This is the first mechanism. Another possible mechanism may be the formation of Pb^{2+} species during the recrystallization of unstable PbO_2 fragments to crystalline β-PbO_2. Accurate description of the processes governing the formation and accumulation of soluble Pb^{2+} species requires consideration of the kinetics for each of the reactions described above. For instance, if Eq. 4-c is the rate-limiting step, Pb(II) species will accumulate in the system; while if the rates of Eq. 4-b and 4-c are similar, Pb_3O_4 dissolution will take place in a closed loop and there will be no net production of Pb(II) species. If rates of Eq.4-b and 4-c are similar, the increase in Pb^{2+} and thus greater formation of lead (II) carbonate phases in experiment 3MB can only be attributed to the first mechanism proposed above (Eq. 1 and 5). The increase in Pb^{2+} ions at higher initial chlorine concentrations may explain why more lead carbonates formed in experiment 3MB than in 3MA, as discussed in Section 4.2.2.2.

It is well established that the transformation of cerussite into hydrocerussite is controlled by pH (Lytle and Schock 2005; Wang et al. 2010). In contrast to Stage I and II, pH values increase significantly during Stage III (Figure 4.2b). At 30 days, cerussite was the only observed carbonate phase and the pH was approximately 8.4 compared to a pH of about 8.1 recorded at day 10 for experiments 3MA and 3MB. We attempted to fit a rate law to the observed pH levels using first order kinetics. However, we are unable to obtain an acceptable fitting over the entire Stage III. Instead, two apparent first order kinetic regimes were observed with different rate constants (Figure 4.12). The change in the apparent rate at around 60-90 days suggests that the changes in pH were caused by at least two different mechanisms during Stage III. The change in apparent rates can be rationalized based on the stoichiometry of the proton-consuming/generating reactions described by Eq. 2, 5, 6 and 7.

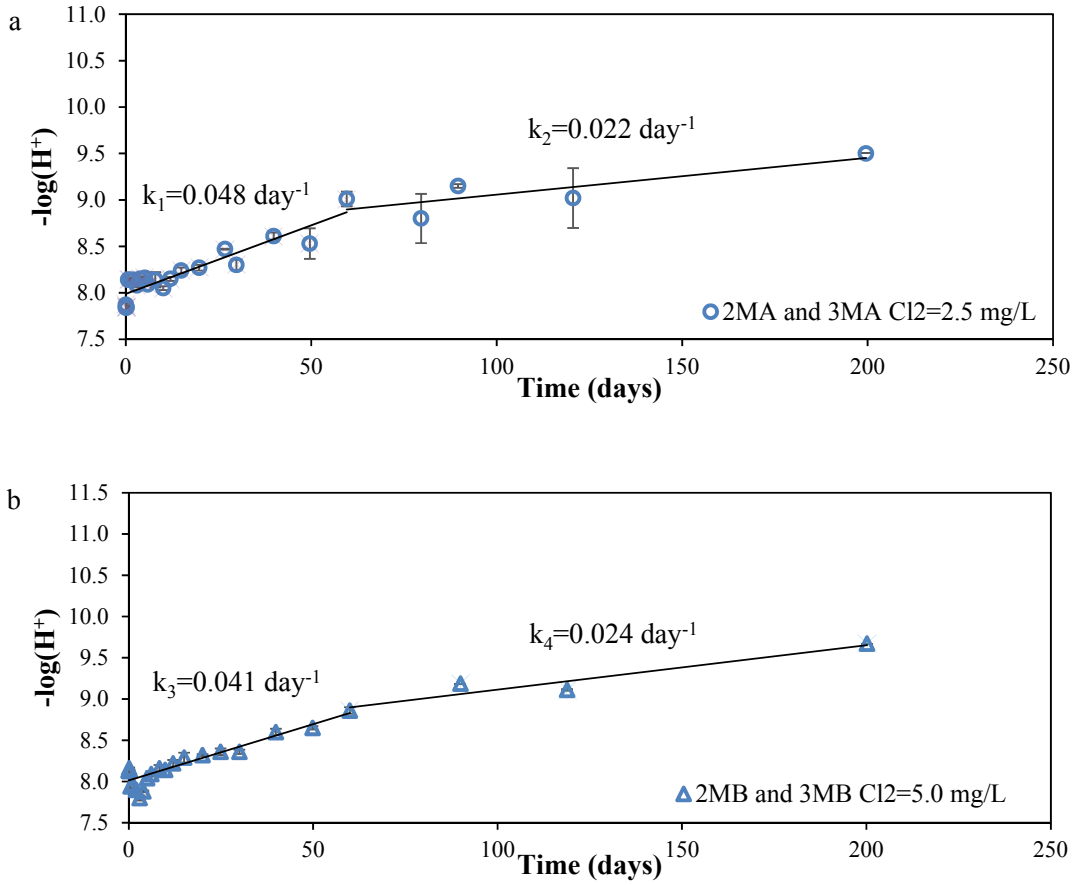

Figure 4.12 pH and first order linear regression obtained for the rate of pH change during a) experiments 2MA and 3MA and b) experiments 2MB and 3MB.

Specifically, during Stage III, the dissolution of Pb_3O_4 by water (chlorine is already depleted) consumes hydrogen ions to form Pb (II) species (Eq. 2). Meanwhile, the newly generated PbO_2 is reduced by water and this produces hydroxide ions (Eq. 5). As previously described, cerussite was also formed during the initial part of Stage III. The formation of cerussite does not consume hydroxide ions (Eq. 6). Thus with these three processes occurring simultaneously, the concentration of hydroxide ions increased during the early part of Stage III and resulted in the observed pH increase. In contrast to Eq. 2, 5 and 6, hydroxide ions were consumed when hydrocerussite formed (Eq. 7) during the latter part of Stage III (as observed by FTIR). Even though the formation of hydrocerussite will consume some hydroxide ions, the stoichiometry of the overall dissolution process (Eq. 2, 5, 6 and 7) results in a net gain in hydroxide ions if indeed PbO_2 is being reduced by water. However, the increase in pH levels would be slower than the increase observed during the early part of Stage III when only cerussite was forming.

4.3 Environmental implications

From our results we expect that PbO_2 would be the final product in the dissolution of Pb_3O_4 if the stoichiometric amount of chlorine was present, or a continuous source of free chorine was available, such as in a DWDS. It is reasonable to propose that Pb_3O_4 acts as an intermediate phase during the Pb(II) → Pb(IV) solid phase transformation. This is also consistent with the fact that few field corrosion scales have been reported to contain Pb_3O_4. The final experimental solubility of Pb_3O_4 under depleting chlorine conditions seems to be as high as those of lead carbonates, and is likely controlled by thermodynamics. This indicates that the equilibrium lead levels of Pb_3O_4 may be controlled by the solubilities of both Pb_3O_4 and lead carbonates formed on the surface. Moreover, the dissolved lead concentrations obtained in the control test (no chlorine present) were about 0.14 mg/L. Such high solubility suggest that elevated lead concentrations in drinking water may occur in a scenario with depleted chlorine where Pb_3O_4 phases are still present.

4.4 References

Dan, A. C., J. H. C. Robin, L. J. M. and O. Marianne (1996). "Studies on the thermal decomposition of basic lead (II) carbonate by Fourier-transform Raman spectroscopy, X-ray diffraction and thermal analysis." Journal of the Chemical Society, Dalton Transactions(18): 3639-3645.

Edwards, M. and A. Dudi (2004). "Role of chlorine and chloramine in corrosion of lead-bearing plumbing materials." Journal of the American Water Works Association **96**(10): 69-81.

Fraser, D. A. and L. T. Fairhall (1959). "Laboratory study of the solubility of red lead paint in water." Public Health Reports **74**(6): 501.

Grimes, S. M., S. R. Johnston and D. N. Batchelder (1995). "Lead carbonate–phosphate system: solid–dilute solution exchange reactions in aqueous systems." Analyst **120**(11): 2741-2746.

Health.Canada. (2012). Guidelines for Canadian Drinking Water Quality - Summary Table. Available: http://www.hc-sc.gc.ca/ewh-semt/pubs/water-eau/2012-sum_guide-res_recom/index-eng.php#t2. Last accessed 15th January 2014.

Hozalski, R. M., E. Esbri-Amador and C. F. Chen (2005). "Comparison of stannous chloride and phosphate for lead corrosion control." Journal of the American Water Works Association **97**(3): 89-103.

Kang, Z. C., L. Machesky, H. A. Eick and L. Eyring (1988). "The solvolytic disproportionation of mixed-valence compounds: III. Pb_3O_4." Journal of Solid State Chemistry **75**(1): 52-59.

Kim, E. J. and J. E. Herrera (2010). "Characteristics of lead corrosion scales formed during drinking water distribution and their potential influence on the release of lead and other contaminants." Environmental Science and Technology **44**(16): 6054-6061.

Lin, Y. and R. L. Valentine (2008). "The release of lead from the reduction of lead oxide (PbO2) by natural organic matter." Environmental Science and Technology **42**(3): 760-765.

Lin, Y. and R. L. Valentine (2009). "Reduction of Lead Oxide (PbO2) and Release of Pb(II) in Mixtures of Natural Organic Matter, Free Chlorine and Monochloramine." Environmental Science and Technology.

Liu, H., G. V. Korshin and J. F. Ferguson (2009). "Interactions of Pb (II)/Pb (IV) solid phases with chlorine and their effects on lead release." Environmental Science and Technology **43**(9): 3278-3284.

Liu, H., A. M. Kuznetsov, A. N. Masliy, J. F. Ferguson and G. V. Korshin (2012). "Formation of Pb(III) intermediates in the electrochemically controlled Pb(II)/PbO(2) system." Environmental Science and Technology **46**(3): 1430-1438.

Lytle, D. A. and M. R. Schock (2005). "Formation of Pb (IV) oxides in chlorinated water." Journal of the American Water Works Association **97**(11): 102-114.

Lytle, D. A., C. White, M. N. Nadagouda and A. Worrall (2009). "Crystal and morphological phase transformation of Pb (II) to Pb (IV) in chlorinated water." Journal of Hazardous Materials **165**(1): 1234-1238.

Marani, D., G. Macchi and M. Pagano (1995). "Lead precipitation in the presence of sulphate and carbonate: testing of thermodynamic predictions." Water Research **29**(4): 1085-1092.

Mosseri, S., A. Henglein and E. Janata (1990). "Trivalent lead as an intermediate in the oxidation of lead (II) and the reduction of lead (IV) species." Journal of Physical Chemistry **94**(6): 2722-2726.

Sánchez-Navas, A., O. López-Cruz, N. Velilla and I. Vidal (2013). "Crystal Growth of Lead Carbonates: Influence of the Medium and Relationship between Structure and Habit." Journal of Crystal Growth.

Schock, M. R., S. M. Harmon, J. Swertfeger and R. Lohmann (2001). "Tetravalent lead: a hitherto unrecognized control of tap water lead contamination." Proceedings AWWA Water Quality Technology Conference, Nashville: 11-15.

Schock, M. R., D. A. Lytle, A. M. Sandvig, J. Clement and S. M. Harmon (2005). "Replacing polyphosphate with silicate to solve lead, copper, and source water iron problems." Journal of the American Water Works Association **97**(11): 84-93.

Schock, M. R., I. Wagner and R. Oliphant (1996). The corrosion and solubility of lead in drinking water. Internal corrosion of water distribution systems. Denver, CO., AWWA Research Foundation/TZW**:** 131-230.

Schrrrz, B. E. and W. B. White (1977). "Vibrational spectra of the alkaline earth double carbonates." American Mineralogist **62**: 36-50.

Trettenhahn, G. L. J., G. E. Nauer and A. Neckel (1993). "Vibrational spectroscopy on the PbO-$PbSO_4$ system and some related compounds: Part 1. Fundamentals, infrared and Raman spectroscopy." Vibrational spectroscopy **5**(1): 85-100.

U.S.EPA (1991). Maximum contaminant level goals and national primary drinking water regulations for lead and copper. Fianl rule., Federal Register **56, 26460**.

Vigouroux, J. P., E. Husson, G. Calvarin and N. Q. Dao (1982). "Etude par spectroscopié vibrationnelle des oxydes Pb3O4, SnPb2O4 et SnPb(Pb2O4)2." Spectrochimica Acta Part A: Molecular Spectroscopy **38**(4): 393-398.

Wang, Y., Y. Xie and D. E. Giammar (2012). Lead(IV) oxide formation and stability in drinking water distribution systems.

Wang, Y., Y. Xie, W. Li, Z. Wang and D. E. Giammar (2010). "Formation of lead (IV) oxides from lead (II) compounds." Environmental Science and Technology **44**(23): 8950-8956.

Xie, Y., Y. Wang and D. E. Giammar (2010). "Impact of chlorine disinfectants on dissolution of the lead corrosion product PbO2." Environmental Science and Technology **44**(18): 7082-7088.

Chapter 5

5 Dissolution of plattnerite (β-PbO_2) in water under depleting chlorine conditions

5.1 Introduction

PbO_2 is often found in corrosion scales of lead-bearing plumbing in DWDS. Tetragonal plattnerite (β-PbO_2) and orthorhombic scrutinyite (α-PbO_2) are both generally observed in the surface layer of corrosion scales as dissolved lead(II) species are oxidized by free chlorine to form these solid lead(IV) phases (Schock et al. 2001; Schock and Giani 2004; Schock et al. 2005; Kim and Herrera 2010) It is well recognized that the stability of PbO_2 can significantly impact dissolved lead levels in drinking water (Schock et al. 2001). Many studies have examined the effects of water quality parameters such as pH, dissolved inorganic carbon (DIC), and disinfectant type on PbO_2 stability, together with the effect of reductants that are naturally present in drinking water such as Fe^{2+} and natural organic matter (NOM) (Lin and Valentine 2009; Shi and Stone 2009; Lin and Valentine 2010; Xie et al. 2010a; Xie et al. 2010b; Wang et al. 2012).

PbO_2 is less soluble than solid lead(II) carbonates ($PbCO_3$ and $Pb_3(OH)_2(CO_3)_2$) according to tabulated thermodynamic data and experimental results (Schock et al. 1996; Schock et al. 2001). PbO_2 is generally stable when high oxidation-reduction potential (ORP) is maintained in a DWDS by free chlorine. However, a decrease in ORP due to, for example, a change in disinfectant, may destabilize PbO_2 and cause dissolved lead concentrations to rapidly increase. This was observed in the DWDS of Washington D.C. when the disinfectant was switched from free chlorine to chloramine (Edwards and Dudi 2004; Switzer et al. 2006). Understanding PbO_2 dissolution under depleting chlorine, and thus decreasing ORP conditions, is essential to evaluate and predict lead levels in drinking water and for developing effective long-term corrosion control strategies. Only a few prior studies have examined these experimental conditions (Lytle and Schock 2005; Lin and Valentine 2009). However, the long-term solid phase transformations and subsequent dissolved lead concentrations in drinking water have not been comprehensively investigated under depleting chlorine conditions.

As mentioned in Chapter 2, β-PbO_2 was thermodynamically stable phase in chlorinated water with relatively low pH levels (8~10) than α-PbO_2 (pH>10) (Bagshaw et al. 1966; Lytle and Schock 2005; Liu et al. 2008; Wang et al. 2010; Li et al. 2011). For most DWDS, drinking water is slightly basic (pH<10), indicating the favored β-PbO_2 formation. Therefore, in this chapter, the effects of free chlorine on the β-PbO_2 solubility under depleting chlorine conditions are investigated via long-term batch dissolution experiments. Characterization of solid samples collected during these experiments provides important insights into the β-PbO_2 dissolution mechanisms. Relatively high initial concentrations of free chlorine (up to 5 mg Cl_2/L) were used in experiments to completely oxidize the labile surface of PbO_2 and provide sufficient oxidant for characterization of structural changes.

5.2 Results and discussion

5.2.1 Influence of free chlorine on lead release profile and equilibrium concentrations

Three long-term experiments (1PA, 1PB, and 1PC) with different initial free chlorine concentrations were conducted to evaluate the equilibrium solubility of β-PbO_2. The lead levels in experiments 1PA (2.5 mg Cl_2/L), 1PB (5.0 mg Cl_2/L), and 1PC (6.0 mg Cl_2/L) were low (ranged from 2 - 8 μg/L) after 100 days based on ICP-OES analysis (Table 5.1). The depletion of free chlorine, pH, and ORP levels over time for these experiments are shown in Figures S.B.1 and S.B.2 in Appendix B. Free chlorine was not depleted until around 100 days for experiment 1PA and 336 days for experiment 1PB. Equilibrium was reached after 100 days for experiment 1PA. For experiment 1PC, 1.2 mg Cl_2/L still remained after 330 days, and as a result, equilibrium was not reached during the experimental period (330 days). The dissolved lead concentration observed at 336 days in experiment 1PB may have reached equilibrium since free chlorine was depleted completely at this time. The final observed equilibrium lead concentrations were 1.3 μg/L for experiment 1PA at 239 days and 2.4 μg/L for experiment 1PB at 336 days as determined by ICP-MS analysis.

Experiments 2PA and 2PB were performed under similar conditions as Experiments 1PA and 1PB but with more frequent sampling during the first three days of the experiments to

evaluate the lead dissolution profiles. Details of the experimental conditions are provided in Table 5.2. Experiments 3PA and 3PB were performed under similar conditions as experiments 2PA and 2PB, respectively (Table 5.2). Solid samples were collected from experiments 3PA and 3PB, in addition to aqueous samples.

The free chlorine and lead concentrations observed during experiments 2PA and 3PA (2.5 mg/L nominal free chlorine) are shown in Figure 5.1. The free chlorine concentrations decreased exponentially - during the first 10 days, the free chlorine decreased rapidly from 2.51 mg/L to 0.97 mg/L, followed by a decrease to 0.13 mg/L by 80 days, and complete consumption by 120 days. Although the observed dissolved lead levels (Figure 5.1b) from experiment 3PA are more than from experiment 2PA, the lead levels should be similar for both these experiments as their conditions were the same except for the reactor volume. Based on the observations in Chapter 4 and also free chlorine concentrations shown in Figure 5.1a, the reactor volume has negligible effect. The dissolved lead concentrations remained relatively constant from 0 - 90 days, after which time a slight increase in concentration was observed (~4 μg/L at 90 days) even though free chlorine was still available (~0.2 mg/L) and the ORP was approximately 450 mV (vs. Ag/AgCl) (Figure 5.2a). This is consistent with the study of Wang et al. (2010) which reported that there was a threshold value of free chlorine for PbO_2 formation. During this stage (0 - 90 days) free chlorine likely oxidized the dissolved lead species ($Pb^{2+}_{(aq)}$) released from the reduction of β-PbO_2 by water (Eq. 1) (Edwards and Dudi 2004; Lytle and Schock 2005; Switzer et al. 2006; Wang et al. 2010). This results in the reprecipitation of PbO_2 and consumption of free chlorine (Eq. 2). The pH levels remained relatively stable at 8.1±0.2 throughout experiments 2PA and 3PA (Figure 5.2b).

$$PbO_{2(s)} + H_2O_{(l)} \leftrightarrow Pb^{2+}{}_{(aq)} + 2OH^-{}_{(aq)} + 0.5O_{2(aq)} \quad (1)$$

$$Pb^{2+}{}_{(aq)} + OCl^-{}_{(aq)} + H_2O_{(l)} \leftrightarrow Cl^-{}_{(aq)} + PbO_{2(s)} + 2H^+{}_{(aq)} \quad (2)$$

Table 5.1 Summary of β-PbO_2 dissolution experimental conditions and results for Test 1

Experiment	Initial solid phase	Free chlorine (mg/L as Cl_2)	Elapsed time (days)	Initial pH	DIC (mg C/L)	$[Pb]_{diss.}$ mg/L				Final pH
						10 days	100 days	200 days		
						ICP-OES	ICP-OES	ICP-OES	ICP-MS	
1PA	β-PbO_2	2.35	330	7.93	20	0.010	0.006	0.006	0.0013	8.30
1PB		5.13	336	8.12	20	0.009	0.002	0.008	0.0024	8.16
1PC		6.16	330	7.94	20	0.008	0.004	0.007	N/A	8.38

Note: Test 1 experiments were conducted in 25 ml vials.

Table 5.2 Summary of β-PbO_2 dissolution experimental conditions and results for Tests 2 and 3

Experiment	Initial solid phase	Free chlorine (mg/L as Cl_2)	Sampling times (days)	Initial pH	DIC (mg C/L)	Final pH
2PA	β-PbO_2	2.51	0, 0.5h, 1h, 6h, 12h, 1, 2, 3, 4, 5, 6, 8, 12,	8.00	20	8.37
2PB		4.85	15, 20, 25,40, 50, 80, 120, 200	7.96	20	8.13
3PA		2.51	0, 10, 30, 60, 90, 200	8.00	20	8.16
3PB		4.85	0, 1, 10, 30, 60, 90, 120, 200	7.96	20	8.11
CP		0	0, 10, 30, 60	8.01	20	7.97

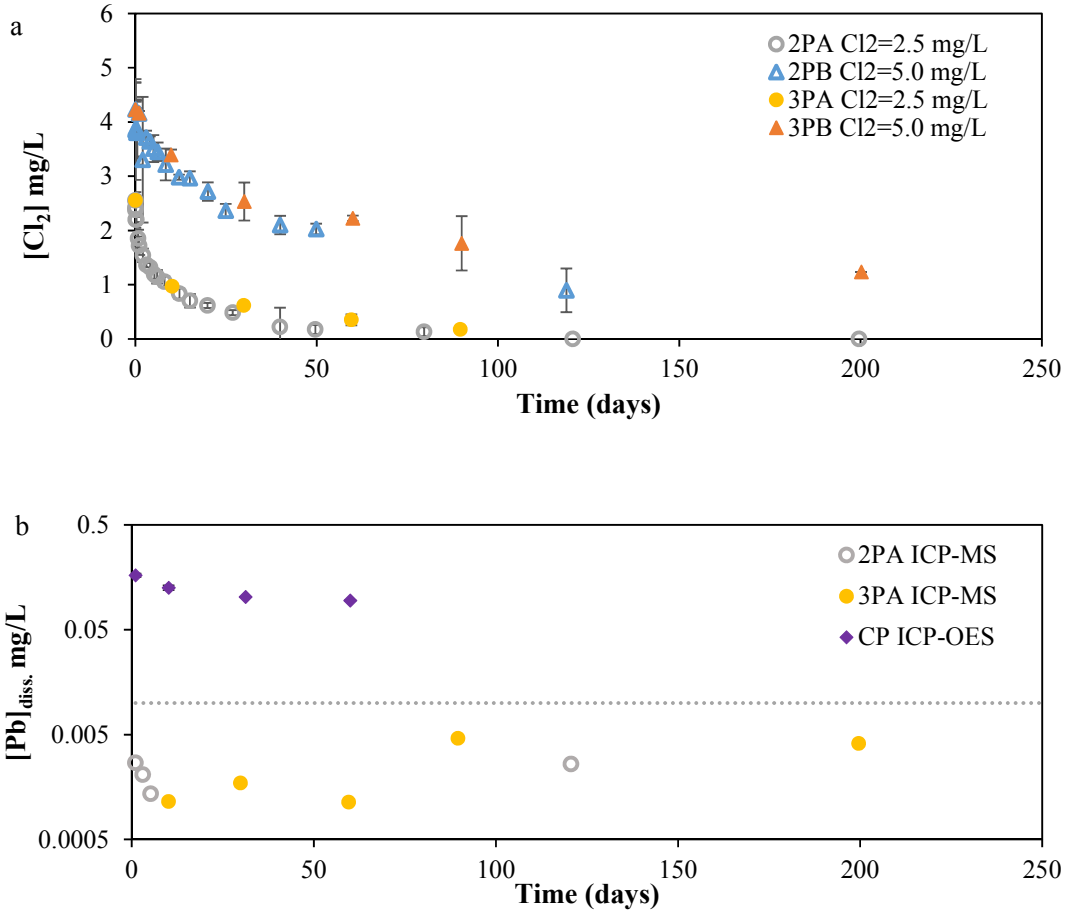

Figure 5.1 a) Free chlorine and b) dissolved lead concentrations observed during experiments 2PA, 2PB, 3PA, 3PB and CP (control test).

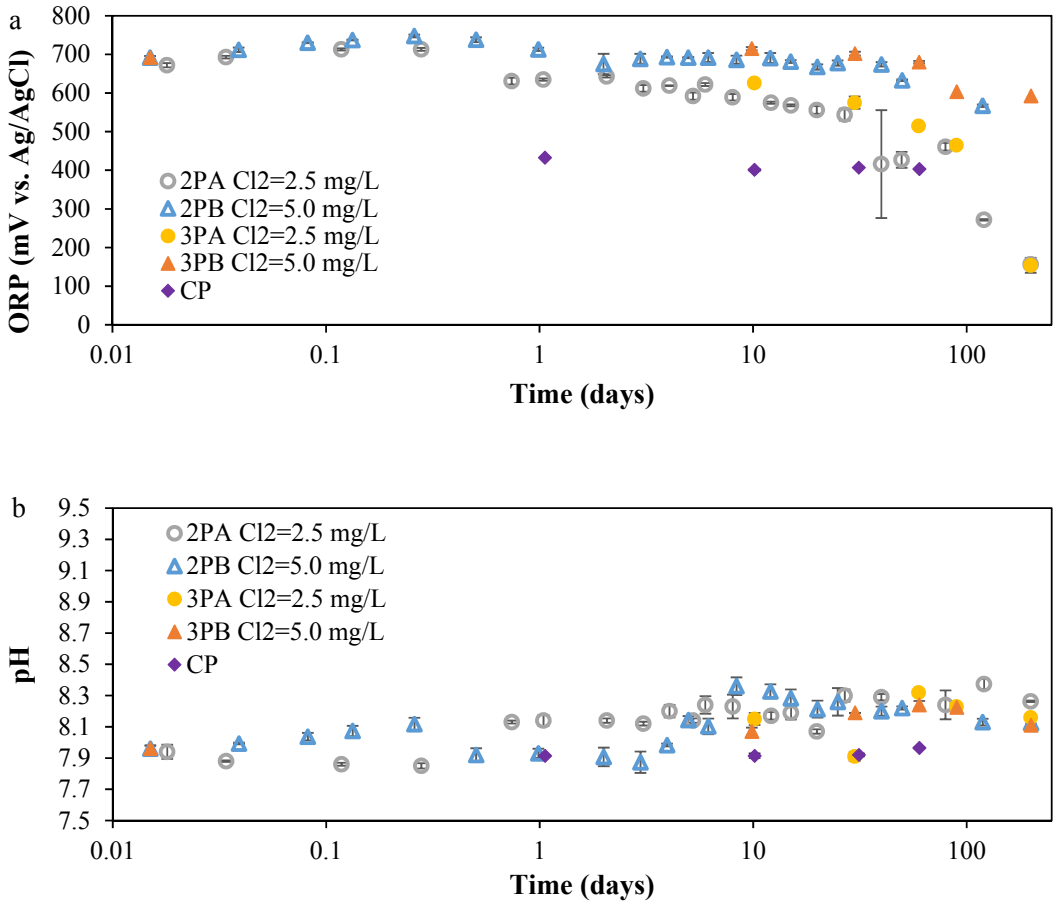

Figure 5.2 a) ORP and b) pH values measured during experiments 2PA, 2PB, 3PA, 3PB and CP (control test).

The lead levels observed in Tests 1, 2, and 3 before 90 days under the depleting chlorine conditions are similar to those presented previously (Lin and Valentine 2009; Xie et al. 2010a). For instance, Wang et al. (2010) performed batch β-PbO_2 dissolution experiments at pH 6, 7.5, and 8.5 for 25 days (50 mg C/L DIC, at constant free chlorine concentration of 2 mg Cl_2/L). They observed that the dissolved lead concentrations reached a plateau after 17 days for all three conditions (<1 µg/L, ~10 µg/L, and ~30 µg/L, respectively). Wang et al. (2010) proposed these lead concentrations were equilibrium concentrations although they were higher than expected based on thermodynamic constraints. Lin and Valentine (2009) reported dissolved lead concentrations around 8 µg/L after 21 days of a β-PbO_2 batch dissolution experiment conducted at pH 7 with 2 mg/L initial free chlorine (no redosing). Although this experiment was conducted under depleting chlorine conditions, residual chlorine was still available at the end of the experiment (21 days).

In experiments 2PA and 3PA, the dissolved lead concentration remained low (about 5 μg/L) until 200 days, even though free chlorine was depleted around 120 days. The final lead concentrations for 3PA (Figure 5.1b), as well as 2PA, are in agreement with that observed in experiment 1PA (Table 5.1). Compared with Tests 1, 2 and 3, much higher dissolved lead concentrations (~0.1 mg/L) were observed in a control experiment conducted with no free chlorine (Figure 5.1b). The low final lead levels in Tests 1, 2 and 3 after chlorine depleted are surprising based on our control experimental results and also previous studies that have reported lead concentrations as high as 50 μg/L during β-PbO_2 batch dissolution experiments with no free chlorine (Lin and Valentine 2009). In addition, ORP values in experiments 2PA and 3PA at 200 days were about 150 mV (vs. Ag/AgCl) – this was lower than the ORP levels in the control experiment (~ 400 mV vs. Ag/AgCl) (Figure 5.2a). The observed low lead concentrations at low ORP in experiments 2PA and 3PA suggest that once chlorine is depleted the prevailing ORP is not the critical factor controlling the stability of β-PbO_2 in our system. This result is contradictory with prior studies that suggest ORP regulates PbO_2 stability (Delahay et al. 1951; Pourbaix 1974; Schock et al. 1996). However, by comparison with the control test results it is evident that the prior availability of chlorine does affects the long-term β-PbO_2 stability.

We expected the dissolved lead concentrations to increase once chlorine became depleted. To our knowledge, only one long-term β-PbO_2 dissolution experiments under depleting chlorine conditions (105 - 395 days) has been reported previously (Lytle and Schock (2005). In this study it was reported that dissolved lead levels increased and lead carbonates formed once free chlorine was depleted. In this study, however, pure β-PbO_2 was not used as initial solid phase. Precipitated solid phase from solution containing dissolved lead and free chlorine (0 – 105 days) was used to investigate the PbO_2 dissolution pathway. Although the XRD analysis suggested that the solid phase was PbO_2, the authors reported that the color of solid was different from pure β-PbO_2 and therefore the crystal size, impurities and other factors may be different from the pure β-PbO_2 used in our experiments. Another major difference is that well mixed condition (stirrer) was used by Lytle and Schock (2005), while our experiments were under comparatively static conditions (shaker). Our experiments are the first time that low dissolved lead levels have been observed in a depleting chlorine system after chlorine is completely consumed. To better understand

these observations, detailed characterization of the solid phase transformations occurring over the Test 3 dissolution experiments were performed.

5.2.2 Solid phase characterization

5.2.3.1 NIR spectra

Figures 5.3 and 5.4 show the NIR spectra of solid samples collected during experiments 3PA and 3PB together with the spectrum of pure β-PbO_2. The NIR spectrum of β-PbO_2 shows a sharp characteristic peak centered at 1300 nm. This peak was also observed for the solid samples collected from experiments 3PA and 3PB, but the position of the peak shifted to longer wavelengths as the experimental time increased. The shift of the NIR peak (in nm) with time closely followed the consumption of free chlorine in the system (Figure 5.5). This suggests that changes in the morphology of β-PbO_2 observed via the NIR peak shift are linked to the consumption of chlorine. In contrast to the shift of the peak to higher wavelengths as experiments 3PA and 3PB progressed, samples collected from the control experiment without free chlorine present showed a general shift of the peak to shorter wavelengths (Figure S.B.3 in Appendix B).

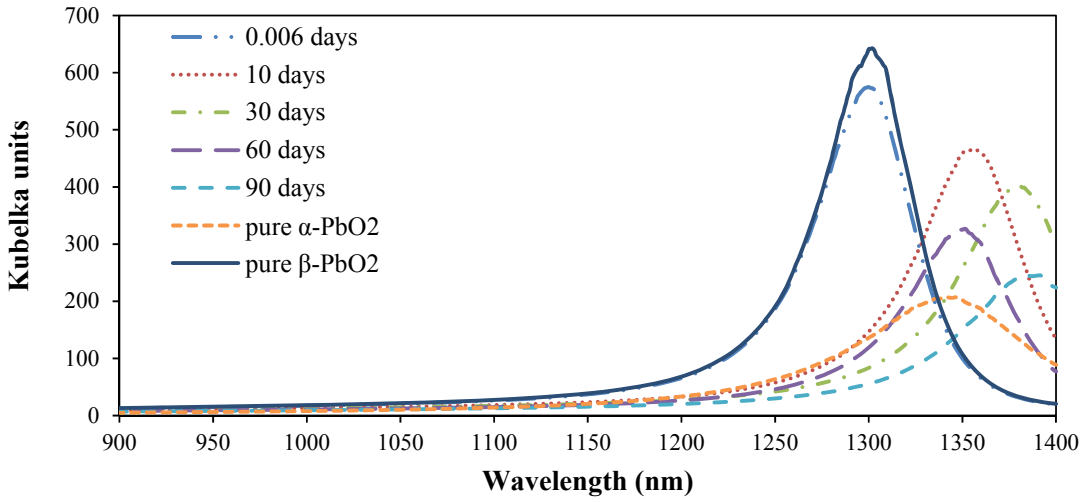

Figure 5.3 NIR spectra of solids collected during experiment 3PA (initial chlorine concentration of 2.5 mg Cl_2/L).

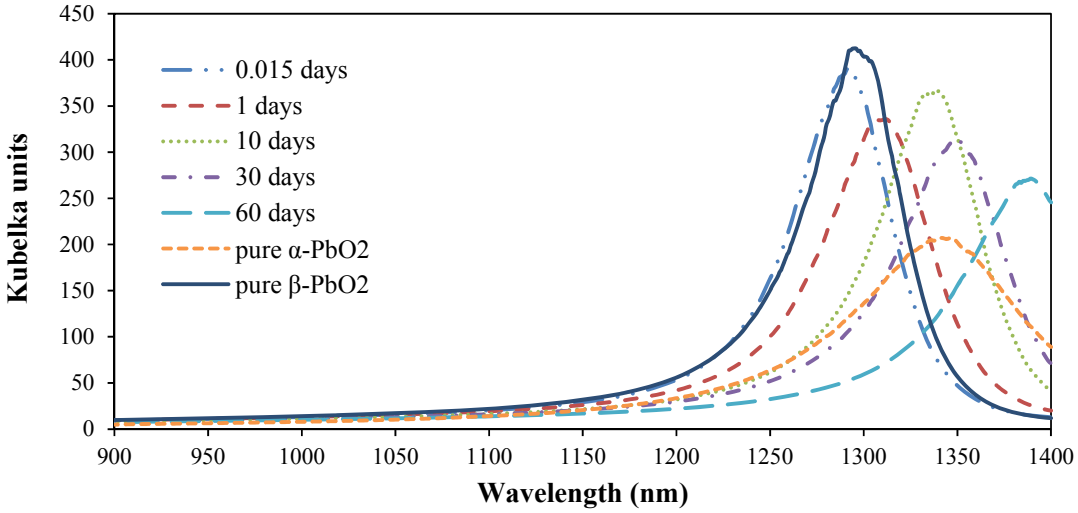

Figure 5.4 NIR spectra of solids collected during experiment 3PB (initial chlorine concentration of 5.0 mg Cl_2/L).

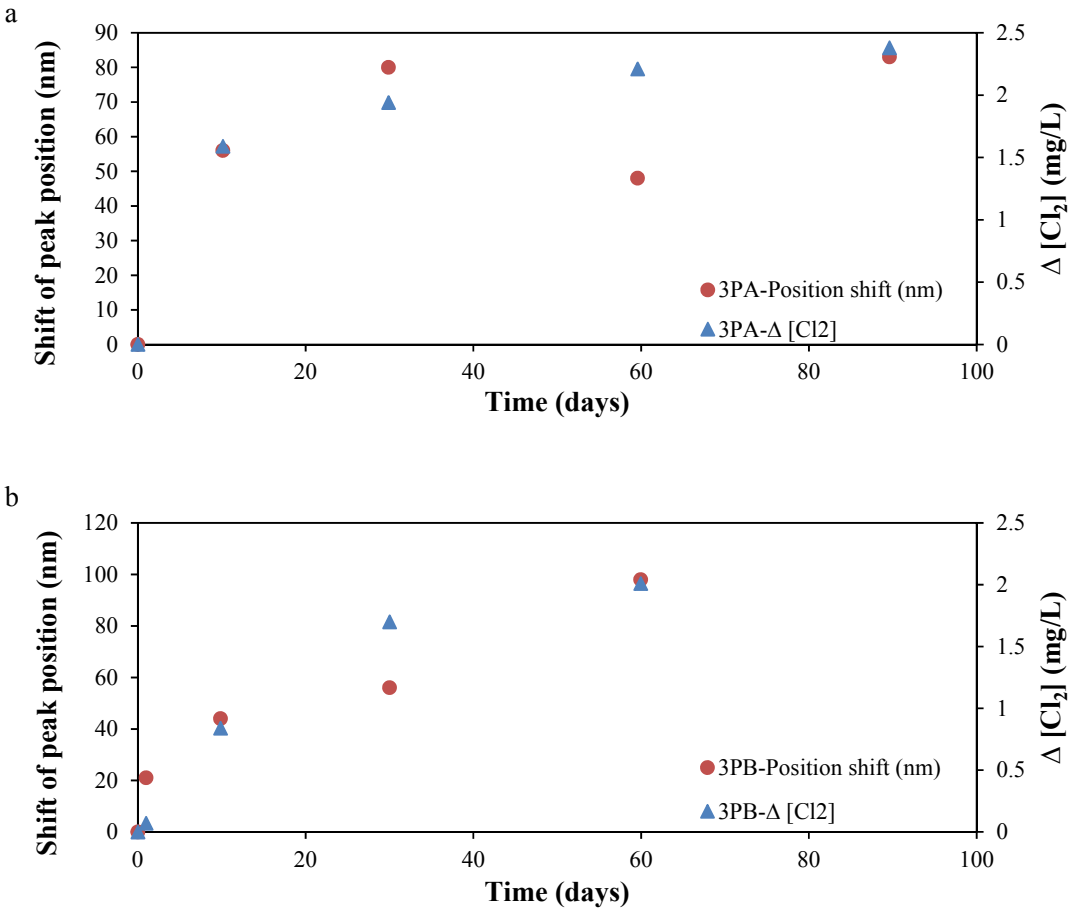

Figure 5.5 Shift of the PbO_2 NIR peak from ~1300nm and the rate of depletion of free chlorine over time for experiments a) 3PA and b) 3PB.

We attempted to correlate the observed shift in this NIR peak to possible changes occurring in the solid phase. By comparing the NIR peak observed with NIR spectra for crystalline pure phases of PbO and lead carbonates (cerussite and hydrocerussite) (Figures S.A.4 in Appendix A), it is apparent that the NIR peak observed is characteristic of PbO_2 only. The NIR peak shift was therefore not caused by the formation of an amorphous Pb(II) oxides/carbonates surface layer on the solid β-PbO_2 (Wang et al. 2013). To confirm that the peak shift was not caused by a physical mix of additional phases present on the β-PbO_2 surface, physical mixtures of β-PbO_2 with hydrocerussite at different molar ratio were analyzed (Table S.B.1 in Appendix B). The results obtained for the NIR spectra of these mixtures are presented in Figure S.B.4 in Appendix B. It is evident that the intensity of the NIR peak at 1300 nm is very sensitive to solid phases surrounding β-PbO_2. In other words, the intensity of the peak changes considerably with different mixture compositions, thereby indicating that the NIR peak observed is a distinct feature of crystalline PbO_2.

We also obtained the NIR spectra of synthesized α-PbO_2 (Figures 5.3 and 5.4), and interestingly, the position of the NIR peak of α-PbO_2 also shows a bathochromic shift relative to β-PbO_2. While it is tempting to propose that the shifts observed in the NIR spectra of the aging β-PbO_2 indicate a phase transformation to α-PbO_2, the position of the NIR peak for the samples obtained at 30 and 90 days shows a shift to even higher wavelengths (more than 50 nm) compared to the peak observed for α-PbO_2. Thus the changes in the observed spectra cannot be solely linked to a phase transition from the β to the α structure of PbO_2.

To interpret the NIR spectra, it is necessary to understand the spectroscopic origin of the NIR peak. The NIR peak observed for both α and β structures of PbO_2 is linked to an electronic transition in the band gap present in these solids. Features in the electronic spectra of lead oxides have been well studied for the applications of lead-containing thin films and glasses often used in optical technology, and more recently, for the development of transparent conducting materials (Lappe 1962; Keester and White 1969; Salagram et al. 2002a; Salagram et al. 2002b; Scanlon et al. 2011; Aly et al. 2013; Walsh et al. 2013). From these prior studies, features present in the NIR spectra of PbO_2 shown in Figure S.B.5 (Appendix B), 5.3, and 5.4 can be rationalized in terms of symmetry forbidden electronic

transitions from the upper valence band into the solid's conduction band (Scanlon et al. 2011; Walsh et al. 2013). The band gap is defined as the energy difference between the upper valence band and lower conduction band in the solid phase. Kester and White (1969) obtained a linear correlation between band edge calculated from the optical spectra of solid lead oxides and the average oxidation state, suggesting that the NIR feature arises from small amounts of Pb^{2+} present in the β and α forms of PbO_2. Since the seminal work of Kester and White (1969) much progress has been made (Salagram et al. 2002b; Scanlon et al. 2011; Walsh et al. 2013). While the electronic structures of PbO and Pb_3O_4 are now relatively well understood, the band structure of PbO_2 is still controversial. It has however been established that the NIR peak arises due to the presence of Pb^{2+} impurities that result in charge compensation occurring through electrons in the PbO_2 conduction band (Payne et al. 2009; Scanlon et al. 2011).

Using the work by Keester and White (1969) as starting point, we attempted to link the average Pb oxidation state in lead oxides with the band gap energies calculated from the UV/Vis/NIR spectra of pure PbO, Pb_3O_4, and both α and β-PbO_2. The band gap energy (E_g) was calculated using Davis and Mott's (1970) model which relates the absorption coefficient (α) to the photon energy ($h\nu$) for various electronic transitions prevalent in semiconductors. This model is given by:

$$(h\nu\alpha)^{1/n} = A\left(h\nu - E_g\right) \tag{3}$$

where h is Planck's constant, ν is the frequency of vibration, A is a proportionality constant, and n describes the electronic transition, taking values of 1/2, 3/2, 2, or 3, depending of the type of transition: direct allowed, direct forbidden, indirect allowed, and indirect forbidden. When diffuse reluctance spectra are used to calculate the band gap, Eq. 3 becomes:

$$(h\nu F(R))^{1/n} = A\left(h\nu - E_g\right) \tag{4}$$

where $F(R)$ is the Kubelka-Munk function quantifying light absorption for the solid. Although the prior studies described above indicate that the type of electronic transition observed in PbO_2 is likely to be indirect forbidden (n=3), the exact mechanism is uncertain. It is common to select the n value based on the best linear fit of the band gap edge region

in the spectra (Khan and Hogarth 1991; Hossein et al. 1994). Thus, to select the value for *n*, all the four values (1/2, 3/2, 2 and 3) were tested and used to plot $(h\nu F(R))^{1/n}$ against $h\nu$ for pure lead oxide phases (PbO, Pb_3O_4, α and β-PbO_2). We observed that n=1/2 (Table 5.4) gave the best linear fit for the edge absorption region. Thus we used the power of 2 of the Kubelka–Munk function multiplied by the photon energy, which provides the edge energy value after extrapolation to zero absorbance for amorphous semiconductors. We also performed this calculation for $Pb_{12}O_{19}$ and Pb_2O_3 after digitalizing the data originally reported for these solids by Keester and White (1986). The linear correlation between average oxidation state and calculated band gap energy is shown in Figure 5.6 for the solid phases PbO, Pb_3O_4, $Pb_{12}O_{19}$, and Pb_2O_3.

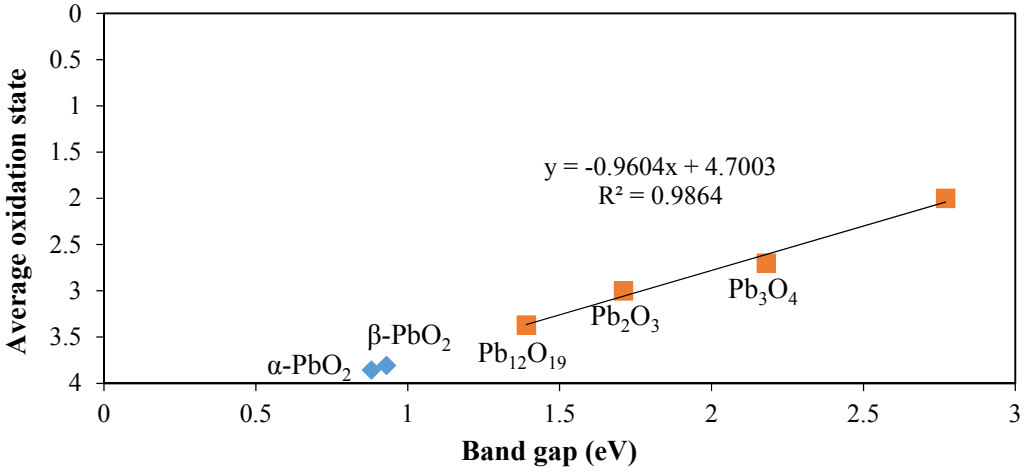

Figure 5.6 Correlation between average oxidation state and band gap edge energy obtained using PbO (massicot), Pb_3O_4, $Pb_{12}O_{19}$, and Pb_2O_3. The experimental values obtained for β-PbO_2 and α-PbO_2 are also shown.

It is well acknowledged that the NIR spectra peak (~1300 nm) is linked to the presence of Pb^{2+} defects in the PbO_2 crystalline structure. Thus we used the data shown in Figure 5.6 to extrapolate the expected band gap energy for a perfect (100% of lead species as Pb^{4+}) PbO_2 solid. Using the same correlation, we calculated the apparent number of Pb^{2+} defects present in both β-PbO_2 and α-PbO_2 solids based on their gap energies and obtained values of 9.4% and 6.8% of Pb^{2+} present in these solids, respectively (Table 5.3). Despite the uncertainty generated by the spectral resolution of the optical absorption data, this approach provides an upper limit reference for the number of defects present in the PbO_2 sample.

The values obtained for the apparent number of Pb^{2+} defects are within the same order of magnitude as those reported by Scanlon et al. (2011) using neutron scattering results.

Table 5.3 Band gap energy at different exponent n values

	Band gap				Average oxidation state	Predicted oxdiation state (n=0.5)	Pb(II)	Pb(IV)
	n=3	n=2	n=1.5	n=0.5			Amount (%)	
PbO	2.34	2.505	2.59	2.77	2		100	0
Pb_3O_4	2	2.067	2.1	2.18	2.7		65	35
Pb_2O_3	1.65	1.69	1.7	1.71	3		50	50
$Pb_{12}O_{19}$	1.34	1.36	1.36	1.39	3.37		31	69
α-PbO_2	0.787	0.825	0.84	0.88		3.86	6.8	93.2
β-PbO_2	0.89	0.905	0.91	0.93		3.81	9.4	90.6

From this analysis the changes in the NIR spectra shown in Figures 5.3 and 5.4 may be attributed to the oxidation of Pb^{2+} defects in the PbO_2 lattice by free chlorine. In contrast, the shift to shorter wavelengths observed in the control experiment (no chlorine) may be due to the formation of additional Pb^{2+} moieties resulting from PbO_2 reduction by water. If a similar approach as the one described above, which relates the calculated band gap to the number of Pb^{2+} defects in the reference lead oxides, is applied to the spectra of the solids collected during experiments 3PA and 3PB, a profile describing the amount of Pb^{4+} over time can be obtained. This plot is shown in Figure 5.7. It can be seen that the percentage of Pb^{4+} species present in the solid increases similar to the depletion of chlorine over 90 days. This increase in Pb^{4+} species is dependent of the amount of free chlorine consumed rather than the absolute value of initial chlorine concentrations. The bathochromic shift in the NIR band is, therefore, caused by a decrease in the amount of Pb^{2+} defects in PbO_2 by oxidation. This is in agreement with Izvozchikov (1972) who showed experimentally that the band gap energy value decreases as the oxidation state of Pb increases. It should be noted that the NIR band does not shift back to its original position even though the free chlorine level was lower than the threshold value for PbO_2 formation (Wang et al. 2010). This indicates that the newly generated Pb^{4+} sites remain in the crystal lattice. Thus we can propose that the NIR peak shift is not caused by adsorption of Pb^{2+} reduced from PbO_2 as this adsorption only affects the surface of the crystal. Furthermore, we can hypothesize that the new form of crystalline PbO_2 oxidized by free chlorine with less Pb^{2+} impurities has a more stable crystalline structure than the initial β-PbO_2 phase in

our system. The formation of a more stable structure explains why low final dissolved lead concentrations were observed even when chlorine was completely consumed and the ORP levels were low.

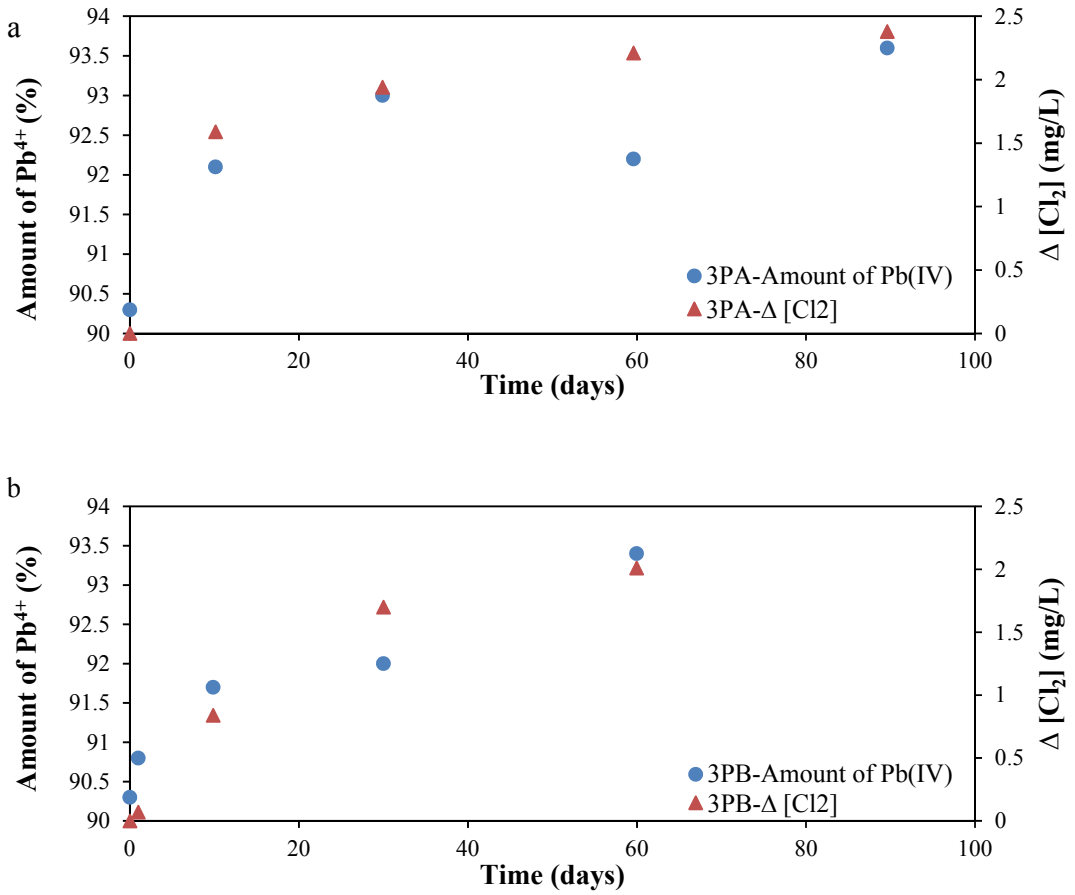

Figure 5.7 Correlation obtained between the percentage lead atoms present as Pb^{4+} ions in PbO_2 as obtained from the NIR band edge energy calculation and the consumption of free chlorine over time for experiments a) 3PA and b) 3PB.

5.2.3.2 Raman spectra

To correlate the observed NIR peak shift and associated band gap changes with morphological changes to β-PbO_2 that may have taken place during dissolution, we attempted to obtain the IR spectra of the solid samples. Previous studies indicate that heavy metal oxides such as PbO_2 do not exhibit IR bands above 400 cm^{-1}, but they appear below the detection limit of most IR detectors, even though they have relatively large cross sections (Nelson and Exarhos 1979). In contrast, PbO_2 phase displays Raman allowed transitions but it has extremely low cross sections (Black et al. 1995; Burgio et al. 2001;

Aze et al. 2008). We characterized samples from experiment 3PB using a 633 nm laser at 613 uW power under which conditions the degradation of PbO_2 and other lower valence lead oxide phases is unlikely to occur (Burgio et al. 2001). The Raman spectra for pure crystalline reference compounds are provided in Appendix A (Figure S.A.6). For β-PbO_2, characteristic peaks appear at 147, 286, and 337 cm^{-1} and are attributed to the vibrational stretching of Pb-O bonds (Trettenhahn et al. 1993; Black et al. 1995; Dan et al. 1996; Burgio et al. 2001).

The Raman spectra obtained for the experiment 3PB solid samples are shown in Figure 5.8, together with the spectra obtained for crystalline PbO and β-PbO_2. The Raman spectra for PbO shows similar characteristic peaks as pure β-PbO_2 and samples from experiment 3PB (Figure 5.8). This observation is consistent with the fact that oxygen vacancies and Pb^{2+} coexist in crystalline PbO_2. PbO_2 is known to be an extremely weak light scatterer because of the intense absorption of any scattered radiation by the crystal itself and fluorescence phenomena (Bullock et al. 1983; Black et al. 1995; Burgio et al. 2001). Compared with PbO_2, Pb(II) oxides give a more intense Raman signal. Thus it is plausible to assume that the spectral features observed at 147, 286, and 337 cm^{-1} reflect the presence of Pb(II)-O rather than Pb(IV)-O, as Raman scattering by Pb^{2+} overwhelms the Pb^{4+} signal. This is consistent with our earlier calculations which indicate that more than six percent of the total lead content in the aging β-PbO_2 samples is present as Pb^{2+}.

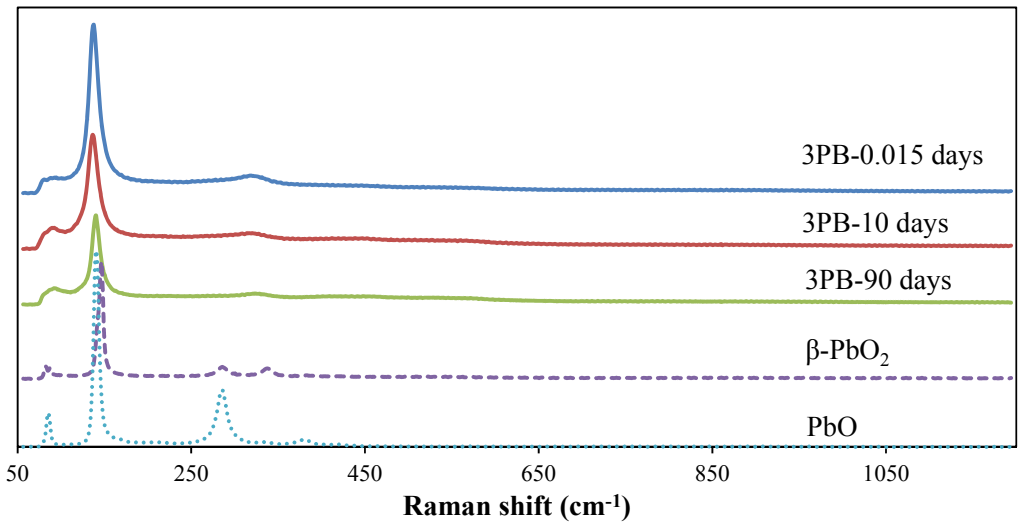

Figure 5.8 Raman spectra obtained on the solids collected during experiment 3PB.

The characteristic peak in the spectra obtained for the experiment 3PB samples shifted from 147 cm^{-1} (β-PbO_2) to 138 cm^{-1} at 20 minutes and to 136 cm^{-1} at 10 days (Figure 5.8). At 90 days, this peak shifted back to 140 cm^{-1} - the same position as the characteristic peak of PbO and also of α-PbO_2 (Figure S.A.6 in Appendix A). This indicates after 90 days the Pb(II)-O bonds in the aging β-PbO_2 sample tended to be organized similarly to those in PbO or α-PbO_2. It is worth noting that Raman signals around 1045 cm^{-1} which indicate C-O symmetric stretching of carbonates were not observed (Dan et al. 1996). This suggests that lead carbonates were not formed during the experiment. The Raman results thus suggest that either the Pb(II)-O structure is being changed or that a phase transformation (β- to α-PbO_2) is taking place due to oxidation by chlorine through the dissolution experiment.

5.2.3.3 XRD

Since PbO_2 is more sensitive to X-ray diffraction (XRD) than Raman, XRD was used to characterize the aging soild samples from experiment 3PA (Figure 5.9). Pure β-PbO_2 shows characteristic diffraction peaks at 29.6°, 37.4°, and 57.7°(Bullock et al. 1983). No characteristic peak shift or new peak was present in the diffractogram even after 200 days, indicating that β-PbO_2 is the only crystalline phase through the dissolution experiment.

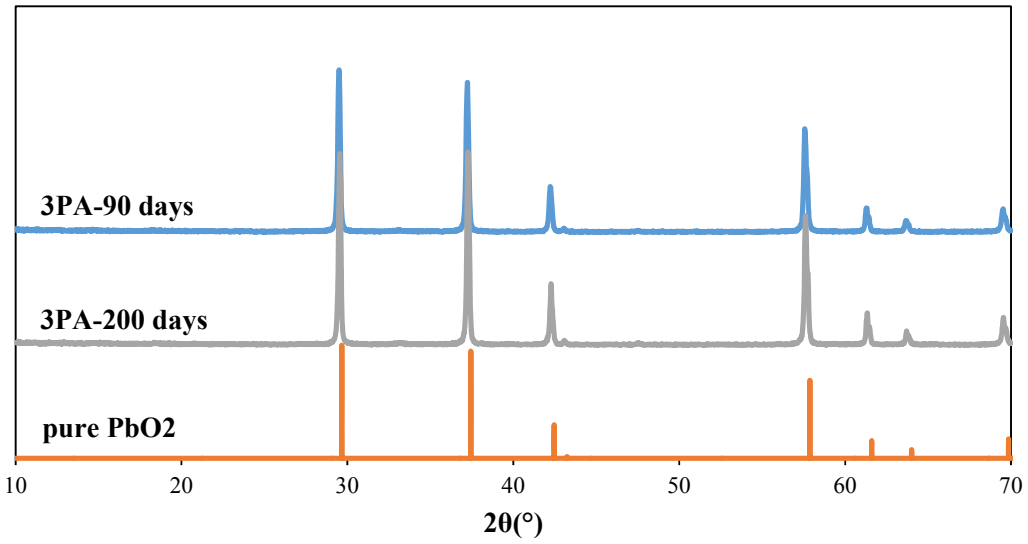

Figure 5.9 XRD patterns obtained on solids collected during experiment 3PA (initial chlorine concentration of 2.5 mg/L).

5.2.3 Proposed dissolution mechanism

The solid phase analysis indicates that the dominant crystalline phase through the dissolution experiment was β-PbO_2. As observed in the XRD, this phase did not transform to another crystalline phase. However, the shift in the peak position in the Raman spectra suggests that the Pb-O bond in the crystal changed over time at the molecular level. The NIR spectra of samples collected from experiments 3PA and 3PB are the most informative (Figure 5.5). For both experiments 3PA and 3PB, the shift in the NIR peak position and the associated changes in average oxidation state of the Pb in PbO_2 directly followed the consumption of free chlorine. This result suggests that the driving force for these changes is the amount of oxidant consumed over time rather than the absolute value of initial oxidant available. It is expected that further changes in the electronic structure of β-PbO_2 would occur over time if there more initial chlorine was available for consumption. Aging samples collected from the control test (no chlorine) showed a slightly hypsochromic shift in the NIR peak position supporting our observation that the consumption of free chlorine governs changes to the electronic structure of β-PbO_2.

The Pb(IV) oxide phase with a different electronic structure than the initial β-PbO_2 phase likely formed on the surface of the solid matrix, controlling the dissolution of lead into the aqueous phase over time. This new form of the solid phase had a relatively low solubility under our experimental conditions when chlorine was completely depleted and water was the only available reductant. The presence of this surface phase also explains why dissolved lead concentrations were higher in the control test (no chlorine) compared to experiments 2PA and 3PA, despite the higher ORP values in the control test. The different final dissolved lead levels between the control test and experiments 2PA and 3PA indicate that free chlorine changed the morphology of the β-PbO_2 phase to a more stable structure. These further suggests that the changes in the structure of β-PbO_2 has a controlling influence on the solubility of the more stable PbO2 phase compared with the ORP, even though theoretically ORP governs the solubility of β-PbO_2. The morphological changes observed to PbO_2 may be the main reason why much lower dissolved lead concentrations were observed in our experiments, compared with prior experiments conducted without free

chlorine (e.g. (Lin and Valentine 2008a; Lin and Valentine 2008b; Lin and Valentine 2009)).

In contrast to our experimental findings, higher dissolved lead concentrations have been observed in DWDS that use a disinfectant other than free chlorine even though PbO_2 is found uniformly layered on the surface of the corrosion scale. Prior studies have attributed the higher lead concentrations to the reduction of PbO_2 which is triggered by the low ORP levels associated with the use of chloramines. Our results however show that lead concentrations below actions level (10 μg/L) can occur even under low ORP conditions. Reductants naturally present in drinking water, such as NOM and reductive ions (Fe^{2+} and Mn^{2+}), may be able to reduce this more stable PbO_2 phase and transform it into more soluble Pb(II) solids. These reductive species may be the reason for inconsistent observations between our work and prior field studies. Our results indicate that the priority for corrosion control strategies should be to decrease the concentration of reductants in drinking water, especially for municipalities with lead-bearing plumbing that intend to switch disinfectant. Oxidative treatment or granular activated carbon may be used to remove the reductants.

5.3 References

Aly, S. A., M. A. Kaid and N. Z. El-Sayed (2013). "Some Optical Aspects of Thermally Evaporated Lead Oxide Thin Films." Acta Physica Polonica, A. **124**(4).

Aze, S., P. Delaporte, J. M. Vallet, V. Detalle, O. Grauby and A. Baronnet (2008). Towards the restoration of darkened red lead containing mural paintings: A preliminary study of the β-PbO2 to Pb3O4 reversion by laser irradiation. Lasers in the Conservation of Artworks: Proceedings of the International Conference Lacona VII, Madrid, Spain, 17-21 September 2007, CRC Press.

Bagshaw, N. E., R. L. Clarke and B. Halliwell (1966). "The preparation of lead dioxide for X-ray diffraction studies." Journal of Applied Chemistry **16**(6): 180-184.

Black, L., G. C. Allen and P. C. Frost (1995). "Quantification of Raman spectra for the primary atmospheric corrosion products of lead." Applied spectroscopy **49**(9): 1299-1304.

Bullock, K. R., G. M. Trischan and R. G. Burrow (1983). "Photoelectrochemical and microprobe laser Raman studies of lead corrosion in sulfuric acid." Journal of The Electrochemical Society **130**(6): 1283-1289.

Burgio, L., R. J. Clark and S. Firth (2001). "Raman spectroscopy as a means for the identification of plattnerite (PbO2), of lead pigments and of their degradation products." Analyst **126**(2): 222-227.

Dan, A. C., J. H. C. Robin, L. J. M. and O. Marianne (1996). "Studies on the thermal decomposition of basic lead (II) carbonate by Fourier-transform Raman spectroscopy, X-ray diffraction and thermal analysis." Journal of the Chemical Society, Dalton Transactions(18): 3639-3645.

Delahay, P., M. Pourbaix and P. Van Rysselberghe (1951). "Potential-pH Diagram of Lead and its Applications to the Study of Lead Corrosion and to the Lead Storage Battery." Journal of the Electrochemical Society **98**(2): 57-64.

Edwards, M. and A. Dudi (2004). "Role of chlorine and chloramine in corrosion of lead-bearing plumbing materials." Journal of the American Water Works Association **96**(10): 69-81.

Hossein, A. A., C. A. Hogarth and J. Beynon (1994). "Optical absorption in CeO_2-V_2O_5 evaporated thin films." Journal of Materials Science Letters **13**(15): 1144-1145.

Keester, K. L. and W. B. White (1969). "Electronic spectra of the oxides of lead and of some ternary lead oxide compounds." Materials Research Bulletin **4**(10): 757-764.

Khan, G. A. and C. A. Hogarth (1991). "Optical absorption spectra of evaporated V_2O_5 and co-evaporated V_2O_5/B_2O_3 thin films." Journal of Materials Science **26**(2): 412-416.

Kim, E. J. and J. E. Herrera (2010). "Characteristics of lead corrosion scales formed during drinking water distribution and their potential influence on the release of lead and other contaminants." Environmental Science and Technology **44**(16): 6054-6061.

Lappe, F. (1962). "Some physical properties of sputtered PbO_2 films." Journal of Physics and Chemistry of Solids **23**(11): 1563-1566.

Li, X. H., D. Pletcher and F. C. Walsh (2011). "Electrodeposited lead dioxide coatings." Chemical Society Reviews **40**(7): 3879-3894.

Lin, Y.-P. and R. L. Valentine (2008a). "Release of Pb (II) from monochloramine-mediated reduction of lead oxide (PbO2)." Environmental Science and Technology **42**(24): 9137-9143.

Lin, Y. and R. L. Valentine (2008b). "The release of lead from the reduction of lead oxide (PbO2) by natural organic matter." Environmental Science and Technology **42**(3): 760-765.

Lin, Y. and R. L. Valentine (2009). "Reduction of Lead Oxide (PbO2) and Release of Pb(II) in Mixtures of Natural Organic Matter, Free Chlorine and Monochloramine." Environmental Science and Technology.

Lin, Y. P. and R. L. Valentine (2010). "Reductive dissolution of lead dioxide (PbO2) in acidic bromide solution." Environmental Science and Technology **44**(10): 3895-3900.

Liu, H., G. V. Korshin and J. F. Ferguson (2008). "Investigation of the kinetics and mechanisms of the oxidation of cerussite and hydrocerussite by chlorine." Environmental Science and Technology **42**(9): 3241-3247.

Lytle, D. A. and M. R. Schock (2005). "Formation of Pb (IV) oxides in chlorinated water." Journal of the American Water Works Association **97**(11): 102-114.

Nelson, B. N. and G. J. Exarhos (1979). "Vibrational spectroscopy of cation-site interactions in phosphate glasses." Journal of Chemical Physics **71**(7): 2739-2747.

Payne, D. J., G. Paolicelli, F. Offi, G. Panaccione, P. Lacovig, G. Beamson, A. Fondacaro, G. Monaco, G. Vanko and R. G. Egdell (2009). "A study of core and valence levels in β-PbO_2 by hard X-ray photoemission." Journal of Electron Spectroscopy and Related Phenomena **169**(1): 26-34.

Pourbaix, M. (1974). Atlas of electrochemical equilibria in queous solutions. Houston, TX, National Association of Corrosion Engineers.

Salagram, M., V. Krishna Prasad and K. Subrahmanyam (2002a). "Optical band gap studies on xPb_3O_4–$(1-x)$ P_2O_5 lead [(II, IV)] phosphate glasses." Optical Materials **18**(4): 367-372.

Salagram, M., V. K. Prasad and K. Subrahmanyam (2002b). "IR and optical study of Pb_3O_4 (2PbO. PbO_2) glass containing a small amount of silica." Journal of Alloys and Compounds **335**(1): 228-232.

Scanlon, D. O., A. B. Kehoe, G. W. Watson, M. O. Jones, W. I. F. David, D. J. Payne, R. G. Egdell, P. P. Edwards and A. Walsh (2011). "Nature of the Band Gap and Origin of the Conductivity of PbO_2 Revealed by Theory and Experiment." Physical Review Letters **107**(24): 246402.

Schock, M. R. and R. Giani (2004). Oxidant/disinfectant chemistry and impacts on lead corrosion. Proceedings of 2004 American Water Works Association Water Quality and Technology Conference.

Schock, M. R., S. M. Harmon, J. Swertfeger and R. Lohmann (2001). "Tetravalent lead: a hitherto unrecognized control of tap water lead contamination." Proceedings AWWA Water Quality Technology Conference, Nashville: 11-15.

Schock, M. R., K. Scheckel, M. DeSantis and T. L. Gerke (2005). Mode of occurrence, treatment, and monitoring significance of tetravalent lead. Proceedings AWWA Water Quality Technology Conference. Quebec City, Quebec.

Schock, M. R., I. Wagner and R. Oliphant (1996). The corrosion and solubility of lead in drinking water. Internal corrosion of water distribution systems. Denver, CO., AWWA Research Foundation/TZW**:** 131-230.

Shi, Z. and A. T. Stone (2009). "PbO2 (s, plattnerite) reductive dissolution by aqueous manganous and ferrous ions." Environmental Science and Technology **43**(10): 3596-3603.

Switzer, J. A., V. V. Rajasekharan, S. Boonsalee, E. A. Kulp and E. W. Bohannan (2006). "Evidence that monochloramine disinfectant could lead to elevated Pb levels in drinking water." Environmental Science and Technology **40**(10): 3384-3387.

Trettenhahn, G. L. J., G. E. Nauer and A. Neckel (1993). "Vibrational spectroscopy on the PbO-$PbSO_4$ system and some related compounds: Part 1. Fundamentals, infrared and Raman spectroscopy." Vibrational spectroscopy **5**(1): 85-100.

Walsh, A., A. B. Kehoe, D. J. Temple, G. W. Watson and D. O. Scanlon (2013). "PbO2: from semi-metal to transparent conducting oxide by defect chemistry control." Chemical Communications **49**(5): 448-450.

Wang, Y., J. Wu and D. E. Giammar (2012). "Kinetics of the reductive dissolution of lead(IV) oxide by iodide." Environmental Science and Technology **46**(11): 5859-5866.

Wang, Y., J. Wu, Z. Wang, A. Terenyi and D. E. Giammar (2013). "Kinetics of lead(IV) oxide (PbO2) reductive dissolution: role of lead(II) adsorption and surface speciation." Journal of Colloid Interface Science **389**(1): 236-243.

Wang, Y., Y. Xie, W. Li, Z. Wang and D. E. Giammar (2010). "Formation of lead (IV) oxides from lead (II) compounds." Environmental Science and Technology **44**(23): 8950-8956.

Xie, Y., Y. Wang and D. E. Giammar (2010a). "Impact of chlorine disinfectants on dissolution of the lead corrosion product PbO2." Environmental Science and Technology **44**(18): 7082-7088.

Xie, Y., Y. Wang, V. Singhal and D. E. Giammar (2010b). "Effects of pH and carbonate concentration on dissolution rates of the lead corrosion product PbO2." Environmental Science and Technology **44**(3): 1093-1099.

Chapter 6

6 Conclusions and recommendations

6.1 Conclusions

Both minium (Pb_3O_4) and plattnerite (β-PbO_2) have been previously identified in lead corrosion scales present in DWDS. The destabilization of these lead oxides by changes in water treatment processes can result in elevated dissolved lead in drinking water. The solubility and dissolution mechanisms for Pb_3O_4, hypothesized as an intermediate lead-oxide phase, are not well understood. In contrast, some literature investigated the dissolution mechanisms for β-PbO_2, however, very few studies have examined long-term dissolution for both Pb_3O_4 and β-PbO_2 under depleting chlorine conditions.

In this thesis, the solubility of Pb_3O_4 was studied under representative drinking water conditions. The lead release profile revealed three distinct stages during 200 days long-term dissolution experiments. Free chlorine acted as driving force in the dissolution of Pb_3O_4, and affected the rate of Pb_3O_4 dissolution in the first stage. With free chlorine depleting in Stage II, the dissolved lead levels rebounded and reached a spike. Final dissolved lead concentrations at equilibrium in Stage III were about 0.1 mg/L and independent of the initial free chlorine concentrations.

The Pb_3O_4 dissolution mechanisms were explored by detailed characterization of the solid samples via FTIR, UV/Vis/NIR, XRD, and Raman spectrometry, and detailed analysis of the changes in water quality during the dissolution experiments. The proposed dissolution mechanism included the transient formation of amorphous PbO species from 30 to 90 days in Stage III during dissolution. As the time progressed β-PbO_2 formed together with cerussite and hydrocerussite. Shifts of characteristic peak of Pb_3O_4 in the IR spectra suggested that the Pb(IV)-O bond present in the octahedral arrangement hosting the Pb^{4+} ions in Pb_3O_4 was distorted from its original form during dissolution. Based on these characterization results we proposed that Pb_3O_4 dissolves through a disproportionation reaction followed by the reduction of β-PbO_2 by water in the absence of free chlorine.

A similar experimental approach was used to study β-PbO_2 dissolution under depleting chlorine conditions. Results indicated that while initial free chlorine concentrations play a minor role in determining the final dissolved lead levels, they do affect the long-term PbO_2 stability. Steady low dissolved lead levels were observed even in the absence of residual chlorine for more than 100 days after chlorine was depleted. This result contradicts previous literature studies that have examined β-PbO_2 in the absence of free chlorine.

Characterization of solid samples collected through the β-PbO_2 dissolution experiments using NIR spectroscopy indicated that the consumption of chlorine caused changes in the electronic structure of the solid resulting in the depletion of Pb^{2+} defects in the PbO_2 structure. The XRD patterns of the solid samples indicated that the only crystalline phase present during the experiment was still β-PbO_2. However the Raman spectra revealed a shift in the Pb(II)-O vibrational peaks, suggesting changes in Pb-O bonds or the formation of amorphous PbO species on surface layer of β-PbO_2 crystal. Our overall observations were rationalized in terms of lead (IV) oxide with a distinct electronic structure forming on the surface of crystalline β-PbO_2 during dissolution.

6.2 Recommendations

In this thesis, we found that the initial availability of free chlorine can effectively depress the release of dissolved lead from Pb_3O_4. However, our experiments showed that lead concentrations will rebound to above action levels immediately when residual chlorine depletes. We hypothesized that if chloramine is used as disinfectant dissolved lead concentrations could potentially be elevated in customers' tap when Pb_3O_4 is present in the lead corrosion scale formed in the DWDS. This scenario needs to be further explored. Further research on the dissolution of Pb_3O_4 under constant free chlorine concentration conditions is also necessary to fully understand the solid phase transformations taking place under high ORP conditions. This will also complement the work conducted by groups in the U.S. on the study of the dissolution of β-PbO_2 at constant chlorine residuals.

Our results also indicated that the solubility of β-PbO_2 with a modified electronic structure was well below action levels even after chlorine depleted completely. This contradicts previous studies suggested that β-PbO_2 transforms into phases with high solubility under

low ORP conditions. On the other hand, this result suggests that the changes in electronic structure of β-PbO_2 govern the dissolution and solubility of this solid phase. Low dissolved lead concentrations have not been observed in real DWDS in the absence of free chlorine. This indicates that concentrations of reductant species such as NOM and Fe^{2+} in treated water play a role in lead dissolution. The impact of the reductants on the dissolution of β-PbO_2 with a modified electronic structure needs to be addressed in future work.

Scrutinyite (α-PbO_2) has been observed in corrosion scales, and identified as the final product obtained in chlorinated water under relatively high pH conditions (>10). Thus the study of the dissolution of α-PbO_2 under depleting chlorine conditions could provide information on the solid phase transformations taking place during this process.

Actual field lead corrosion scales collected from lead pipes extracted from a DWDS should also be analyzed and subjected to the experimental protocols presented in this work as their composition and transformation are strongly linked to the water quality and historic changes in the DWDS. This information is needed to better understand the stability of corrosion scales in real DWDS, and to evaluating the effectiveness of long-term corrosion control strategies.

Appendix A

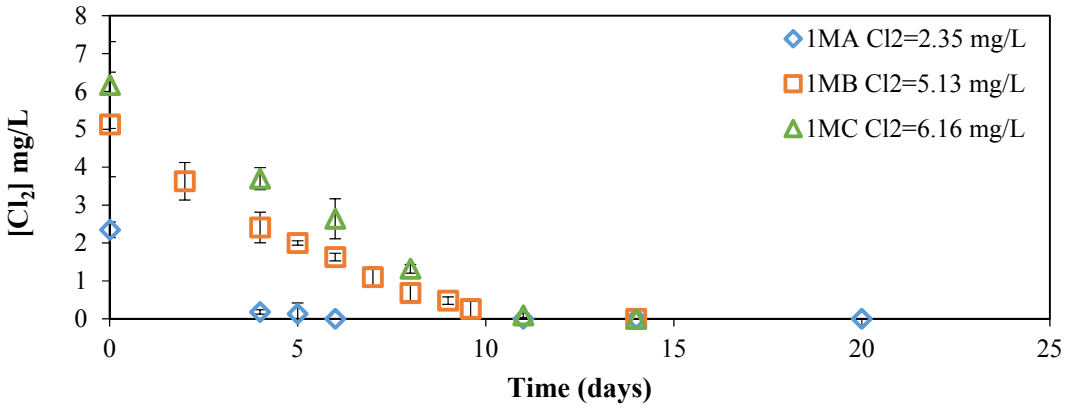

Figure S.A.1 Free chlorine concentrations observed during experiments 1MA, 1MB, and 1MC.

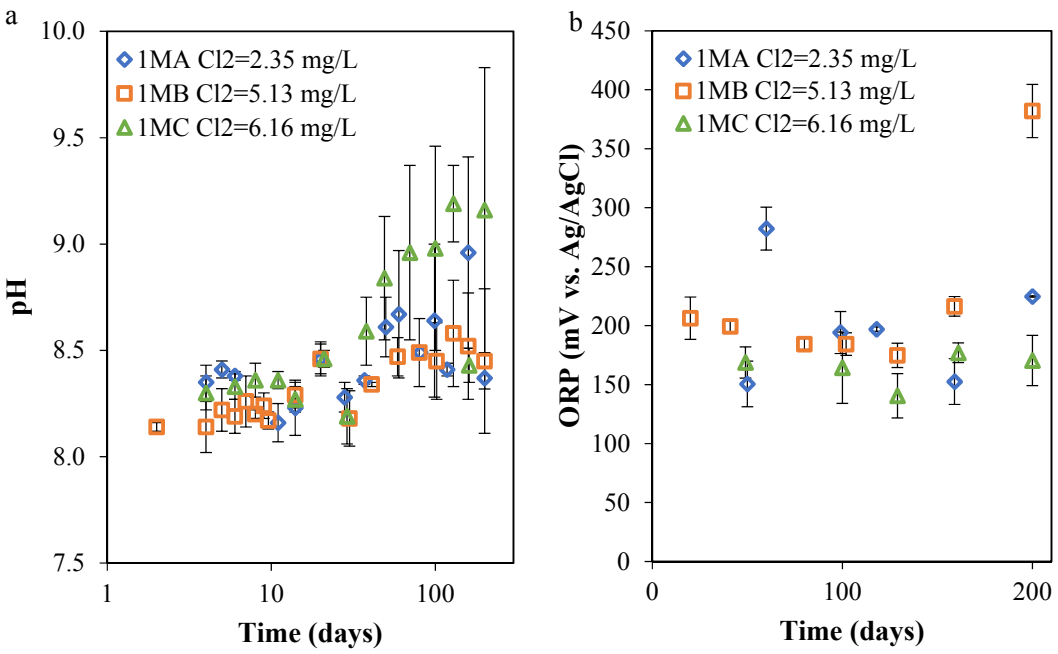

Figure S.A.2 a) pH and b) ORP values obtained during experiments 1MA, 1MB, and 1MC.

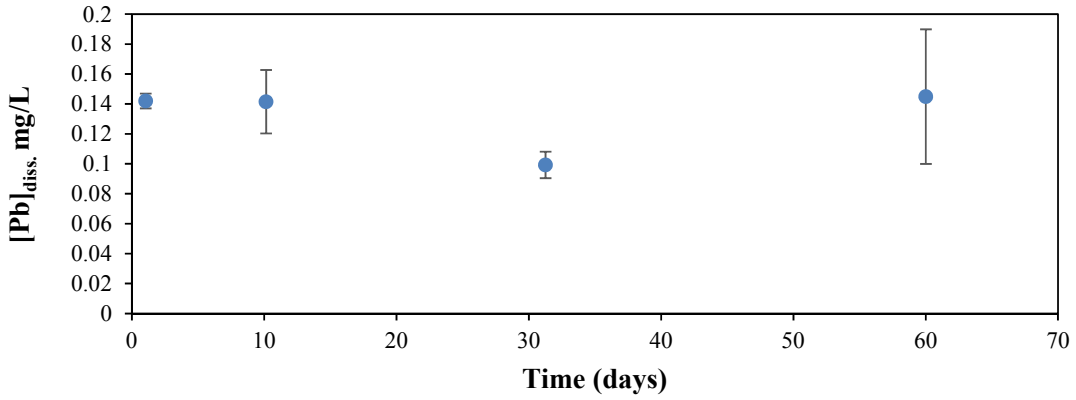

Figure S.A.3 Dissolved lead concentrations observed during Pb_3O_4 dissolution of the control test.

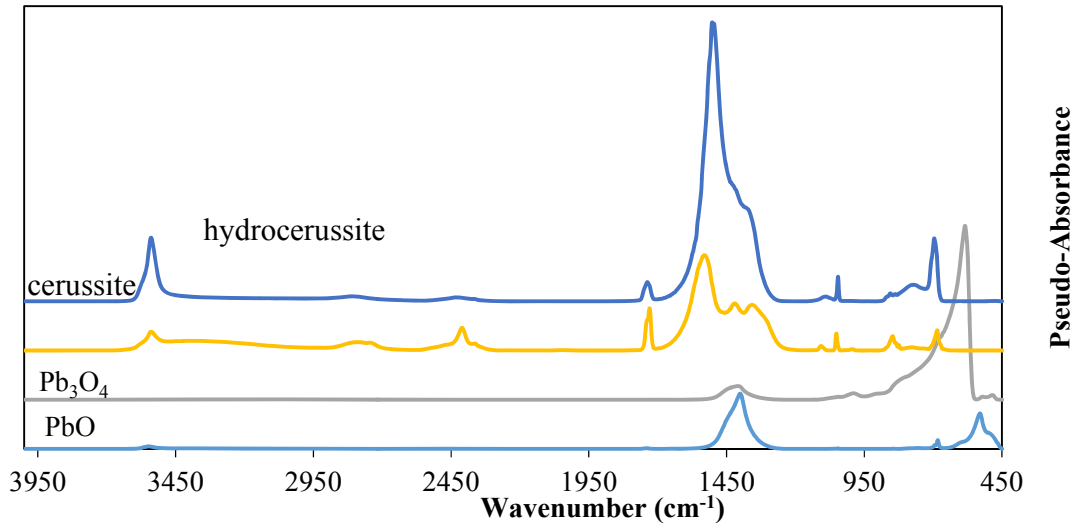

Figure S.A.4 FTIR spectra of pure hydrocerussite, cerussite, PbO, and Pb_3O_4.

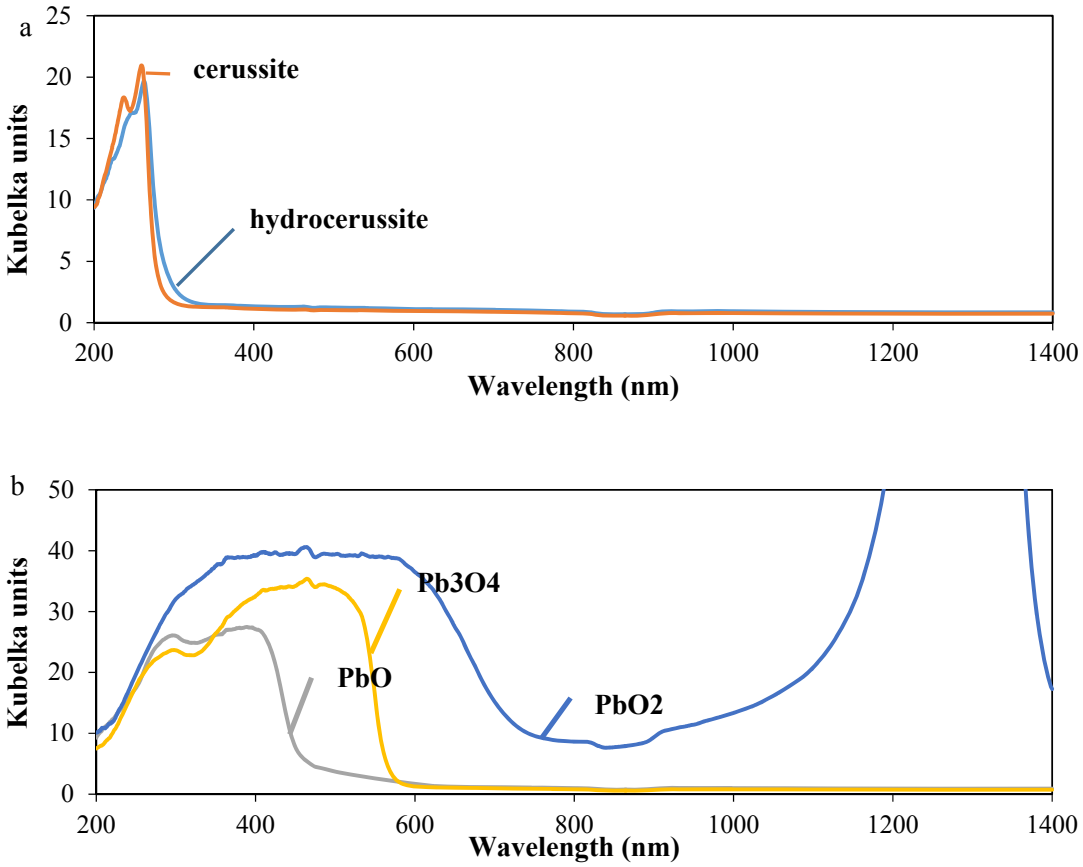

Figure S.A.5 UV/Vis/NIR spectra of pure a) hydrocerussite and cerussite, b) PbO, Pb_3O_4, and PbO_2 as standard.

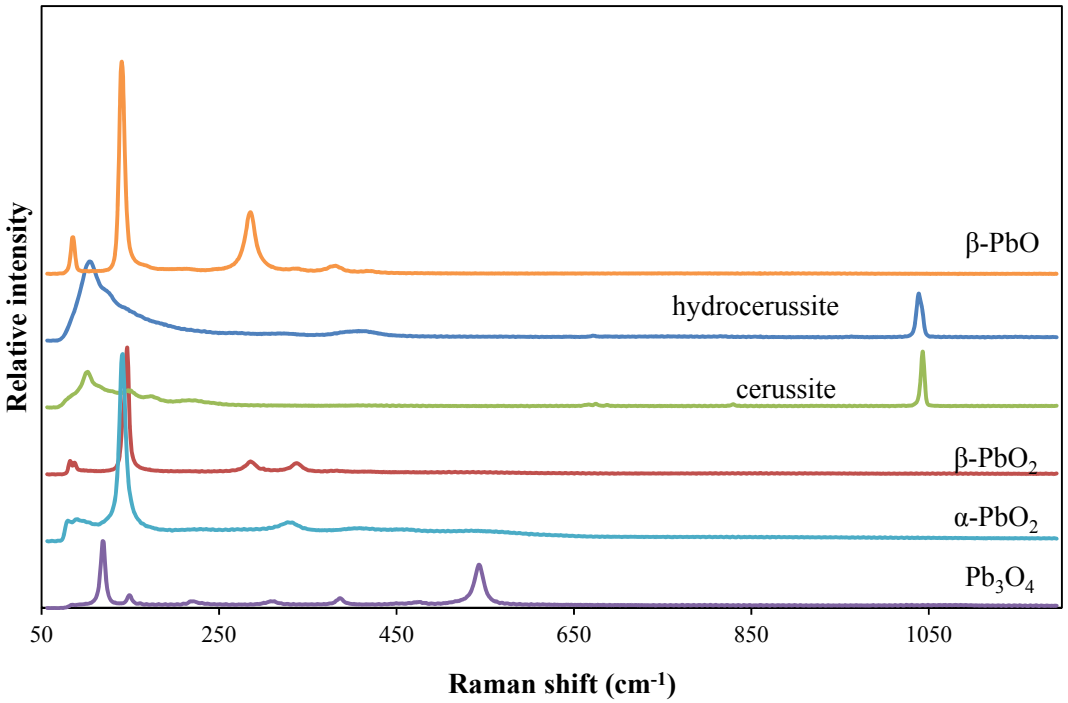

Figure S.A.6 Raman spectra of pure hydrocerussite, cerussite, β-PbO, Pb_3O_4, and PbO_2.

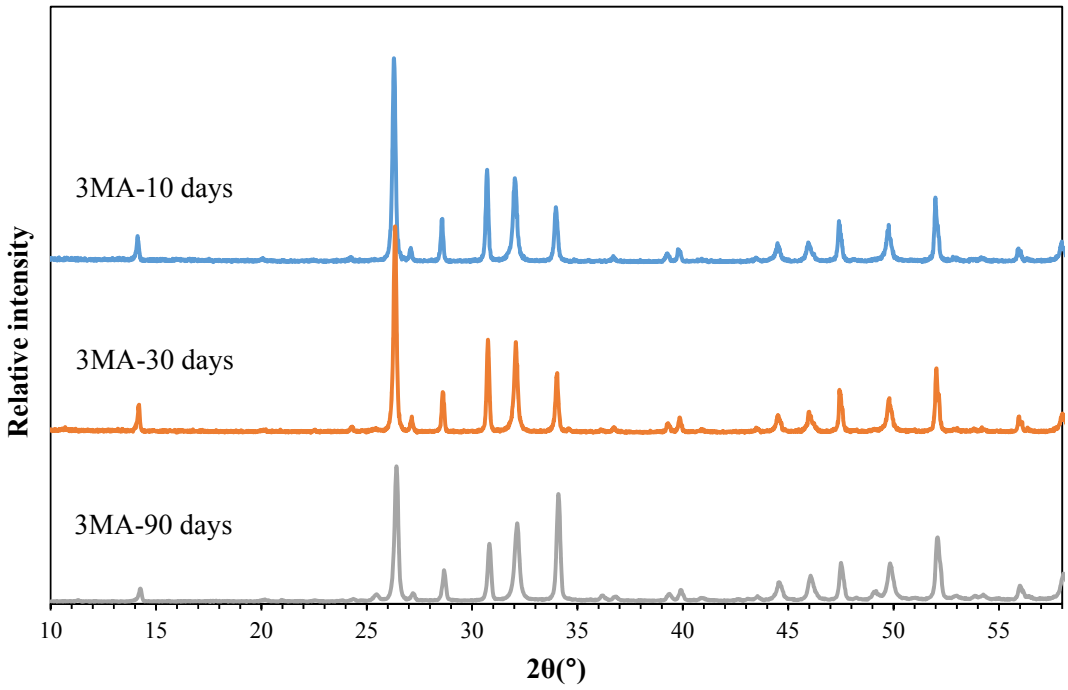

Figure S.A.7 XRD patterns obtained on solid samples collected for experiment 3MA

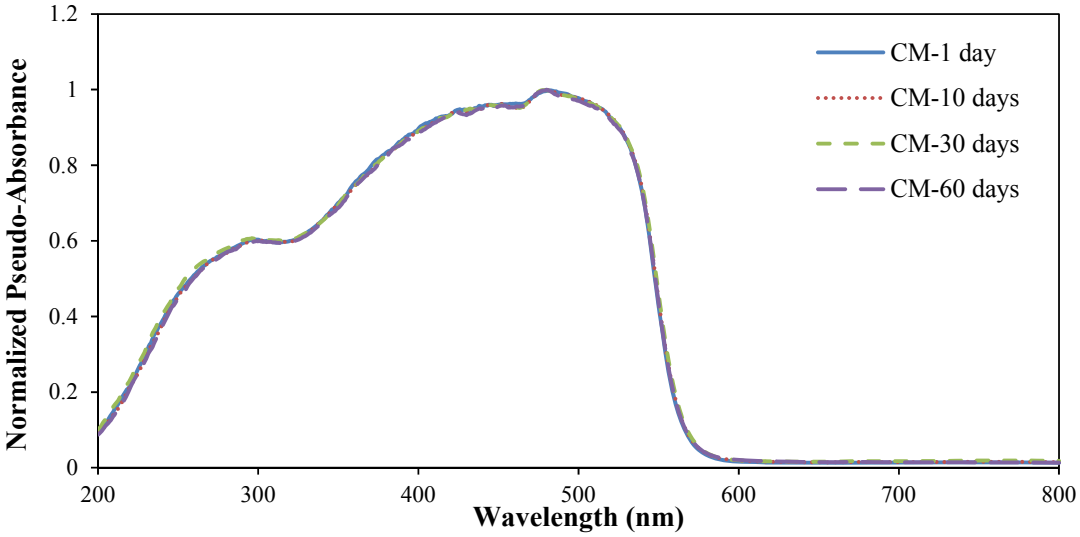

Figure S.A.8 Normalized NIR spectra of solids from control test of Pb_3O_4 dissolution experiment (CM) without free chlorine.

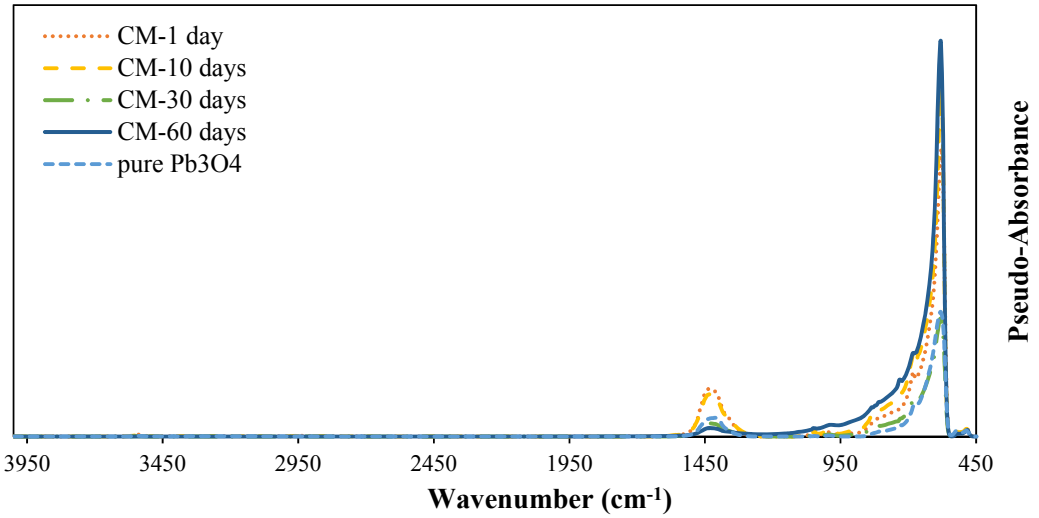

Figure S.A.9 FTIR spectra of solids from control test of Pb_3O_4 dissolution experiment (CM) without free chlorine.

Appendix B

Table S.B.1 Synthetic lead compounds

Hyc^{*}/Pb_xO_y	Molar ratio								Corresponding mass ratio							
No.	1	2	3	4	5	6	7	8	1	2	3	4	5	6	7	8
Pb_3O_4	0.1	N/A	0.2	0.33	1	3	5	10	0.12	N/A	0.23	0.39	1.13	3.35	5.60	11.08
PbO	0.1	0.167	0.2	N/A	1	3	5	N/A	0.35	0.58	0.7	N/A	3.39	10.35	17.13	N/A
β-PbO_2	0.1	N/A	0.2	0.33	1	3	5	N/A	0.32	N/A	0.65	1.08	3.21	9.45	16.24	N/A

Note: *Hyc is hydrocerussite

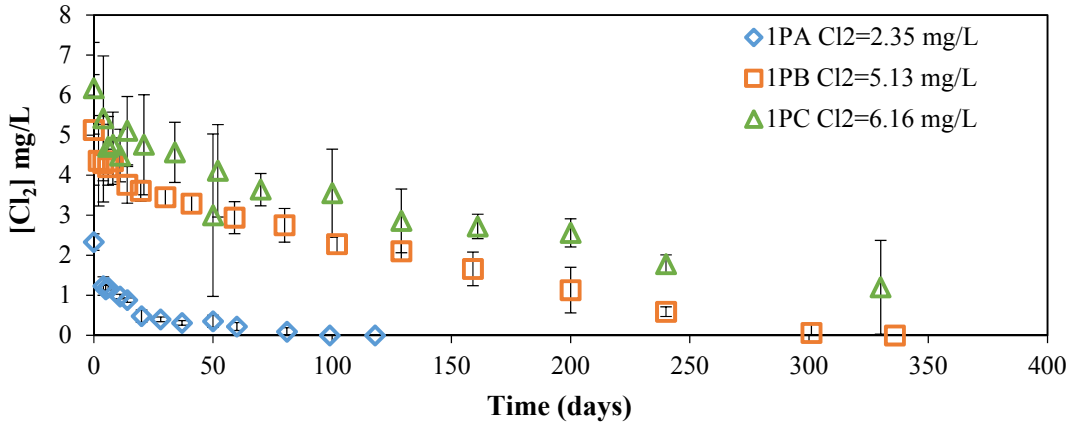

Figure S.B.1 Free chlorine concentrations observed during experiments 1PA, 1PB, and 1PC.

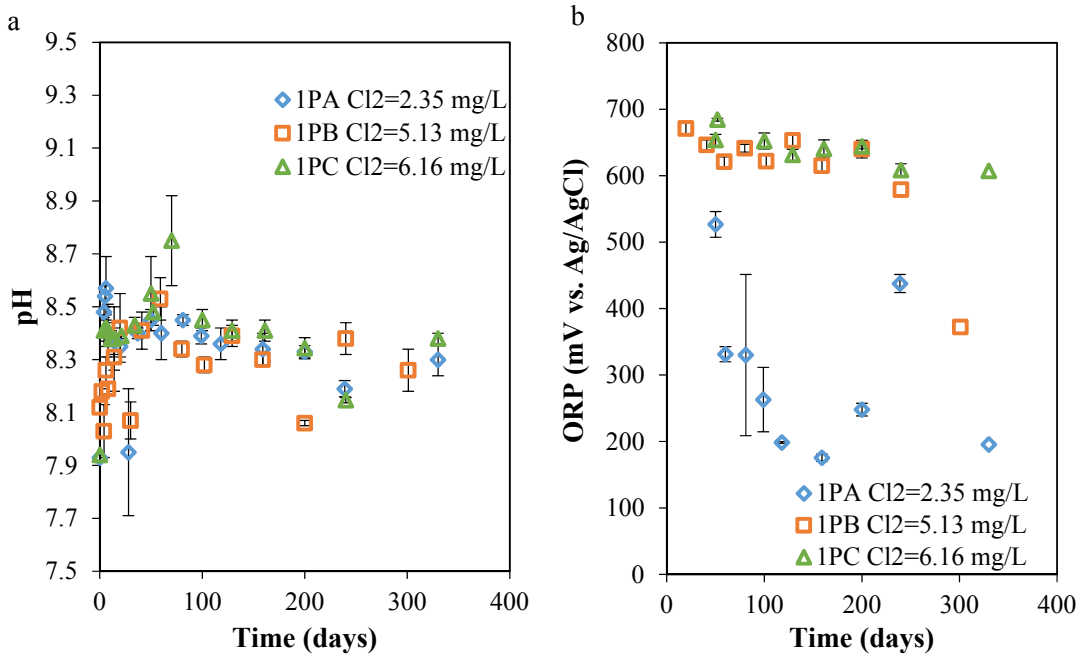

Figure S.B.2 a) pH and b) ORP values obtained during experiments 1PA, 1PB, and 1PC.

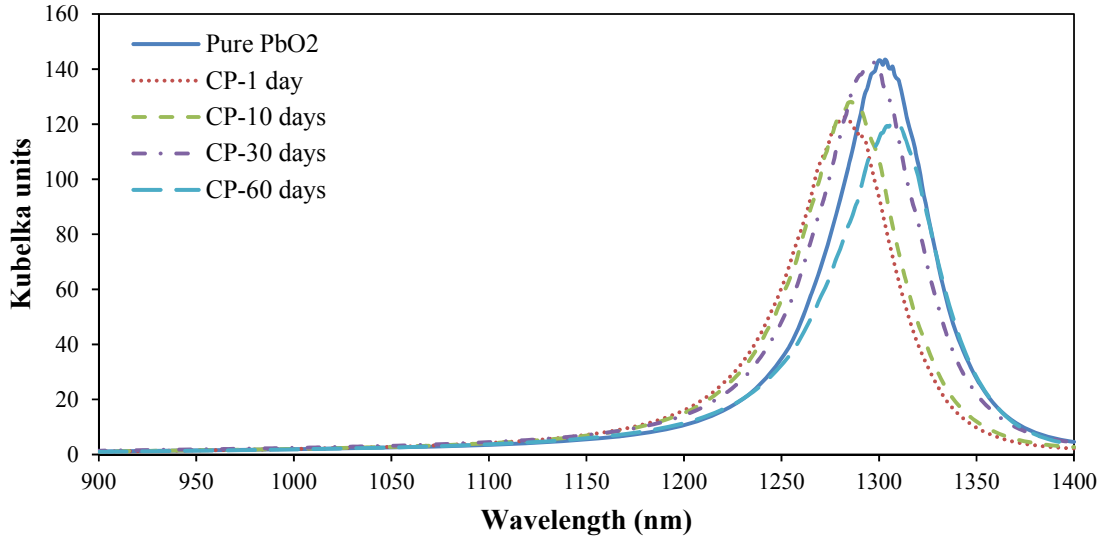

Figure S.B.3 NIR spectra of solids from the control test of β-PbO_2 reaction (CP) in the absence of free chlorine.

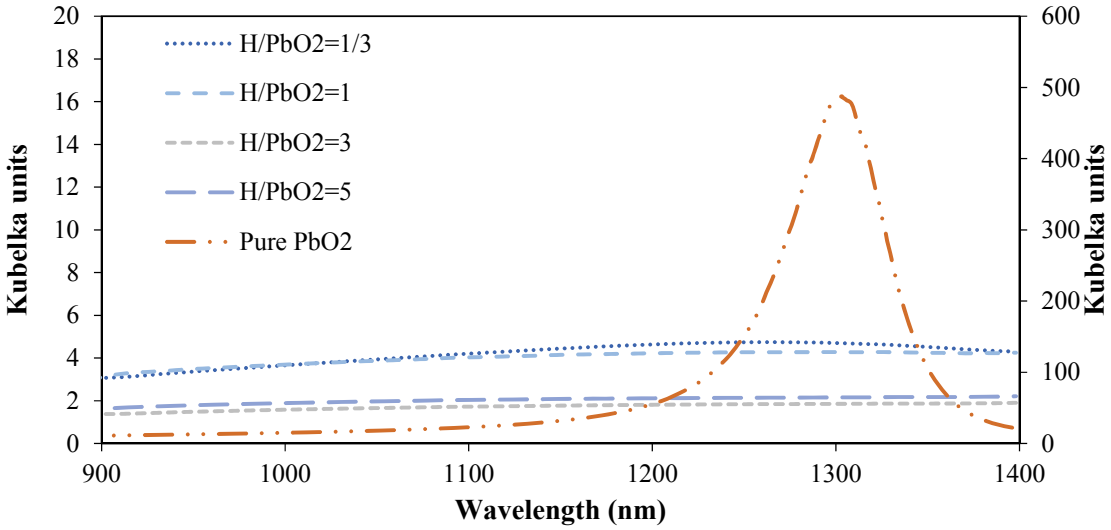

Figure S.B.4 NIR spectra of physical mixtures of β-PbO_2 and hydrocerussite (H) with different molar ratios. The NIR spectra of pure phase β-PbO_2 is also shown (right y axis).

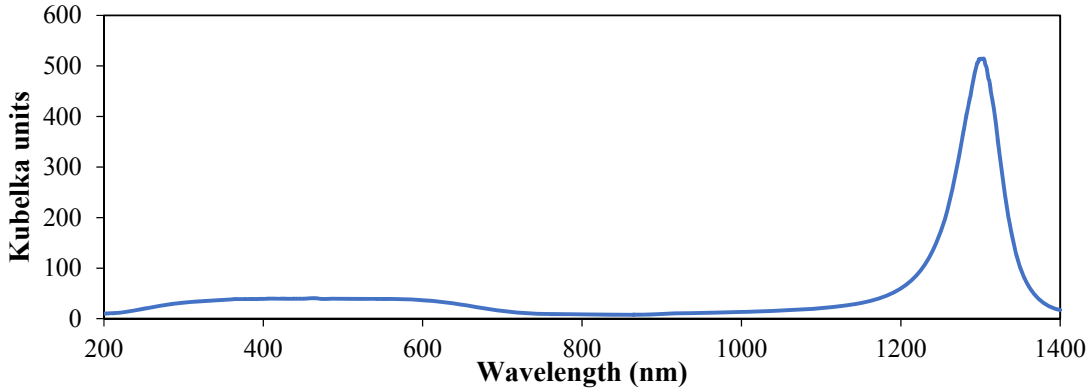

Figure S.B.5 UV/Vis/NIR spectra of pure β-PbO_2.

Curriculum Vitae

Name:	Daoping Guo
Post-secondary Education and Degrees:	University of Science and Technology Beijing Beijing, China 2006-2010 B.E. Western University London, Ontario, Canada 2012-2014 M.E.
Related Work Experience	Research Assistant Western University 2012-2014 Teaching Assistant Western University 2012-2014